

**THEORETICAL STUDIES OF DIPOLE-BOUND ANIONS AND SMALL WATER
CLUSTERS**

by

Kadir Diri

BS Chemical Education, Bogazici University, Turkey, 1999

MS Chemistry, Bogazici University, Turkey, 2001

Submitted to the Graduate Faculty of
Arts and Sciences in partial fulfillment
of the requirements for the degree of
Doctor of Philosophy

University of Pittsburgh

2007

UNIVERSITY OF PITTSBURGH
FACULTY OF ARTS AND SCIENCES

This dissertation was presented

by

Kadir Diri

It was defended on

June 26, 2007

and approved by

David J. Earl, Ph.D.

Hyung J. Kim, Ph.D.

Peter E. Siska, Ph.D.

Dissertation Advisor: Kenneth D. Jordan, Ph.D.

THEORETICAL STUDIES OF DIPOLE-BOUND ANIONS AND SMALL WATER CLUSTERS

Kadir Diri, PhD

University of Pittsburgh, 2007

Part I of this work deals with dipole-bound anions of moderately and highly polar molecules. High level electronic structure calculations are performed on nitrile, carbonate, and sulfite containing molecules. The results are compared against experimental data obtained from Rydberg electron transfer, photoelectron spectroscopy, and field detachment studies. Explanations to the unusual trends in the electron binding energies of the series of nitrile containing molecules are suggested. Calculation results also help in suggesting an explanation to the interesting dissociative electron attachment observed in ethylene sulfite.

Part II of the thesis is devoted to theoretical studies of neutral and anionic water clusters. Neutral water clusters are important in establishing the bridge between a single water molecule and its bulk phase, while still allowing for accurate quantum mechanical calculations. Anionic water clusters on the other hand, are valuable species in the study of electron capture, solvation, and transfer, which are important chemical and biological processes.

Here, we focus mainly on the energetic and spectroscopic features of water clusters. Namely, we consider the effects of anharmonicity and high-level electron correlation to the vibrational frequencies and to the binding energies of the $(\text{H}_2\text{O})_n$, $n = 2-6$ neutral clusters. We also attempt to assign the vibrational spectrum of the $(\text{H}_2\text{O})_7^- \text{Ar}_m$ cluster, which shows unusual complexity and Ar solvation dependence, when compared with smaller clusters.

TABLE OF CONTENTS

| | |
|------------------------------------------------------------------------------------------------------------------------|------------|
| PREFACE..... | XVI |
| PART I: ELECTRONIC STRUCTURE CALCULATIONS ON DIPOLE-BOUND ANIONS..... | 1 |
| 1.0 INTRODUCTION..... | 2 |
| 1.1 EXPERIMENTAL TECHNIQUES FOR MEASURING THE ELECTRON BINDING ENERGIES OF DIPOLE-BOUND ANIONS..... | 5 |
| 1.1.1 Rydberg Electron Transfer (RET)..... | 5 |
| 1.1.2 Field Detachment (FD)..... | 7 |
| 1.1.3 Photoelectron Spectroscopy..... | 8 |
| 1.2 AB INITIO CALCULATIONS ON DIPOLE-BOUND ANIONS..... | 9 |
| 1.2.1 Methods..... | 9 |
| 1.2.2 Basis Sets..... | 11 |
| 2.0 DIPOLE-BOUND ANIONS OF MODERATELY POLAR MOLECULES: A STUDY OF A SERIES OF NITRILE CONTAINING MOLECULES..... | 13 |
| 2.1 INTRODUCTION..... | 13 |
| 2.2 CALCULATIONS, RESULTS, AND DISCUSSION..... | 15 |
| 2.3 CONCLUSIONS..... | 22 |

| | | |
|----------------------------------------------------------------------------------|-------------------------------------------------------------------------------------------------------------------------------------|-----------|
| 3.0 | DIPOLE-BOUND ANIONS OF HIGHLY POLAR MOLECULES: ETHYLENE CARBONATE AND VINYLENE CARBONATE..... | 23 |
| 3.1 | ABSTRACT..... | 23 |
| 3.2 | INTRODUCTION | 24 |
| 3.3 | RESULTS AND DISCUSSION..... | 27 |
| 4.0 | NEGATIVE IONS OF ETHYLENE SULFITE | 35 |
| 4.1 | ABSTRACT..... | 35 |
| 4.2 | INTRODUCTION | 36 |
| 4.3 | THEORY | 37 |
| 4.4 | DISCUSSION..... | 38 |
| 4.5 | CONCLUSIONS..... | 45 |
| PART II: VIBRATIONAL SPECTRA AND ENERGETICS OF SMALL WATER CLUSTERS | | |
| 48 | | |
| 5.0 | INTRODUCTION..... | 49 |
| 6.0 | THE ROLE OF ANHARMONICITY AND HIGH-ORDER ELECTRON CORRELATION EFFECTS ON THE VIBRATIONAL FREQUENCIES OF WATER CLUSTERS | 50 |
| 6.1 | INTRODUCTION | 50 |
| 6.2 | METHODOLOGY | 51 |
| 6.3 | RESULTS..... | 52 |
| 6.4 | CONCLUSIONS..... | 62 |
| 7.0 | ON THE CONTRIBUTION OF VIBRATIONAL ANHARMONICITY TO THE BINDING ENERGIES OF WATER CLUSTERS | 63 |

| | | |
|-------|----------------------------------------------------------------------------------------------------------------------------------|-----|
| 7.1 | ABSTRACT..... | 63 |
| 7.2 | INTRODUCTION | 64 |
| 7.3 | METHODOLOGY | 68 |
| 7.4 | RESULTS | 68 |
| 7.5 | CONCLUSIONS..... | 76 |
| 8.0 | ISOLATION AND SPECTROSCOPIC CHARACTERIZATION OF A NEW HIGH ELECTRON BINDING ENERGY ISOMER OF $(\text{H}_2\text{O})_7^-$ | 78 |
| 8.1 | INTRODUCTION | 78 |
| 8.2 | EXPERIMENTAL..... | 80 |
| 8.3 | THEORETICAL..... | 81 |
| 8.4 | RESULTS AND DISCUSSION | 84 |
| 8.4.1 | Photoelectron spectra: Ar dependence of the isomer distribution..... | 84 |
| 8.4.2 | Theoretical expectations..... | 87 |
| 8.4.3 | Evolution of the HOH bending spectra with argon..... | 91 |
| 8.4.4 | Isomer-specific predissociation spectra using VDE-dependent photodepletion | 94 |
| 8.4.5 | Isolation of the isomer II spectrum | 94 |
| 8.4.6 | Characterization of the type I and I' isomers in the bending region..... | 99 |
| 8.4.7 | Spectra of isomers I and I' in the OH stretching region | 103 |
| 8.5 | SUMMARY OF THE M-DEPENDENCE OF THE $(\text{H}_2\text{O})_7^- \text{AR}_M$ SPECTRA: EMERGENCE OF COMPLEXITY..... | 107 |
| 8.5.1 | Theoretical considerations of plausible structures for isomers I, I', and II | 108 |

| | | |
|---------------------------|-----------------------------------------------|------------|
| 8.6 | RECOMMENDATIONS FOR FURTHER WORK | 116 |
| APPENDIX A | 117 | |
| APPENDIX B | 133 | |
| BIBLIOGRAPHY | 136 | |

LIST OF TABLES

| | |
|-------------------------------------------------------------------------------------------------------------------------------------------------------------------------------------------------------------------------------------------------------------------------------------------|----|
| Table 1. Dipole moments, molecular polarizabilities, and electron affinities for the nitrile molecules studied here..... | 15 |
| Table 2. Comparison of calculated and experimental electron affinities (in meV) for the nitrile-containing compounds. For butanenitrile, pentanenitrile, and 3-methylbutanenitrile two different conformers labeled 1 and 2 are considered. In each case conformer 2 is more stable. | 18 |
| Table 3. Dipole Moments of Vinylene Carbonate and Ethylene Carbonate..... | 26 |
| Table 4. Calculated Vertical Electron Affinities (meV) of Vinylene Carbonate and Ethylene Carbonate..... | 32 |
| Table 5. Calculated vibrational frequencies of H_2O^a | 52 |
| Table 6. Calculated anharmonic vibrational frequencies ^a of $(\text{H}_2\text{O})_2^b$ | 53 |
| Table 7. Calculated anharmonic vibrational frequencies ^a of $(\text{H}_2\text{O})_3^b$ | 54 |
| Table 8. Calculated vibrational frequencies ^a of $(\text{H}_2\text{O})_4^b$ | 55 |
| Table 9. Calculated vibrational frequencies ^a of $(\text{H}_2\text{O})_5^b$ | 56 |
| Table 10. Contributions of anharmonicity and higher-order correlation corrections to the frequency shifts ^a (cm^{-1}) of the single-donor OH stretch vibrations of the $(\text{H}_2\text{O})_n$, $n = 2-4$, clusters ^b | 57 |

| | |
|---------------------------------------------------------------------------------------------------------------------------------------------------------------------------------------------------------------------------------------------------------------|----|
| Table 11. Changes in the OO distances (\AA) of the $(\text{H}_2\text{O})_n$, $n = 2-6$, clusters due to vibrational averaging (ΔR_{OO}) ^a | 57 |
| Table 12. Harmonic and Anharmonic Vibrational Frequencies and Zero-Point Energies (cm^{-1}) of $(\text{H}_2\text{O})_2$ | 70 |
| Table 13. Harmonic and Anharmonic ZPEs and ZPE Contributions to the Binding Energies (cm^{-1}) of the $(\text{H}_2\text{O})_n$, $n = 1 - 6$, Clusters Calculated at the B3LYP/aug-cc-pVDZ Level of Theory ^a .. | 72 |
| Table 14. Harmonic and Anharmonic ZPEs and ZPE Contributions to the Binding Energies (cm^{-1}) of the $(\text{H}_2\text{O})_n$, $n = 1 - 6$, Clusters Calculated at the MP2/aug-cc-pVDZ Level of Theory ^a | 72 |
| Table 15. Vibrational ZPE Contributions (cm^{-1}) to the Binding Energies Reported per Monomer and Calculated at the B3LYP/aug-cc-pVDZ Level of Theory. | 73 |
| Table 16. ZPE Contributions (cm^{-1}) of Various Classes of Vibrations to the Binding Energies of the $(\text{H}_2\text{O})_n$, $n = 2 - 6$, Clusters Calculated in the Harmonic Approximation at the B3LYP/aug-cc-pVDZ Level. | 75 |
| Table 17. ZPE Contributions (cm^{-1}) of Various Classes of Vibrations to the Binding Energies of the $(\text{H}_2\text{O})_n$, $n = 2 - 4$, Clusters Calculated in the Harmonic Approximation at the QCISD/aug-cc-pVDZ Level ^a | 76 |
| Table 18. The exponents of the supplemental set of diffuse functions for the basis sets used..... | 87 |
| Table 19. Relative energies, VDEs, and dipole moments of the isomers considered, calculated at the MP2 and CCSD(T) levels of theory utilizing the 6-31(1+,3+)G* basis set, and with the Drude model. ^a | 89 |
| Table 20. Relative zero point energies (meV) of selected isomers calculated using the 6-31(1+,3+)G* basis set. | 90 |

Table 21. Relative energies, VDEs, and dipole moments of selected isomers, calculated at the MP2/aug-cc-pVDZ (2s2p,1s) level of theory.^a 91

Table 22. Relative energies (meV) of the structures shown in Figure 32..... 115

LIST OF FIGURES

| | |
|-----------------------------------------------------------------------------------------------------------------------------------------------------------------------------------------------|----|
| Figure 1. The direction of the dipole moment (a) and the shape of the orbital occupied by the excess electron (b) in butanenitrile. | 4 |
| Figure 2. Dipole-bound anion spectra of cyclohexanone, | 6 |
| Figure 3. Measured electron binding energies of various compounds as a function dipole moment. | 14 |
| Figure 4. The position of the supplemental diffuse set. | 17 |
| Figure 5. The direction of the dipole moment (the arrows) in two different conformers of butanenitrile. | 17 |
| Figure 6. Pictures of the orbitals occupied by the excess electron in (a) butanenitrile and (b) 3-methylbutanenitrile conformers. The value of the isosurface is the same for all plots. | 21 |
| Figure 7. Relative anion signal for ethylene carbonate (left) and vinylene carbonate (right) as a function of effective Rydberg quantum number n^* (from nd states) of rubidium..... | 28 |
| Figure 8. Photoelectron spectrum of ethylene carbonate negative ion. | 30 |
| Figure 9. Shapes of the dipole-bound molecular orbitals (electron density) of vinylene carbonate (left) and ethylene carbonate (right) using an isosurface of 0.003. | 32 |

Figure 10. Electron affinities of a number of dipole-bound anions. The various shapes indicate the source of the measurements: squares,³⁵ diamonds,¹⁸ asterisk,¹⁰ circle,⁵³ and triangles (current work). 34

Figure 11. Relative Rydberg electron transfer cross sections as a function of n^* for reactions of Rb^{**} with ES. (a) shows the ion signal as a function of the two-photon excitation wavelength of ns and nd Rydberg states whereas (b) represents the ion signal as a function of the effective quantum number n^* . The solid lines in (b) indicate simulated results using the RET curve crossing model.⁶² The peak at $n^*_{max} \sim 16.8$ corresponds to the expected dipole-bound anion. The broader feature at $\sim n^*_{max} \sim 13.5$ is attributed to ring breaking and the formation of a distorted $C_2H_4SO_3^-$ anion..... 39

Figure 12. (a) Structures and (b) their relative energies (in parentheses) compared to the neutral ethylene sulfite (ES1 in this figure). Energies have been corrected for vibrational zero-point energy..... 42

Figure 13. Relative dissociative electron attachment cross sections for the ions created from electron attachment to ES. SF_6^- is included as a reference..... 44

Figure 14. Relative dissociative electron attachment cross sections for SO_2^- ions created from electron attachment to ES using a TEM. SF_6^- is included as a reference..... 45

Figure 15. Water clusters studied in this work. 67

Figure 16. Vibrational ZPE contributions per monomer (cm^{-1}) to the dissociation energies of the $(H_2O)_n$, $n = 2 - 6$, clusters..... 73

Figure 17. Acceptor-acceptor (AA) binding motif of the isomer I variants of $(H_2O)_n^-$. In this scheme, a single water molecule serves as the binding site for an excess electron, pointing both

free hydrogens into the electron's diffuse orbital. This AA molecule is easily revealed in infrared spectra by the presence of its very red-shifted ($>50\text{ cm}^{-1}$) HOH bend..... 80

Figure 18. The calculated most stable 28 possible structures of $(\text{H}_2\text{O})_7^-$ 83

Figure 19. Photoelectron spectra of the $(\text{H}_2\text{O})_7^- \cdot \text{Ar}_m$ ($m = 0-10$) species. Expected electron binding energies of isomers I and II, along with the emergence of a new, higher-binding isomer (I'), are indicated by the dashed lines. The arrows indicates the energy of the infrared bleaching laser used to selectively remove isomers II and I from the population (0.372 and 0.471 eV, respectively)..... 86

Figure 20. Calculated vertical detachment energies (VDE) of the $(\text{H}_2\text{O})_7^-$ structures shown in Figure 18, plotted as a function of the dipole moments of their neutral scaffolds. The dramatic separation of the AA and non-AA type binding motifs qualitatively supports the structural assignments of isomers I and II for $(\text{H}_2\text{O})_7^-$ 90

Figure 21. Infrared spectra of $(\text{H}_2\text{O})_7^- \cdot \text{Ar}_m$ ($m = 0-10$) in the HOH bending region. The red-shifted bend at $\sim 1535\text{ cm}^{-1}$ indicates the existence of the AA binding motif throughout the $m = 0-10$ series. The bending vibrational frequency of a free H_2O molecule is represented by the dashed line at 1595 cm^{-1} . Features labeled α , β , γ , and δ , whose presence coincides with the emergence of a new peak in the photoelectron spectrum (see Figure 19) between $m = 4$ and 6 , suggest that this new peak is created by a $(\text{H}_2\text{O})_7^-$ isomer which is structurally different than isomer I. 93

Figure 22. Infrared spectrum of $(\text{H}_2\text{O})_7^- \cdot \text{Ar}_4$ (a) before and (b) after bleaching the ion packet with an infrared laser tuned to 3000 cm^{-1} (0.372 eV). The bleaching laser removes isomer II from the population, leaving only isomer I for interrogation by the second infrared laser. The persistence

of the red-shifted HOH bend transition at 1535 cm^{-1} after photobleaching establishes that isomer I exhibits an AA-type electron binding motif. 95

Figure 23. Infrared HOH bending spectrum of the isomer II variant of $(\text{H}_2\text{O})_7^- \cdot \text{Ar}_4$ (trace b), determined by subtraction of trace (b) from trace (a) in Figure 22, shown in comparison with the analogous spectra for $(\text{D}_2\text{O})_6^-$ (trace a) and $(\text{H}_2\text{O})_8^-$ (trace c) species from previous studies.^{170,183}

All three species exhibit intensity that is either at or slightly red-shifted from the free H_2O bending frequency (1595 cm^{-1} for H_2O and 1178 cm^{-1} for D_2O), indicative of similar electron binding motifs, in which one or more dangling OH groups serve as the capture point for the excess electron. The dashed line indicates the position of the red-shifted AA band present in isomer I species. 97

Figure 24. Calculated structure and infrared spectrum of a $(\text{H}_2\text{O})_7^-$ species with a non-AA type electron binding motif (a). The isomer shown is Pr-b, together with the orbital occupied by the excess electron. Vibrational frequencies were calculated at the MP2/6-31(1+,3+)G* level and scaled by 0.93. Peaks were given line widths of 9 cm^{-1} to facilitate comparison with the experimental spectrum (b). 99

Figure 25. Infrared spectra of the isomer I species for $(\text{H}_2\text{O})_6^-$ (top panel), $(\text{H}_2\text{O})_7^-$ (center panel), and $(\text{H}_2\text{O})_8^-$ (bottom panel). The red-shifted peak at $\sim 1535\text{ cm}^{-1}$ that is present in all species establishes that isomer I displays the AA-type electron binding motif. The similarity of the spectra in the $1600\text{-}1650\text{ cm}^{-1}$ range suggests that the supporting scaffolds of isomer I clusters in this size range share similar structural aspects. 101

Figure 26. Comparison of the infrared spectra of $(\text{H}_2\text{O})_7^-$ (a) isomer I' and isomer I species in the HOH bending region. The isomer I' spectrum is obtained by photobleaching the ion packet with

a laser tuned to 3800 cm^{-1} before interaction with the second infrared laser, thereby removing both isomers I and II from the population. 102

Figure 27. Argon dependence of $(\text{H}_2\text{O})_7^-\cdot\text{Ar}_m$ ($m = 0-10$) in the OH stretching region. The transition from isomer I to I' is most obvious at $m = 5$, where new distinguishable peaks emerge at $3200, 3250,$ and 3300 cm^{-1} 104

Figure 28. OH stretch region vibrational spectrum of $(\text{H}_2\text{O})_7^-\cdot\text{Ar}_6$ (a) and the spectrum of isomer I' (b) obtained by hole burning at 0.47 eV 106

Figure 29. Calculated spectra of Pf24a (top) and Pnf-a (bottom), together with the experimental ones. Note that the experimental spectra here are not those of isolated isomers. 110

Figure 30. Comparison of isomers I' and I in the HOH bending region. (a) is the calculated spectrum for Af-a, and (b) is the corresponding experimental data. (c) shows the experimental spectrum of isomer I, while (d) depicts the corresponding calculated spectra of I ($m < 5$) and I ($m > 5$) [i.e., Pnf-a (bold) and Pf24a (pale), respectively]. 112

Figure 31. Calculated vibrational spectra of Af-e* (a) and Af-a (b), together with the experimental data from the hole burning experiment at 0.47 eV (c). 113

Figure 32. Barriers (meV) for interconversion between selected structures. "ts" denotes a transition state. 114

PREFACE

I am indebted to my advisor Prof. Ken Jordan for all his help, support, understanding, and patience throughout grad school. I would also like to thank him and all the other past and current group members for creating the wonderful atmosphere at school, which made me enjoy my PhD journey! The lab was a nice place to hang out even on the weekends thanks to Valerie, Jun, Alex, and Wendy. I should thank Seymour, Richard, and Albert for their help with computer stuff. It was fun playing ping pong with Eugene, Brad, Hanbin, and Tae Hoon during our breaks. I should also thank Thomas and Daniel for the nice scientific and non-scientific discussions, and Jing for being my night-shift buddy. I almost forgot to mention Glen, Jiawei, Hao, and Li :)

I could not survive without my other friends which are too many to fit in this page, but I should mention Sebnem, Mehmet, and my eternal roommate Alpay, who have all been like a family to me. Thanks to Erikah, for being my failsafe for all kinds of activities and for teaching me organic chemistry :) Ozlem, Murat, Isil, Bill, Marti, and Pinar also made my life much nicer.

Many thanks to Drs. Earl, Kim, and Siska for serving in my thesis committee and for the nice chats we had. My “2 min stops” to Dr. Siska’s office often turned into long conversations. I should also acknowledge the whole P-chem division and Toni and Elaine. Also, Fran rules!

Prof. Anna Krylov and her wonderful group deserve a lot of credit for making my phase transition to the west coast easier, and for their patience while I was writing this thesis.

And my family... Thanks to you, I am still sane :) This work is dedicated to you.

**PART I: ELECTRONIC STRUCTURE CALCULATIONS ON DIPOLE-BOUND
ANIONS**

1.0 INTRODUCTION

The problem of an electron binding to a dipole has attracted the attention of experimentalists and theoreticians. It was shown that if the value of a finite-dipole, which can be represented by two charges (+Q and -Q) separated by a distance R, exceeds 1.625 D and if the Born-Oppenheimer approximation holds, there are infinitely many bound states.¹ The Schrödinger equation for this system in atomic units is:

$$\left(-\frac{1}{2}\nabla^2 - \frac{Q}{r_+} + \frac{Q}{r_-} - \frac{Q^2}{R} \right) \Psi = E\Psi \quad [1]$$

where r_+ is the distance of the electron to the positive (+Q) charge, and r_- is the distance to the negative (-Q) charge. The above Hamiltonian is similar to that for the H_2^+ molecule except for having one “negative nucleus” in the finite-dipole case. Consequently, this equation can be solved exactly to obtain the energy levels. Including a short-range repulsion term in the electron-finite-dipole case does not change the value of the critical dipole moment mentioned above.^{1,2}

The same critical dipole moment value and infinitely many bound states are obtained¹ for a point dipole binding an electron. However, in the absence of a repulsive term, there are no discrete eigenfunctions for this system, and the model is unphysical. When such a term is added, it accounts for the “excluded-volume effect” and the model resembles more closely a real molecule.

The spectrum of the excess electron/finite-dipole problem is drastically altered by corrections to the Born-Oppenheimer approximation. The critical value of the dipole moment is raised depending on the moment of inertia of the molecule, but is typically around 2.4 D,³⁻⁵ and the number of bound states becomes finite (often only one).

The anions that are formed when neutral polar molecules capture a free electron due to their dipole moments are called dipole-bound anions. The excess electron in such anions occupies a very diffuse orbital as shown in Figure 1. The arrow in (a) shows the direction of the dipole moment and points towards its positive end, where the electron is expected to be bound. This is exactly what is seen in (b) which depicts the orbital occupied by the excess electron. The extent to which that orbital is diffuse and its “distance” from the molecule depend on the dipole moment of the neutral host; the larger the moment, the less diffuse the orbital, and the closer the electron to the molecule. However as it will be shown later, looking only at the dipole moment of a polar molecule is not enough to characterize its dipole-bound state, since other factors such as higher-order multipole moments, molecular shape, and dispersion interactions also play important roles.

Since the excess electron occupies a very diffuse orbital, and since it is far away from the neutral molecule (typically 10-100 Å),⁶ its binding energy is small, typically ranging from a few to tens of meV. However, in cases where the dipole moment of the neutral host is very large (such as in small water clusters, which will be discussed in later chapters), the electron binding energy can easily reach hundreds of meV.

Interest in dipole-bound anions has been invoked by advances in experimental techniques, which allow one to do spectroscopic measurements on single molecules or molecular clusters such as the water hexamer anion.⁷ Traces of such weakly bound anions have also been

observed in the photodetachment spectra⁸ of some valence anions and therefore it has been suggested that the dipole-bound state is a “doorway” to the valence-bound anion.⁹⁻¹¹ In addition, many biological molecules are actually zwitterions, and thus can bind electrons due to their large dipole moments.

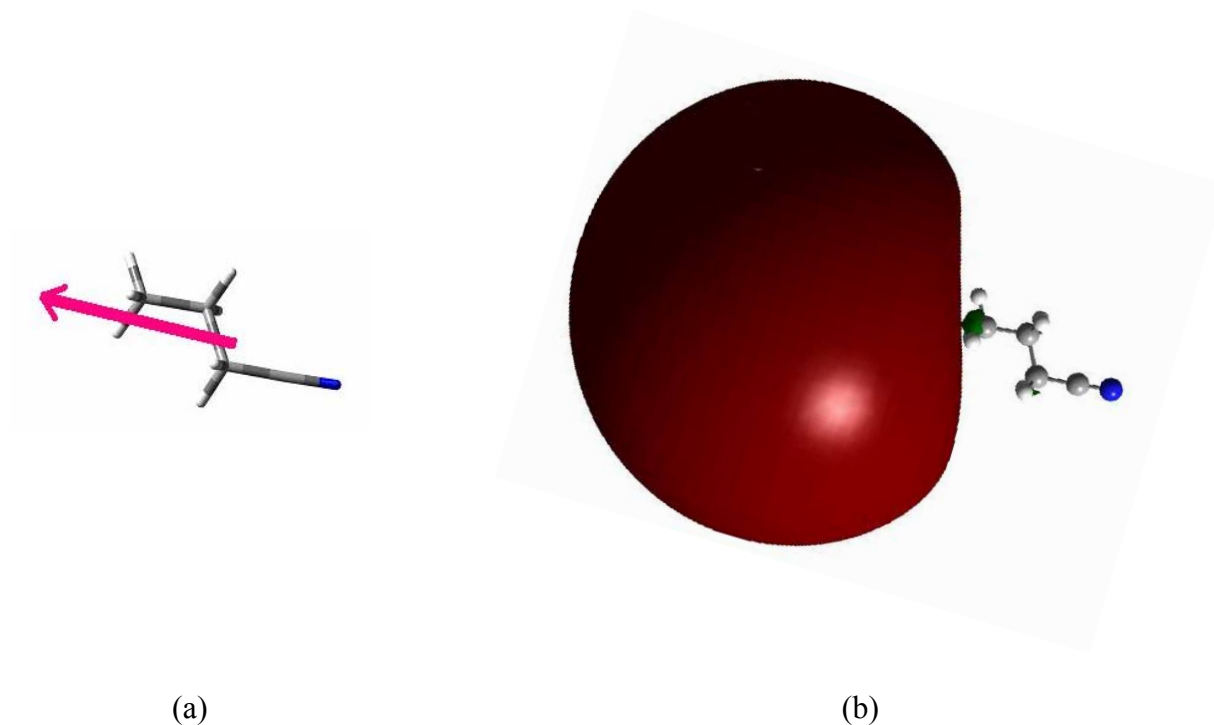


Figure 1. The direction of the dipole moment (a) and the shape of the orbital occupied by the excess electron (b) in butanenitrile.

The first experimental evidence for the existence of dipole-bound anions came in the 1970's from electron scattering measurements,^{12,13} and from Rydberg Electron Transfer (RET) experiments on acetonitrile.¹⁴

1.1 EXPERIMENTAL TECHNIQUES FOR MEASURING THE ELECTRON BINDING ENERGIES OF DIPOLE-BOUND ANIONS

Dipole-bound anions can be formed by a charge transfer from an excited Rydberg atom to a polar molecule during a collision, or by crossing a molecular jet expansion with an electron beam.¹⁵ Acetonitrile dipole-bound anions have also been obtained after the photodissociation of iodine atom/acetonitrile neutral clusters.¹⁶

The most widely used methods to measure the binding energies of dipole-bound anions are RET and Field Detachment (FD) experiments. Photoelectron spectroscopy can also be applied, however that method is not as accurate as RET or FD for very weakly-bound electrons, since the uncertainty imbedded in photoelectron spectroscopy (~ 10 meV) is often of the same order of magnitude as the binding energy of the electron in a dipole-bound anion.

1.1.1 Rydberg Electron Transfer (RET)

Dipole-bound anions can readily be formed by colliding polar molecules (with a dipole moment exceeding the critical value mentioned before) with a Rydberg alkali atom (such as Rubidium) excited to various ns and nd levels.^{17,18} The result is a charge transfer from the Rydberg atom to the neutral molecule. This transfer occurs over a narrow range of n^* values, where n^* is the effective principal quantum number of the Rydberg atom. The newly formed anions then can be sent to a mass spectrometer and the relative anion formation rate can be observed for a range of ns and nd values of the Rydberg atom. A typical spectra obtained from such an experiment can be seen in Figure 2.

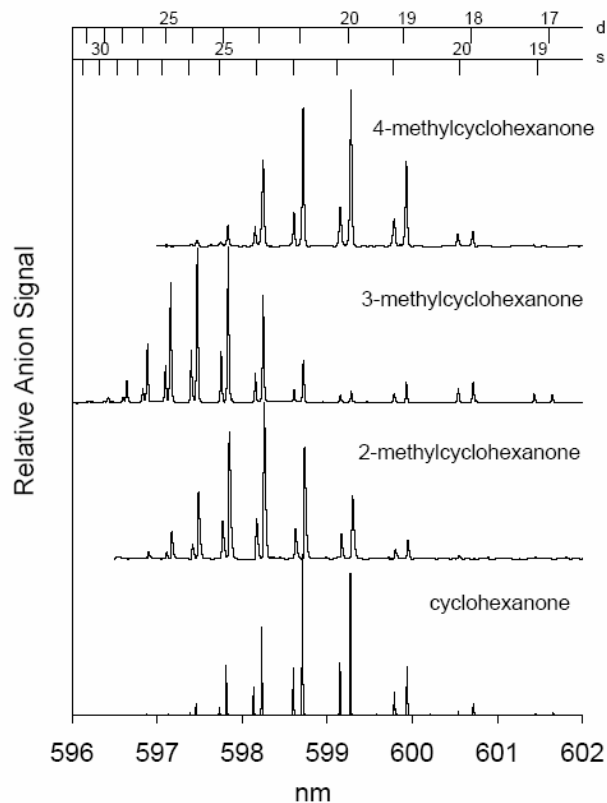


Figure 2. Dipole-bound anion spectra of cyclohexanone, 2-methylcyclohexanone, 3-methylcyclohexanone, and 4-methylcyclohexanone. (Figure taken from Reference 18)

In spectra such as those shown in Figure 2, one can fit a curve passing through the top of each peak and therefore obtain the relationship between the intensity of the relative anion signal and the ns or nd level of the Rydberg atom. Consequently the maximum n^* number (n^*_{\max}) can be determined. Note that n^*_{\max} is not necessarily an integer since it is simply the point where the fitted curve has its maximum. The value of n^*_{\max} is related to the electron binding energy in the dipole-bound anion that forms through the empirical relationship:

$$E_{bind} = \frac{23 eV}{n_{max}^{*2.8}} \quad [2]$$

which was derived from a curve-crossing model introduced by Desfrancois.¹⁹ The binding energies obtained from this model have been recently compared to those from field detachment experiments and were found to be in excellent agreement with them.¹⁸

1.1.2 Field Detachment (FD)

Field detachment of an excess electron from a dipole-bound anion is a method widely used in determining the electron binding energies of such species. The method can be more accurate than the curve-crossing analysis mentioned above and can be used as a good check of the values obtained from Equation 2 presented before.

The field detachment process is very similar to atomic field ionization. In the latter case, an external electric field is applied that can ionize the atom, so one can measure the magnitude of the field required to detach the electron and this way the binding energy of an electron can be determined. In most spectrometers, the time required for ionization through electron tunneling is larger than the time for normal ionization, so very accurate electron binding energies can be obtained.¹⁸

In a dipole-bound anion, the potential V experienced by the excess electron is given by:

$$V(r) = -\frac{\mu}{r^2} - Fr, \quad [3]$$

where μ is the dipole moment of the neutral molecule, r is its distance to the excess electron, and F is the magnitude of the external electric field.¹⁸ Again, the electron can be detached from the molecule by the application of an appropriate field F . In this case however, electron tunneling may be important, and therefore the process is more complicated than the analogous atomic field ionization. Fortunately, field detachment of dipole-bound anions considering electron tunneling has been studied and explained in the literature^{19,20} and at present this is the most accurate way of measuring such small electron binding energies. The disadvantage of the method is that very high voltages are required when the neutral molecule has a large dipole moment, so often this technique may not work for such molecules with conventional pulsed voltage supplies.

1.1.3 Photoelectron Spectroscopy

Photoelectron spectroscopy is a very powerful technique which is well suited for measuring the detachment energies of valence anions. The energy conservation principle

$$h\nu = E_{bind} + E_k, \quad [4]$$

is applied. Here $h\nu$ is the energy of the photon that causes the electron to be detached from the molecule, E_{bind} is the electron binding energy, and E_k is the kinetic energy of the free electron once detached. The energy of the photon used in the experiment is known and the kinetic energy of the free electron can also be measured. Thus E_{bind} can be easily determined.

Caution should be used when interpreting the results from photoelectron spectroscopy experiments on dipole-bound anions. Namely, the uncertainties in the results should be

considered. As mentioned before, typical uncertainties in such experiments are about ± 10 meV, so it is apparent that the technique is not suitable for measuring very low binding energies. In fact the dipole-bound anions with small binding energy may never be observed on certain instruments because the electron may be detached due to the electric fields in the instrument. That was proposed as one of the possible explanations for the fact that photoelectron spectrum of ethylene carbonate dipole-bound anion (with binding energy of 49 ± 5 meV) giving its neutral was readily observed while the very similar vinylene carbonate anion (with binding energy of 24 meV from RET experiments) was never observed in the same instrument.²¹

1.2 AB INITIO CALCULATIONS ON DIPOLE-BOUND ANIONS

1.2.1 Methods

The theory of dipole-bound anions has been discussed in a recent review by Jordan and Wang.²² Such anions are a real challenge for *ab initio* calculations. Their accurate treatment requires inclusion of electron correlation beyond the MP2 level,²³ although in the past researchers assumed electron correlation is not necessary in these calculations, since the excess electron is “far away” from the molecule, so its interaction with the other electrons was supposed to be negligible. This assumption has led many researchers to use the Koopmans’ theorem²⁴ (KT) to estimate the electron binding energies in dipole-bound anions from self-consistent-field (SCF) calculations. In this approach one assumes that this binding energy is simply the negative of the energy of the lowest unoccupied orbital (LUMO). This is a static approach which does not take into account the orbital relaxation that occurs when an electron is captured.

Hartree-Fock (HF) calculations on both the neutral and the anion on the other hand, solve the problem of orbital relaxation, since the orbitals can be optimized for the anion also. The dependence of the relaxation energy ($E_{bind\ SCF} - E_{bind\ KT}$, where $E_{bind\ SCF}$ is the binding energy calculated by subtracting the total HF energy of the anion from that of the neutral, and $E_{bind\ KT}$ is the KT level electron binding energy) is approximately given by:

$$E_{bind\ SCF} - E_{bind\ KT} = c \alpha_z (E_{bind\ KT})^n, \quad [5]$$

where c and n are constants ($c = 6.445 \times 10^{-4}$, $n = 1.2987$), and α_z is the polarizability of the neutral molecule along its principal axis.²⁵

Including electron correlation usually leads to a large increase in the binding energy.^{6,18,23,25} The contribution of electron correlation has two different sources: first, the dipole moment of the neutral molecule is described better with its inclusion, and the second source is the dynamical correlation between the excess electron and the electrons of the neutral host.⁶ The MP2 correction to the electron binding energy can be decomposed to contribution from dispersion interactions between the extra electron and the other electrons in the molecule, and to a contribution from non-dispersion effects.⁶ In the same reference, it was shown that for all molecules studied, the dispersion contribution term dominates, and its magnitude is larger than the binding energy at KT level. The non-dispersion term on the other hand was found to have an opposite effect (of decreasing the electron binding energy).

MP2 calculations usually do not give electron binding energies that are very accurate. To obtain better, more reliable results, one has to employ higher levels of theory. The coupled-cluster approach with single, double and perturbative triple excitations²⁶ (CCSD(T)) generally

gives numbers that are close to the experimental ones, and in cases where CCSD(T) is not adequate, it may be necessary to do CCSDT²⁷ (where the triple excitations are treated self-consistently) calculations.²²

1.2.2 Basis Sets

The fact that the excess electron in a dipole-bound anion has a very diffuse character, requires the use of very large basis sets including diffuse functions with very small exponents in *ab initio* calculations. An immediate complication arising from the use of such basis sets is convergence difficulties for the wavefunction due to linear dependency problems, so the choice of a proper basis set for the calculations is a crucial step.

A detailed study of the complementary diffuse function sets that need to be added when performing *ab initio* calculations on dipole-bound anions was carried out by Gutowski *et al.*, on a series of molecules with different dipole moments.²⁵ Their findings are summarized in this paragraph. The diffuse sets composed of *s*, *p*, *d*, and *f* functions were chosen to be geometrical series of the form

$$\alpha_n = \alpha_1 q^{n-1}, n = 1, 2, \dots, \quad [6]$$

where α_n is the exponent of the n^{th} diffuse function. The value of α_1 (the exponent of the most diffuse function) depends on the dipole moment of the neutral molecule. The smaller the dipole moment, the more loosely bound the excess electron, so the smaller the exponent has to be to properly describe the diffuse orbital occupied by this electron. One way of deciding about the

value of the first exponent is to monitor the LCAO (linear combination of atomic orbitals) coefficients of the LUMO in an SCF calculation on the neutral. The coefficients of the most diffuse functions in the LUMO should not be dominating, since this would indicate that even more diffuse functions are likely to be required. It was found that for a molecule with a dipole moment μ of about 3.3 D, $\alpha_1 = 4 \times 10^{-5}$ is a good choice, and for one with μ of about 6.3 D, $\alpha_1 = 7 \times 10^{-4}$ is sufficient. In addition, it was found that in the case of smaller dipole moments, larger q can be used. For instance for μ in the range 3.3 - 4.5 D, one can have $q = 5$, while for μ of about 6 D, $q = 3.2$ is more appropriate. Finally, the value of the last (largest exponent) in the series is also important. It should be chosen to be at least two times smaller than the smallest exponent in the primary basis set to avoid linear dependency problems.

2.0 DIPOLE-BOUND ANIONS OF MODERATELY POLAR MOLECULES: A STUDY OF A SERIES OF NITRILE CONTAINING MOLECULES

This work is partially reproduced from:

Hammer, N. I.; Diri, K.; Jordan, K. D.; Desfrancois, C.; Compton, R. N. *J. Chem. Phys.* 2003, 119, 3650.

2.1 INTRODUCTION

Dipole-bound anions form when an excess electron is captured by the dipole field of a polar neutral molecule. Any molecule that has a dipole moment greater than about 2.5 D is expected to bind an extra electron, unless there are functional groups or other atoms/molecules occupying the space where the electron is to be bound. Such an “excluded-volume” effect has been recently observed by Tsai et al.²⁸ in theoretical studies of electron attachment to the water dimer embedded in Ar clusters.

Dipole-bound anions are readily produced through the transfer of an electron from an excited Rydberg atom to a polar molecule.¹⁸ A maximum in the Rydberg Electron Transfer (RET) cross section occurs for those values of n^* for which the binding energy of the Rydberg electron matches that of the excess electron in the dipole-bound anion state.

Generally, it is expected that the binding energy of the excess electron strongly correlates with the magnitude of the dipole moment of the neutral host. Although this trend is observed in Figure 3, it is also evident that there are significant deviations for certain molecules. For example, although the dipole moments of the nitrile-containing molecules plotted in the figure (triangles) are close to each other, the electron binding energies differ appreciably. In fact, as the dipole moment increases in this series, the electron affinity decreases as seen in Table 1 (acetonitrile has the smallest dipole moment, but the largest electron binding energy). These unexpected results in RET experiments raise the question of “What factors other than the dipole moments affect the electron binding energy?”. This behavior is unlikely to be caused by the difference in polarizabilities, since they become larger with the increasing size of the molecules. To gain more insight into the problem, we refer to high-level electronic structure calculations.

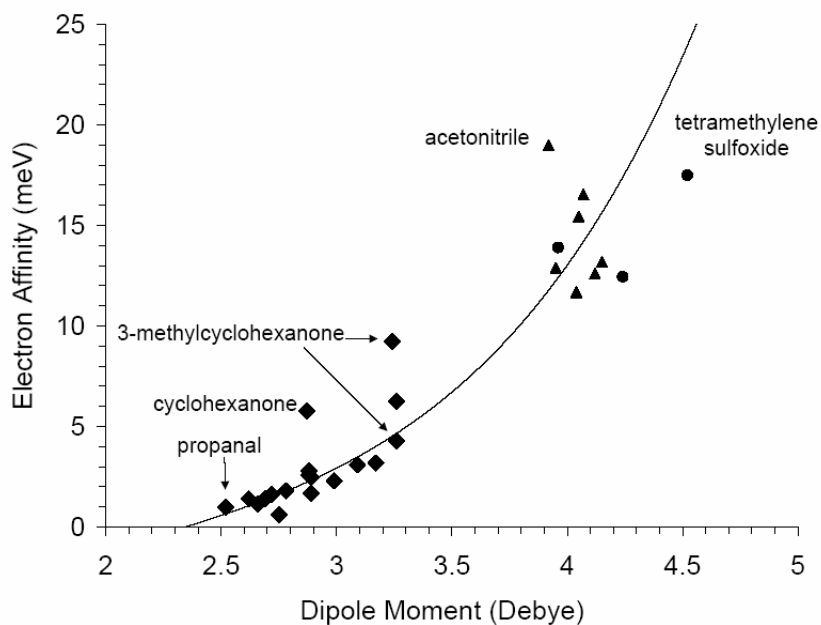


Figure 3. Measured electron binding energies of various compounds as a function dipole moment.

Table 1. Dipole moments, molecular polarizabilities, and electron affinities for the nitrile molecules studied here.

| Molecule | Formula | Dipole Moment (D) | | | Polarizability (10^{-24} cm ³) | | | n^*_{max} | Electron Affinity (meV) | |
|----------------------------|------------------------------------------------------|-------------------|----------|----------|-----------------------------------------------|------|----------|-------------|-------------------------|----------|
| | | MP2 EXP | MP2 PVDZ | MP2 PVTZ | EXP | EMP | MP2 PVDZ | | RET EMP | RET CALC |
| Acetonitrile | CH ₃ CN | 3.92 | 3.92 | 3.94 | 4.44 | 4.42 | 4.36 | 12.7 | 18.7 | 19.3 |
| Propanenitrile | CH ₃ CH ₂ CN | 4.05 | 4.03 | 4.03 | 6.47 | 6.27 | 6.19 | 13.7 | 15.1 | 15.8 |
| 2-Methylpropanenitrile | (CH ₃) ₂ CHCN | 4.29 | 4.04 | | 8.05 | 8.11 | 8.01 | 15.0 | 11.7 | 11.6 |
| Butanenitrile #1 | CH ₃ (CH ₂) ₂ CN | | 4.15 | | | | 8.06 | 13.4 | 16.1 | 17.0 |
| Butanenitrile #2 | | 4.07 | 3.99 | | 8.4 | 8.11 | 7.94 | | | |
| 2,2-Dimethylpropanenitrile | (CH ₃) ₃ CCN | 3.95 | 4.02 | | 9.59 | 9.95 | 9.80 | 14.6 | 12.6 | 13.2 |
| 2-Methylbutanenitrile #1 | CH ₃ CH ₂ CHCH ₃ CN | | 4.15 | | | | 9.81 | 14.5 | 12.9 | 13.5 |
| 2-Methylbutanenitrile #2 | | 3.99 | | | 9.95 | 9.88 | | | | |
| 3-Methylbutanenitrile #1 | (CH ₃) ₂ CHCH ₂ CN | | 4.04 | | | | 9.82 | 15.0 | 11.7 | 11.7 |
| 3-Methylbutanenitrile #2 | | 3.98 | | | 9.95 | 9.71 | | | | |
| Pentanenitrile #1 | CH ₃ (CH ₂) ₃ CN | | 4.26 | | | | 9.92 | 14.6 | 12.6 | 12.6 |
| Pentanenitrile #2 | | 4.12 | 3.95 | | 10.4 | 9.95 | 9.80 | | | |

2.2 CALCULATIONS, RESULTS, AND DISCUSSION

As mentioned previously, inclusion of electron correlation and use of very large basis sets are required in modeling dipole-bound anions.²³ In this study, the optimizations of the neutral molecules were carried out using the aug-cc-pVDZ²⁹ basis set. The resulting geometries were

used for highly correlated single-point CCSD(T) calculations with larger basis sets using the Gaussian98 program.³⁰ Such calculations are very expensive in terms of CPU time and require large disk space even on small molecules with several heavy atoms. Therefore, for the biggest molecules with no symmetry, the calculations were performed up to CCSD level of theory, noting that for the other molecules, the CCSD results were very similar to CCSD(T) ones. Binding energies were also calculated at Koopmans' Theorem (KT), Hartree-Fock (HF), and MP2 levels.

The starting basis set for the single point calculations was the aug-cc-pVTZ²⁹ basis set, from which we have discarded the *f* functions from the heavy atoms, and the *d* functions from the hydrogen atoms. This significantly reduces the computational time without sacrificing too much accuracy.

This starting basis set was supplemented with a set of 7(*sp*)5*d* diffuse primitive Gaussian functions with very small exponents. The exponents of the *sp* functions were: 2.470×10^{-2} , 7.600×10^{-3} , 2.360×10^{-3} , 7.290×10^{-4} , 2.250×10^{-4} , 6.977×10^{-5} , 2.157×10^{-5} , and the exponents of the *d* functions were taken to be the same as those of the first five diffuse *sp* functions.

The diffuse functions were centered on the carbon atom next to the CN group, as shown in Figure 4. One can justify the choice of that location by noting that the dipole moment is almost parallel to the line formed by the α carbon and the CN group (see Figure 5). Test calculations performed at the KT and HF levels show that the binding energy is not appreciably changed upon moving the center of the diffuse functions from the α carbon to either of the adjacent C atoms.

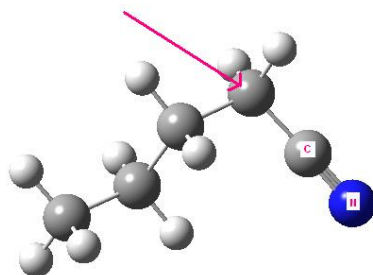


Figure 4. The position of the supplemental diffuse set.



Figure 5. The direction of the dipole moment (the arrows) in two different conformers of butanenitrile.

Table 2 reports the electron binding energies (or more specifically, the vertical attachment energies) calculated at the KT, HF, MP2, CCSD, and CCSD(T) levels of theory. For each molecule, the KT and HF binding energies are quite close, indicating that relaxation effects are relatively unimportant. In contrast, there are large increases in the binding energies in going from the HF to MP2 level, and then again, in going to the CCSD level. Thus, it is seen that electron correlation effects are crucial for describing the electron binding to these molecules, resulting in increases in the binding energies by a factor of 1.9 to 3.8, with the percentage

increase growing with the size of the molecule. As discussed in recent papers, the large contributions of electron correlation in the binding of excess electrons to polar molecules is a consequence of dispersion interactions between the excess electron and the electrons of the molecule.^{6,25,31-33} The binding energies calculated in the CCSD(T) approximation are 3-5% smaller than the corresponding CCSD values.

Table 2. Comparison of calculated and experimental electron affinities (in meV) for the nitrile-containing compounds. For butanenitrile, pentanenitrile, and 3-methylbutanenitrile two different conformers labeled 1 and 2 are considered. In each case conformer 2 is more stable.

| Molecule | Formula | KT | HF | MP2 | CCSD | CCSD(T) | EXP ^a |
|--------------------------|------------------------------------------------------|------|------|------|-------|---------|------------------|
| Acetonitrile | CH ₃ CN | 6.53 | 6.87 | 9.24 | 14.10 | 13.35 | 18.7 |
| Propanenitrile | CH ₃ CH ₂ CN | 4.63 | 4.97 | 6.72 | 11.76 | 11.09 | 15.1 |
| Butanenitrile #1 | CH ₃ (CH ₂) ₂ CN | 3.54 | 3.60 | 4.93 | 9.68 | 9.27 | 16.1 |
| Butanenitrile #2 | | 3.54 | 3.84 | 5.44 | 10.70 | - | |
| 2-Methylpropanenitrile | (CH ₃) ₂ CHCN | 3.81 | 3.93 | 5.32 | 10.33 | 9.85 | 11.7 |
| Pentanenitrile #1 | CH ₃ (CH ₂) ₃ CN | 2.99 | 3.24 | 4.52 | 9.34 | 9.03 | 12.6 |
| Pentanenitrile #2 | | 2.72 | 2.89 | 4.12 | 8.95 | - | |
| 3-Methylbutanenitrile #1 | (CH ₃) ₂ CHCH ₂ CN | 2.72 | 2.81 | 3.98 | 9.01 | - | 11.7 |
| 3-Methylbutanenitrile #2 | | 3.27 | 3.29 | 5.22 | 12.56 | - | |

^a From RET experiments.

The CCSD/CCSD(T) calculations consistently give smaller (by 16-42%) electron binding energies than those deduced from the RET measurements. This could reflect a tendency of the procedure to extract electron binding energies from RET data to overestimate the electron binding, or a tendency of the CCSD and CCSD(T) calculations to underestimate the electron binding energies. The latter possibility could be addressed by performing CCSDT calculations, in which the triple excitations are treated self-consistently rather than perturbatively. Nonetheless, in spite of these discrepancies, there is qualitative agreement in the trends in the calculated and in the RET binding energies. In particular, the calculations predict the largest binding energy for acetonitrile, which is in agreement with experiment.

Another contributing reason for the small discrepancy between the calculated and experimental results might be the fact that RET measures adiabatic electron binding energies whereas the calculated values are vertical attachment energies since in all cases the geometries assumed for the anion were the geometries of the corresponding neutrals. By comparing the dipole moments of the neutrals at their optimized geometries with the dipole moments of the neutrals at the optimized anion geometry, it was found that for acetonitrile and butanenitrile, the geometrical relaxation after capturing an electron is not very important. Therefore there should not be a large difference between the adiabatic and vertical binding energies.

Still another correction to the calculated binding energies to be considered is the role of the zero-point energy. Noting that the geometrical relaxation in going from the neutral to the anion was found to be unimportant for the test molecules mentioned above, the zero-point energies were not calculated, which saves a tremendous amount of computer time. Earlier calculations by Gutowski *et al.*,²³ showed that the zero-point energies of the acetonitrile neutral

and anion are comparable, and therefore their contribution to the final electron binding energy is negligible.

The calculations also confirm that factors other than the net dipole moments and net polarizabilities are important in establishing the electron binding energies. For example, although the dipole moment of conformer 1 of butanenitrile is 0.16 D higher than that of conformer 2, the KT values of the electron binding energies are essentially identical. We believe that this results from the fact that the excess electron interacts strongly with more CH groups in the latter species, as seen from Figure 6 (a). This explanation also appears to account for the greater KT level electron binding energy of conformer 2 (compared to conformer 1) of 3-methylbutanenitrile (see Figure 6 (b)). Apparently, multipole moments higher than the dipole are playing a significant role in the electron binding. We note also that electron correlation effects prove to be more important for the binding of the excess electron to conformer 2 (rather than conformer 1) of both butanenitrile and 3-methylbutanenitrile. This is consistent with an analysis in which the dispersion interaction between the excess electron and the molecule is decomposed into contributions involving individual CH₃, CH₂, CH and CN groups. As seen from Figure 6, for conformer 1 there is only one CH₃ group “near” the excess electron, but three and four CH_n groups “near” the excess electron for conformer 2 of butanenitrile and 3-methylbutanenitrile, respectively.

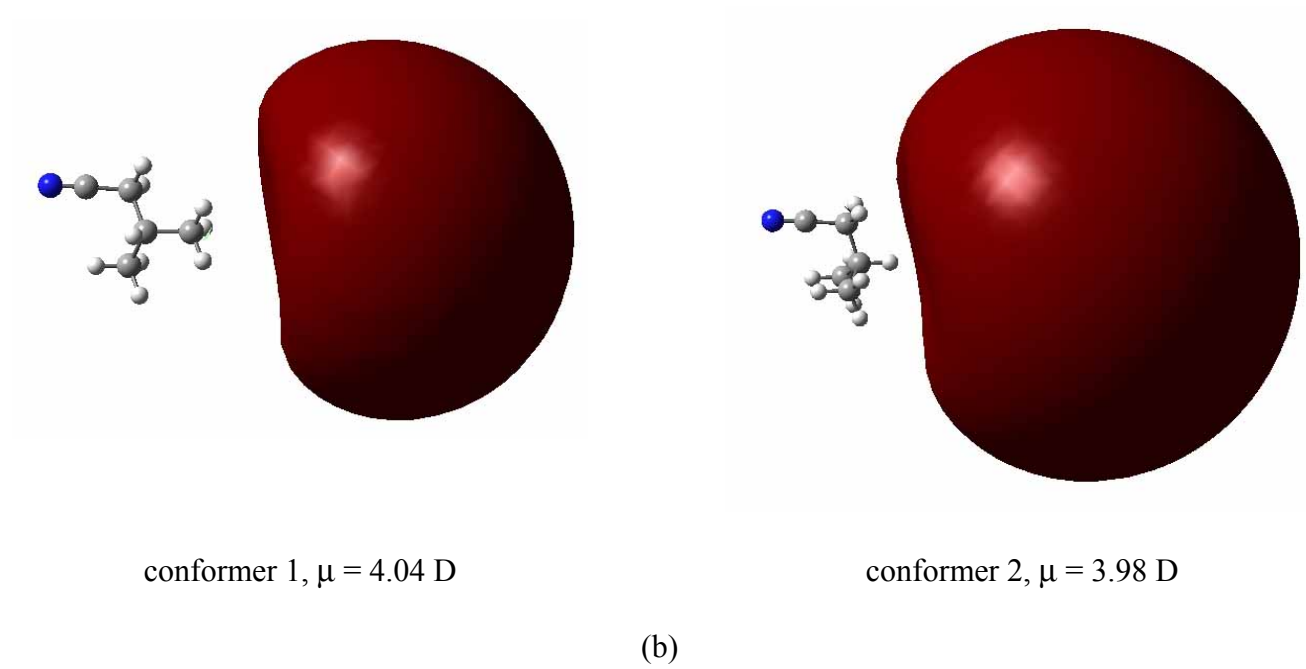
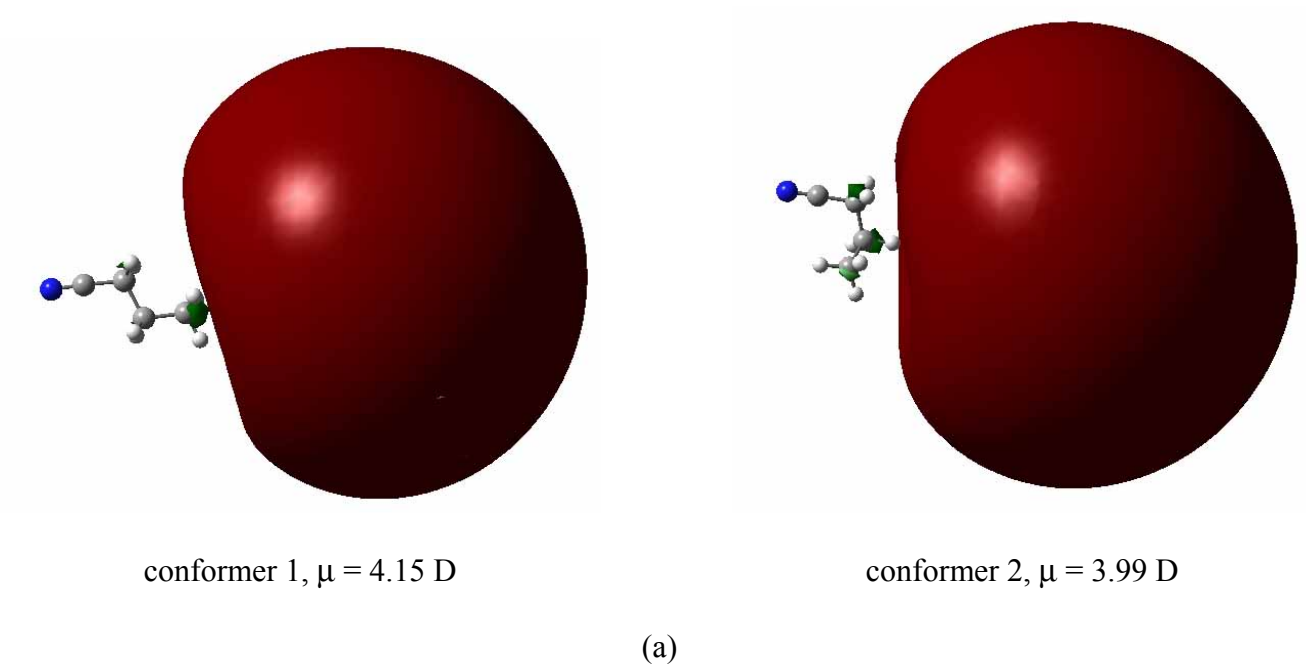


Figure 6. Pictures of the orbitals occupied by the excess electron in (a) butanenitrile and (b) 3-methylbutanenitrile conformers. The value of the isosurface is the same for all plots.

2.3 CONCLUSIONS

High-level (CCSD(T)) electronic structure calculations were carried out on a series of nitrile-containing molecules and these give electron binding energies in qualitative agreement with the experimental trends. Within this series of molecules, the values of the electron affinities do not correlate well with dipole moment or polarizability. It is clear from the experimental¹⁸ and theoretical studies that electron binding energies of dipole-bound anions are mainly dictated by the dipole moment, however other properties of the molecule, *e.g.*, polarizability, molecular size or shape, and, as seen in this study, dispersion interactions all play an important role in determining the electron binding energies.

3.0 DIPOLE-BOUND ANIONS OF HIGHLY POLAR MOLECULES: ETHYLENE CARBONATE AND VINYLENE CARBONATE

This chapter is partially reproduced from

Hammer, N. I.; Hinde, R. J.; Compton, R. N.; Diri, K.; Jordan, K. D.; Radisic, D.; Stokes, S. T.; Bowen, K. H. *J. Chem. Phys.* **2004**, *120*, 685.

3.1 ABSTRACT

Results of experimental and theoretical studies of dipole-bound negative ions of the highly polar molecules ethylene carbonate (EC, $C_3H_4O_3$, $\mu=5.35$ D) and vinylene carbonate (VC, $C_3H_2O_3$, $\mu=4.55$ D) are presented. These negative ions are prepared in Rydberg electron transfer (RET) reactions in which rubidium (Rb) atoms, excited to *ns* or *nd* Rydberg states, collide with EC or VC molecules to produce EC^- or VC^- ions. In both cases ions are produced only when the Rb atoms are excited to states described by a relatively narrow range of effective principal quantum numbers, n^* ; the greatest yield of EC^- and VC^- are obtained for $n^*_{max}=9.0 \pm 0.5$ and 11.6 ± 0.5 , respectively. Charge transfer from low-lying Rydberg states of Rb is characteristic of a large excess electron binding energy (E_b) of the neutral parent; employing the previously derived empirical relationship $E_b = 23/n^*_{max}{}^{2.8}$ eV, the electron binding energies are estimated to be $49 \pm$

8 meV for EC and 24 ± 3 meV for VC. Electron photodetachment studies of EC^- indicate that the excess electron is bound by 49 ± 5 meV, in excellent agreement with the RET results, lending credibility to the empirical relationship between E_b and n^*_{max} . Vertical electron affinities for EC and VC are computed at the CCSD(T) level of theory, employing aug-cc-pVDZ atom-centered basis sets supplemented with a (5s5p) set of diffuse Gaussian primitives to support the dipole-bound electron; the computed electron affinities are 40.9 and 20.1 meV for EC and VC, respectively.

3.2 INTRODUCTION

Many recent experimental studies have confirmed previous theoretical predictions^{3-6,22,34} that molecules with dipole moments above 2.5 Debye may form what are generally described as dipole-bound anions. Three recent review articles^{17,35,36} summarize the considerable experimental progress in this field. The first dipole-bound anion to be observed was CH_3CN^- , which was produced by charge transfer from a rare gas atom in a Rydberg state to the neutral CH_3CN parent.¹⁴ Later work adapted this technique, termed Rydberg electron transfer (RET), to produce dipole-bound anions of several neutral parent species.^{17,18,35,36} RET typically occurs over a narrow range of effective principal quantum numbers n^* of the Rydberg atom; by contrast, electron transfer from Rydberg atoms to produce “normal” valence-bound molecular anions occurs over a wide range of n^* .

Brauman⁸ and Lineberger³⁷ observed narrow intense resonances in the photodetachment spectra of the valence bound anions of several polar molecules; these resonances were located slightly above the photodetachment threshold, and were attributed to rotational autodetachment

via dipole-bound molecular anion states lying in the photodetachment continuum. The experiments showed that molecules that support valence-bound anion states may also exhibit features characteristic of dipole-bound anions. In some cases a dipole-bound anionic state may act as a “doorway” for the formation of a more tightly bound valence anion;^{9,10} in this context, Sommerfeld³⁸ has recently considered the diabatic coupling terms between dipole-bound and valence-bound negative ion states of nitromethane.

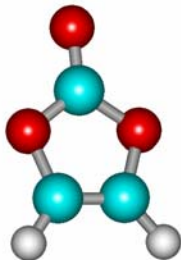
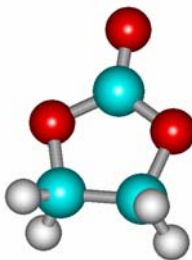
Electron binding energies of both dipole-bound and valence-bound molecular anions can be measured via anion photoelectron spectroscopy; Bowen, *et al.*¹⁵ have recorded the photodetachment spectra of ground-state dipole-bound molecular anions that are prepared by crossing a molecular jet expansion with an electron beam. Dipole-bound anion photoelectron spectra exhibit a distinctive spectral signature, with a single narrow peak at low electron binding energy. Excess electron binding energies of dipole-bound anions can also be inferred by detaching the excess electron via application of an electric field,^{18,35} although the possibility that electrons may tunnel through the potential barrier created by an external electric field makes it somewhat complicated to determine accurate electron binding energies via field detachment experiments. Desfrancois *et al.*³⁵ showed that the excess electron binding energy E_b of a dipole-bound molecular anion produced via RET can be estimated using the empirical relationship

$$E_b = \frac{23 \text{ eV}}{n_{\text{max}}^{*2.8}}, \quad [7]$$

where n_{max}^* is the effective principal quantum number of the Rydberg atom that produces the greatest yield of dipole-bound anions. This method has been recently applied to a large number (27) of molecules possessing dipole moments between 2.5 and 4.3 Debye.¹⁸ The applicability of

this relationship to highly polar molecules such as ethylene carbonate (EC, $C_3H_4O_3$, $\mu=5.35$ D) and vinylene carbonate (VC, $C_3H_2O_3$, $\mu=4.55$ D) is investigated herein. Measured and calculated values of the dipole moments and molecular structures of VC and EC³⁹⁻⁴⁴ are presented in Table 3. This application is confirmed for EC by measuring its electron affinity via anion photoelectron spectroscopy. Theoretical calculations of the electron affinities of EC and VC based on highly correlated electronic structure calculations employing a coupled cluster approach that includes single and double excitations (CCSD)⁴⁵ and a perturbative estimate of triple excitations, or CCSD(T),^{26,46} and a moderately large atom-centered basis set (aug-cc-pVDZ)²⁹ supplemented with a (5s5p) set of diffuse Gaussian primitives to support binding of a dipole-bound electron are also presented. All calculations presented in this work were carried out using the Gaussian 98 program.³⁰

Table 3. Dipole Moments of Vinylene Carbonate and Ethylene Carbonate

|  | |  | |
|-------------------------------------------------------------------------------------|------------------------|--------------------------------------------------------------------------------------|------------------------|
| Vinylene Carbonate $C_3H_2O_3$ | | Ethylene Carbonate $C_3H_4O_3$ | |
| Dipole Moment (D) | Method | Dipole Moment (D) | Method |
| 4.59 | MP2 ^a | 5.39 | MP2 ^a |
| 4.51 +/- 0.05 | Microwave ^b | 5.35 +/- 0.15 | Microwave ^e |
| 4.45 +/- 0.01 | Microwave ^c | | |
| 4.57 +/- 0.05 | Microwave ^d | | |

^a The theoretical dipole moments are from MP2/aug-cc-pVDZ calculations^{29,39} using geometries optimized at this level of theory. ^b Reference 41. ^c Reference 42. ^d Reference 43. ^e Reference 44.

Neither EC nor VC appears to support a stable valence-bound anion state. If these molecules are exposed to a low-energy electron beam, they do not form long-lived (lifetimes $t > 1$ μsec) valence-bound anions, but rather undergo dissociative electron attachment at electron energies above roughly 0.5 eV.^{47,48} For example, electron attachment to VC generates primarily $\text{C}_2\text{H}_2\text{O}^-$ and $\text{C}_2\text{H}_2\text{O}_2^-$ via broad (FWHM roughly 1 eV) dissociative resonances peaking at electron energies of 1.5 ± 0.1 and 3.0 ± 0.2 eV, respectively. Furthermore, studies of fast alkali atom electron transfer to VC show no evidence of a stable parent anion.⁴⁷ Younkin et al. have presented semi-empirical calculations indicating that the $^2\text{A}_2$ and $^2\text{B}_1$ π^* states of VC^- are unbound by -2.0 and -2.1 eV, respectively; they find no evidence of valence-bound anion states for EC or VC. Since valence-bound molecular anions most likely do not exist for EC and VC the anions produced in the experiments presented herein are true dipole-bound anions, and therefore the appropriate species for confirming the validity of Equation 7 in the highly polar regime.

3.3 RESULTS AND DISCUSSION

Using the RET technique described above, dipole-bound anions of EC and VC were produced via collisions between the neutral precursors and excited nd $^2\text{D}_{5/2}$ or $^2\text{D}_{3/2}$ Rb atoms. Figure 7 shows how the relative intensities of the dipole-bound product anions depend on the effective quantum number n^* of the Rb atom. Similar behavior is observed for collisions with Rb atoms excited to ns states, although the absolute signal intensity is much weaker in this case. For dipole-bound anions with excess electron binding energies below 10 meV, the Rb effective quantum numbers n^* that lead to significant RET typically range from 15 to 50. Because the corresponding Rb excited states are closely spaced in energy, the effective quantum number

n^*_{\max} that leads to maximum anion production can usually be estimated with little uncertainty. This is not the case for EC and VC, however; in these molecules, RET takes place at lower effective quantum numbers, where the Rydberg levels of Rb are much more widely spaced.

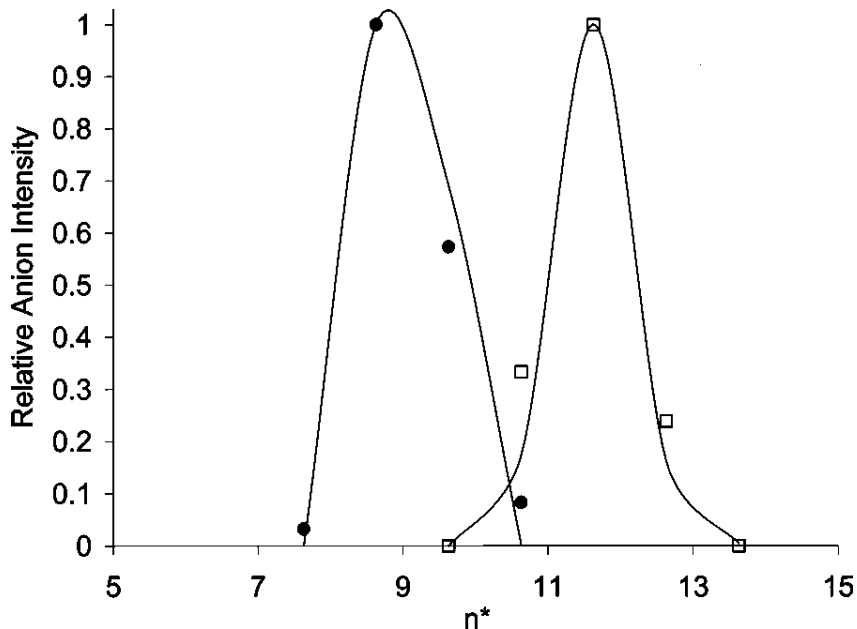


Figure 7. Relative anion signal for ethylene carbonate (left) and vinylene carbonate (right) as a function of effective Rydberg quantum number n^* (from nd states) of rubidium.

The RET profiles observed in Figure 7 could be fitted experimentally more exactly by employing an alternative alkali metal, such as cesium, as the electron donor, or by employing other angular momentum states of Rb. In this study, however, n^*_{\max} for EC and VC is estimated by fitting the available data points in Figure 7 to the curve-crossing model proposed by Desfrançois;¹⁹ the solid lines shown in the figure are the predictions of this model. The best fit to the experimental data is given by $n^*_{\max} = 9.0$ for EC and 11.6 for VC; from these n^*_{\max}

values and Equation 7, the excess electron binding energies of EC^- and VC^- are estimated to be 49 meV and 24 meV, respectively. An uncertainty of 0.5 in n^*_{\max} would correspond to respective uncertainties of 8 meV and 3 meV in the EC^- and VC^- excess electron binding energies.

Figure 8 depicts the photoelectron spectrum of EC^- . The spectrum is clearly that of a dipole-bound anion: such spectra are typically dominated by a single narrow peak at low electron binding energy. The peak shown in Figure 8 is very narrow because the structures of EC and EC^- are very similar, so that the Franck-Condon factor for the underlying transition is close to unity. The electron binding energy is therefore taken at the maximum of this peak (which is very close to the peak centroid) as the adiabatic electron affinity of EC. Using the calibration techniques described previously, the adiabatic electron affinity of EC is determined to be 49 ± 5 meV, in excellent agreement with the value obtained via RET studies. To provide additional confidence in this value, the photoelectron spectrum was measured using three different photon energies (2.41, 2.54, and 2.71 eV) in order to guard against possible complications arising from resonant phenomena;⁴⁹ the same photoelectron spectrum and the same electron binding energy was obtained using all three excitation wavelengths. Repeated efforts were made to obtain the photoelectron spectrum of VC^- , but the VC^- parent ion was never observed in the mass spectrometer. This is not entirely surprising given the relatively low electron binding energy of VC^- ; dipole-bound anions with electron binding energies below 40 meV have never been observed in this particular mass spectrometer. This is most likely due to field detachment of weakly bound electrons as the dipole-bound anions traverse the numerous electric fields associated with the ion optics in the apparatus. The absence of weakly bound dipole anions may also be attributed to the process of formation. The dipole-bound anions in

these experiments may result from RET from Rydberg states of Ar** atoms excited by electron impact. The highly excited atoms necessary to produce anions of molecules with small dipole moments may not survive the harsh conditions of the discharge.

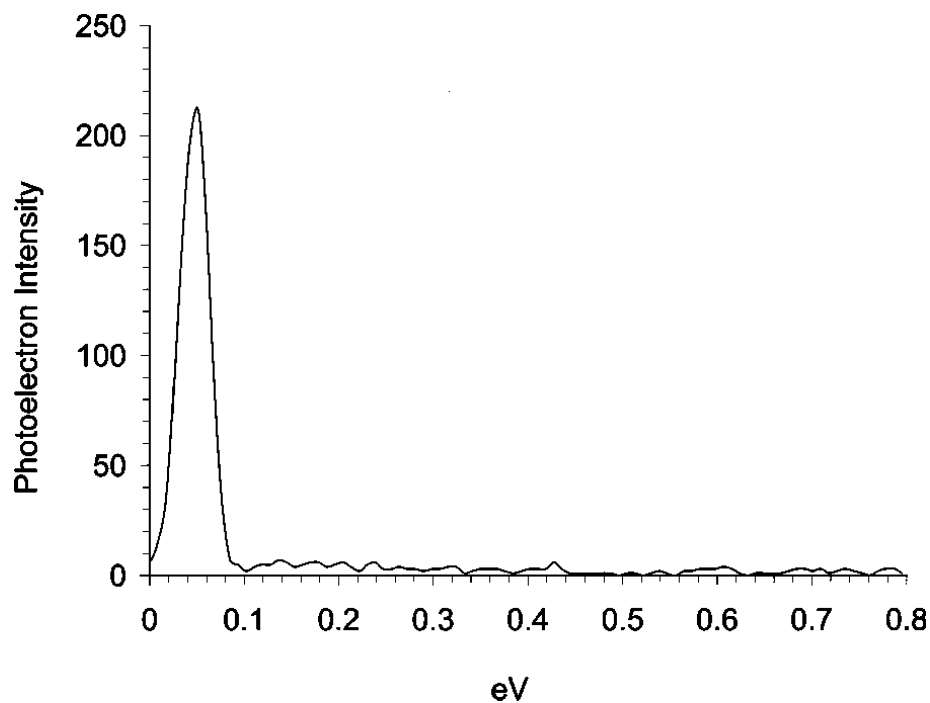


Figure 8. Photoelectron spectrum of ethylene carbonate negative ion.

The vertical electron affinities of EC and VC were computed at various levels of theory: Koopman's theorem (KT), Hartree-Fock (HF), second-order Moller-Plesset (MP2), coupled cluster with single and double excitations (CCSD), and CCSD with a perturbative estimate of triple excitations [CCSD(T)]. These calculations were performed using the MP2/aug-cc-pVDZ equilibrium geometries of the neutral parent molecules; the HF and post-HF calculations for the anions employed unrestricted HF wavefunctions. The computed vertical electron affinities are

defined as the difference between the total energies of the parent neutral and the anion; the total energies of both species are computed using the aug-cc-pVDZ atom-centered basis set augmented with a (5s5p) set of diffuse Gaussian primitive functions located at a point removed from the molecule, but on the twofold rotational symmetry axis of the molecule. The location of this point was determined by maximizing the electron binding energy at the HF level. The exponents for the (5s5p) primitives were chosen to be 0.00025, 0.001, 0.004, 0.016, and 0.064. No significant change in the excess electron binding energies was observed when larger (5s5p1d), (5s5p3d), or (7s7p3d) sets of diffuse functions were used.

The computed excess electron binding energies for EC^- and VC^- are summarized in Table 4. At the highest level of theory employed, CCSD(T), the computed electron binding energies are in reasonably good agreement with experiment. Note that the electron binding energies increase dramatically on going from the KT level of theory to the CCSD(T) level of theory, with a substantial portion of the increase arising from the inclusion of high-order electron correlation effects beyond the MP2 level of theory. This behavior is similar to that observed for several other molecules,^{6,18,22,25,31,50-53} and reflects the importance of dispersion-like interactions between the excess electron and the electrons of the neutral parent. Figure 9 shows the molecular orbitals occupied by the excess electron in EC^- and VC^- . The excess electron density for VC^- is nearly spherically symmetric while that for EC^- is more irregular in shape.

Table 4. Calculated Vertical Electron Affinities (meV) of Vinylene Carbonate and Ethylene Carbonate.

| | Vinylene Carbonate | Ethylene Carbonate |
|--------------------|--------------------|--------------------|
| KT | 11.97 | 23.95 |
| HF | 12.94 | 26.36 |
| MP2 | 15.58 | 31.70 |
| CCSD | 20.43 | 40.43 |
| CCSD(T) | 20.11 | 40.88 |
| Expt. ^a | 24 | 49 |
| Expt. ^b | | 49 |

^a Present work, using RET method. ^b Present work, from photodetachment method.

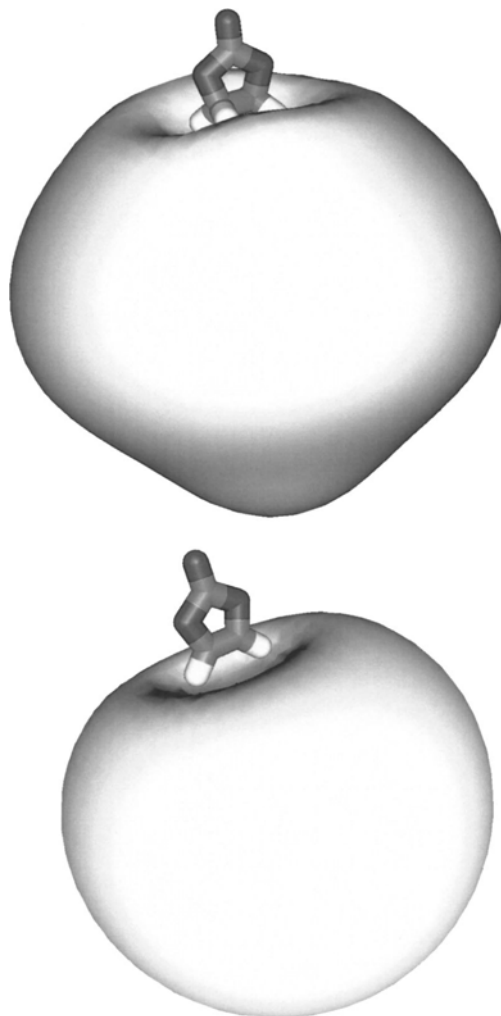


Figure 9. Shapes of the dipole-bound molecular orbitals (electron density) of vinylene carbonate (left) and ethylene carbonate (right) using an isosurface of 0.003.

The computed excess electron binding energies are roughly 20% lower than the experimentally measured binding energies. A similar discrepancy is observed between the electron affinities computed^{18,25} using techniques similar to those described here and measured¹⁸ using RET techniques for a series of alkylnitriles with dipole moments between 3.9 and 4.3 D. The theoretical binding energies presented in Table 4 are vertical electron affinities, while the RET and photodetachment experiments give adiabatic electron affinities and vertical detachment energies, respectively. A substantial change in molecular geometry following attachment of the dipole-bound electron could thus lead to discrepancies between the computed and measured excess electron binding energies. However, the good agreement between the two experimental measurements for EC, and the structure of the photodetachment spectrum shown in Figure 8, suggests that the equilibrium geometries of EC and EC⁻ are very similar, so that nuclear framework relaxation is probably not the source of the discrepancy between the computed and measured electron affinities. Furthermore, framework relaxation effects were explicitly considered in earlier work on CH₃CN and were found to be negligible.⁴⁹ It is possible that for highly polar molecules electron correlation effects beyond those recovered at the CCSD(T) level of theory make significant contributions to the excess electron binding energies.

Shown in Figure 10 is a plot of electron affinity as a function of dipole moment for a number of dipole-bound anions.^{10,18,35,54} For the most part, the electron affinity (EA) values for the compounds are seen to follow a general trend of increasing EA with dipole moment. We include an arbitrary line which attempts to best describe the general trend of all of the data points for discussion purposes. However, EA values for a number of molecules lie above or below this line. Surely part of this scatter can be attributed to the fact that the experimental dipole moments for some of these molecules are not accurately known. Other factors that could contribute to the

scatter include the importance of permanent moments other than the dipole, contributions from dispersion interactions between the excess electron and the electrons of the molecules, and variations in the "excluded volume" effect from molecule to molecule. The overall trend in the observed EA versus dipole moment lends support for this correlation as a means to estimate the unknown dipole moments of molecules. We have recently applied this method to the determination of the dipole moment of camphor ($C_{10}H_{16}O$). The n^*_{\max} for the formation of $C_{10}H_{16}O^-$ is 20.6 ± 0.2 , which gives an electron affinity of 4.8 ± 0.1 meV. Using the general relationship in Figure 10 we estimate the dipole moment for camphor to be 3.1 D. A recent value of the dipole moment for camphor determined from microwave spectroscopy was reported to be 3.08 D.⁵⁵

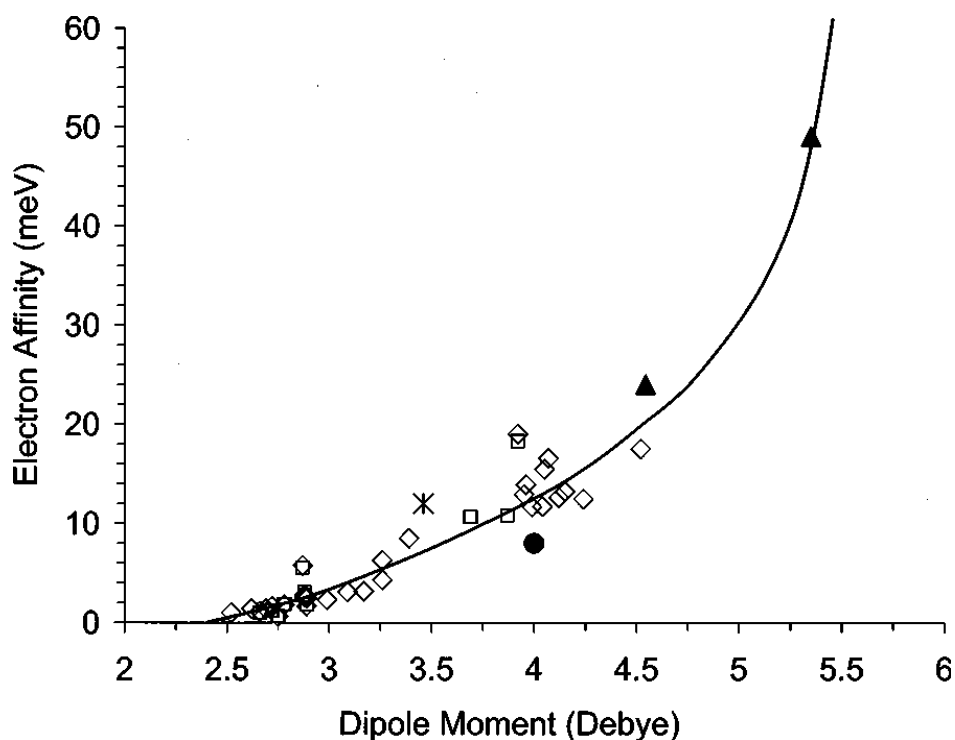


Figure 10. Electron affinities of a number of dipole-bound anions. The various shapes indicate the source of the measurements: squares,³⁵ diamonds,¹⁸ asterisk,¹⁰ circle,⁵³ and triangles (current work).

4.0 NEGATIVE IONS OF ETHYLENE SULFITE

This chapter is partially reproduced from

Robertson, W. D.; Hammer, N. I.; Bartmess, J. E.; Compton, R. N.; Diri, K.; Jordan, K. D.
Journal of Chemical Physics **2005**, *122*.

4.1 ABSTRACT

The formation of negative ions in molecular beams of ethylene sulfite (ES, alternately called glycol sulfite or ethylene glycol, $C_2H_4SO_3$) molecules has been studied using both Rydberg electron transfer (RET) and free electron attachment methods. RET experiments with jet-cooled ES show an unexpected broad profile of anion formation as a function of the effective quantum number (n^*) of the excited rubidium atoms, with peaks at $n_{\max}^* \sim 13.5$ and 16.8. The peak at $n_{\max}^* \sim 16.8$ corresponds to an expected dipole-bound anion with an electron binding energy of 8.5 meV. It is speculated that the peak at $n_{\max}^* \sim 13.5$ derives from the formation of a distorted $C_2H_4SO_3^-$ ion. We suggest that quasifree electron attachment promotes the breaking of one ring bond giving a long-lived acyclic anion and term this process incomplete dissociative electron attachment. Theoretical calculations of plausible ionic structures are presented and discussed. Electron beam studies of ES reveal the presence of multiple dissociative attachment channels, with the dominant fragment, SO_2^- , peaking at 1.3 eV and much weaker signals due to SO_3^- , SO^- ,

and (ES-H)⁻ peaking at 1.5, 1.7, and 0.9 eV, respectively. All of these products appear to originate from a broad temporary negative ion resonance centered at ~1.4 eV

4.2 INTRODUCTION

Many polar molecules possessing a dipole moment above ~2.5 D can form a "dipole-bound" negative ion in which the excess electron occupies a very diffuse molecular orbital in the vicinity of the positive end of the dipole.^{17,35} At the present time the most universal method for the production of these dipole-bound anions involves electron transfer from an atom in a high Rydberg state (Rydberg electron transfer, RET). Provided there are no bound valence anion states for the polar molecule the RET cross section is found to exhibit a maximum over a very narrow range of the effective principal quantum number n^*_{\max} of the Rydberg state.

The observed RET cross section can exhibit additional structure as a function of n^*_{\max} if the molecule exists in more than one conformer⁵⁶ or if it possesses a valence-bound anion state.¹⁰ In the case that a molecule has both dipole-bound and valence-bound anion states, the RET cross section can extend over a much wider range of n^* and the dipole-bound anion can serve as a "doorway state" to the more strongly bound valence anion.¹⁰

In the present contribution we examine anion formation by ethylene sulfite (ES). Both RET and dissociative electron attachment (DEA) measurements are carried out. Although negative ion formation by ES has not been previously reported, there are two reports of negative ion formation by the structurally similar molecule, ethylene carbonate (EC, C₂H₄CO₃),^{21,48} which has been found to exhibit a dipole-bound negative ion state with a rather large electron affinity (EA=49±5 meV) as a result of its sizable dipole moment (μ =5.35 D), but not to have a bound

valence-type anion state. DEA resulting in the fragment ions CO_3^- , and $\text{C}_2\text{O}_2\text{H}_3^-$ in the region of 0.5 to 2.0 eV was attributed to dissociation of a vibrationally excited dipole-bound anion.⁴⁸

The RET measurements on ES show evidence for a dipole-bound anion as well as another anion state which we propose results from an incomplete dissociative electron attachment (i.e., single bond cleavage) process. The DEA studies also provide evidence for dissociative processes leading to SO_3^- , SO_2^- , SO^- , and $(\text{ES-H})^-$. The results are analyzed with the aid of electronic structure calculations.

Ethylene sulfite is used as an electrolyte additive for lithium-ion cells using graphite anodes. Ring opening electron transfer reactions involving ethylene sulfite are invoked in the chemistry involving lithium-ion cell batteries.⁵⁷ Ring opening polycondensation of two cyclic monomers involving ethylene sulfite are also considered in schemes involving new polymer synthesis.⁵⁸ In this study, we are interested in the fundamental interactions of free and quasifree electrons with ethylene sulfite.

4.3 THEORY

The geometries of neutral ES and its anion were optimized at the second order Møller-Plesset (MP2) level using the aug-cc-pVDZ²⁹ and aug-cc-pVDZ+5s5p basis sets, respectively. The +5s5p in the latter basis set denotes the presence of five additional diffuse *s* functions with exponents 1.4656×10^{-2} , 4.5801×10^{-3} , 1.4313×10^{-3} , 4.4727×10^{-4} , 1.3977×10^{-4} and five additional *p* functions with exponents 1.2628×10^{-2} , 3.9463×10^{-3} , 1.2332×10^{-3} , 3.8538×10^{-4} , 1.2043×10^{-4} centered on one of the carbon atoms. These geometries were used to carry out single-point calculations using a larger basis set and at levels of theory up to coupled cluster with single and

double excitations with a perturbative estimate of triple excitations CCSD(T). The larger basis set was constructed by adopting a modified aug-cc-pVTZ²⁹ basis set on the heavy atoms, the aug-cc-pVDZ basis set for the hydrogen atoms, and a *5s5p2d* set of diffuse functions with exponents chosen using a procedure previously suggested by Gutowski,²⁵ and centered on one of the carbon atoms. The modified aug-cc-pVTZ basis set was generated by deleting the *f* functions from the aug-cc-pVTZ basis set. The exponents of the diffuse functions were chosen to be 5.0000×10^{-3} , 1.2500×10^{-3} , 3.1250×10^{-4} , 7.8125×10^{-5} , 1.9531×10^{-5} for the *s*-type functions; 1.0983×10^{-2} , 2.7457×10^{-3} , 6.8641×10^{-4} , 1.7160×10^{-4} , 4.2901×10^{-5} for the *p*-type functions; and 2.7457×10^{-3} , 6.8641×10^{-4} for the *d*-type functions. The electron affinities were calculated at the Koopmans' theorem (KT), Hartree–Fock (HF), MP2, CCSD, and CCSD(T) levels of theory. The calculations were performed using the GAUSSIAN 03⁵⁹ and MOLPRO^{60,61} suites of programs.

4.4 DISCUSSION

Ethylene sulfite is unlike the majority of previously studied molecules that form dipole-bound anions in that its RET profile exhibits two peaks at $n^* = 16.8$ and 13.5 (see Figure 11). Using the data in Figure 11 and Equation 2 the RET peak at $n^* = 16.8$ corresponds to a binding energy of 8.5 meV. It was previously shown that the electron binding energy of molecular dipole-bound anions increases regularly with increasing dipole moment.²¹ When compared to this trend, a binding energy of 8.5 meV is indicative of a molecular dipole moment of ≈ 3.5 D, which agrees reasonably well with the 3.39 D calculated (MP2/aug-cc-pVDZ) dipole moment of ethylene sulfite in its equilibrium geometry.

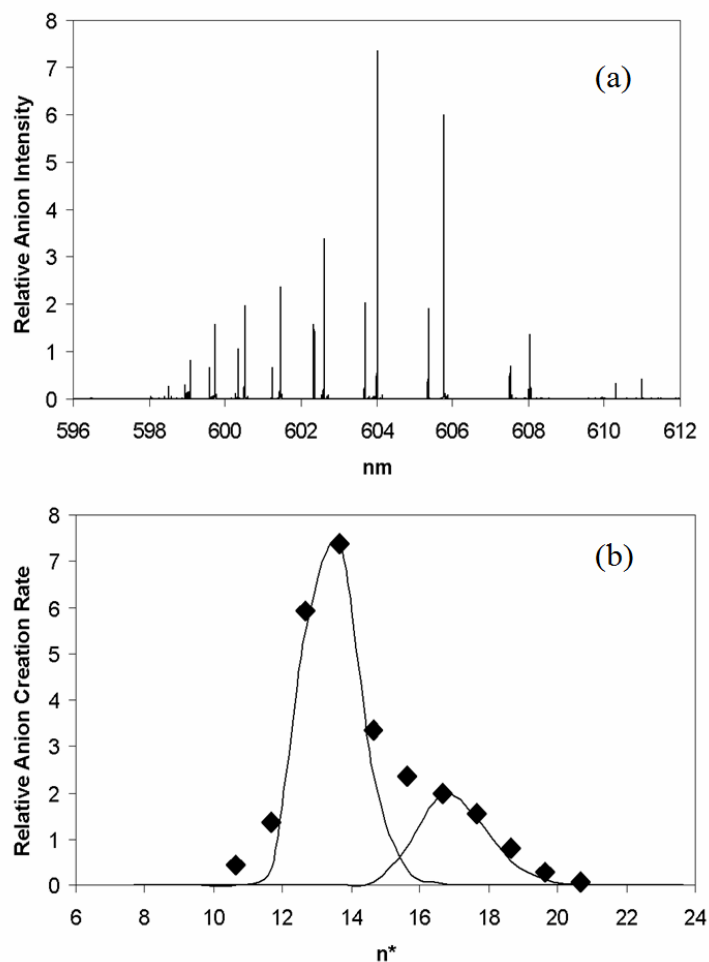


Figure 11. Relative Rydberg electron transfer cross sections as a function of n^* for reactions of Rb^{**} with ES. (a) shows the ion signal as a function of the two-photon excitation wavelength of ns and nd Rydberg states whereas (b) represents the ion signal as a function of the effective quantum number n^* . The solid lines in (b) indicate simulated results using the RET curve crossing model.⁶² The peak at $n^*_{\text{max}} \sim 16.8$ corresponds to the expected dipole-bound anion. The broader feature at $\sim n^*_{\text{max}} \sim 13.5$ is attributed to ring breaking and the formation of a distorted $\text{C}_2\text{H}_4\text{SO}_3^-$ anion.

The calculated vertical electron binding energy at the KT level of theory is 2.72 meV, and the adiabatic electron binding energies at the HF, MP2, CCSD, and CCSD(T) levels are 7.41, 4.37, 6.23, 5.95 meV, respectively. The sizable decrease in the electron binding energy in going

from the HF to the MP2 level is due to the large decrease in the dipole moment of the neutral molecule in going from the HF to the MP2 level (4.02 versus 3.39 D). The electron binding energy obtained at the highest level of theory, 5.95 meV, is about 25% smaller than the experimentally deduced value of 8.5 meV. Similar differences between the calculated and measured electron binding energies were observed in previous studies, and it was speculated that this might be caused by the procedure used in extracting the electron binding energies from RET experiments or by the approximation of treating the triples in the coupled-cluster method perturbatively rather than self-consistently.^{21,63} However, given the small electron binding energy, the agreement between theory and experiment is reasonable.

The second RET peak for ethylene sulfite occurs at $n^* = 13.5$. If this value is substituted into Equation 2, a binding energy of 15.7 meV results. If we assume that the relationship between electron binding energy and dipole moment holds,²¹ a dipole moment of 4.3 D, 0.9 D larger than the calculated (MP2/aug-cc-pVDZ) dipole moment of ES, is deduced. However Equation 2 pertains only to dipole-bound anions, and this suggests that we may be dealing with a valence-bound anion, even though the calculations do not provide evidence for a bound valence-type anion. This suggests the possibility of a stable (or long-lived) valence anion having a geometrical structure very different from the equilibrium geometry of neutral ES. In order to explore this possibility we examined at the MP2/aug-cc-pVDZ level a wide range of distorted structures for ES and its anion. Figure 12 reports the energies and geometrical structures of the stationary points thus identified. ES1 denotes the neutral ethylene sulfite, chosen to be the zero of the energy. ES1⁻ denotes the valence anion, which has a structure similar to ES1 and lies about 0.57 eV above ES1. ES2 is a local minimum of the neutral molecule, lying 3.32 eV above the global minimum. The anion ES2⁻, which was obtained by adding an electron to ES2 (at the same

geometry), lies energetically 0.99 eV above the global minimum of ES, and is much more stable than the neutral at the same geometry, but is found to be a first-order saddle point. Optimizing ES²⁻ to a minimum leads to ES³⁻, which is calculated to lie 0.32 eV below ES1. ES³⁻ has an OCH₂CHOSO structure and thus is derived from ES1 by rupture of one of the SO bonds. Even lower in energy is ES⁴⁻ which resembles a CH₂CH₂O·SO₂⁻ complex. ES³⁻ can dissociate into ethylene oxide + SO₂⁻ products upon cleavage of a CO bond, a near-thermoneutral process. It could also yield the SO⁻ anion upon cleavage of a second SO bond, but that bond is more than 1 eV endothermic, even with further cleavage of the organic fragment to two formaldehyde molecules. ES⁴⁻ can dissociate to either CH₂CH₂O (ethylene oxide) + SO₂⁻ or CH₂CH₂ + SO₃⁻ depending on which bond is broken. Both of these product channels are at roughly the same energy as ES⁴⁻ and a few tenths of an eV below ES1. The potential energy surfaces for the ES1→ES2 and ES1⁻→ES2⁻ transformations cross at about 1.3 eV, which corresponds closely to the positions of the peaks for forming SO₂⁻ and SO₃⁻ *via* DEA, suggesting that this crossing point is the key to the observed DA processes.

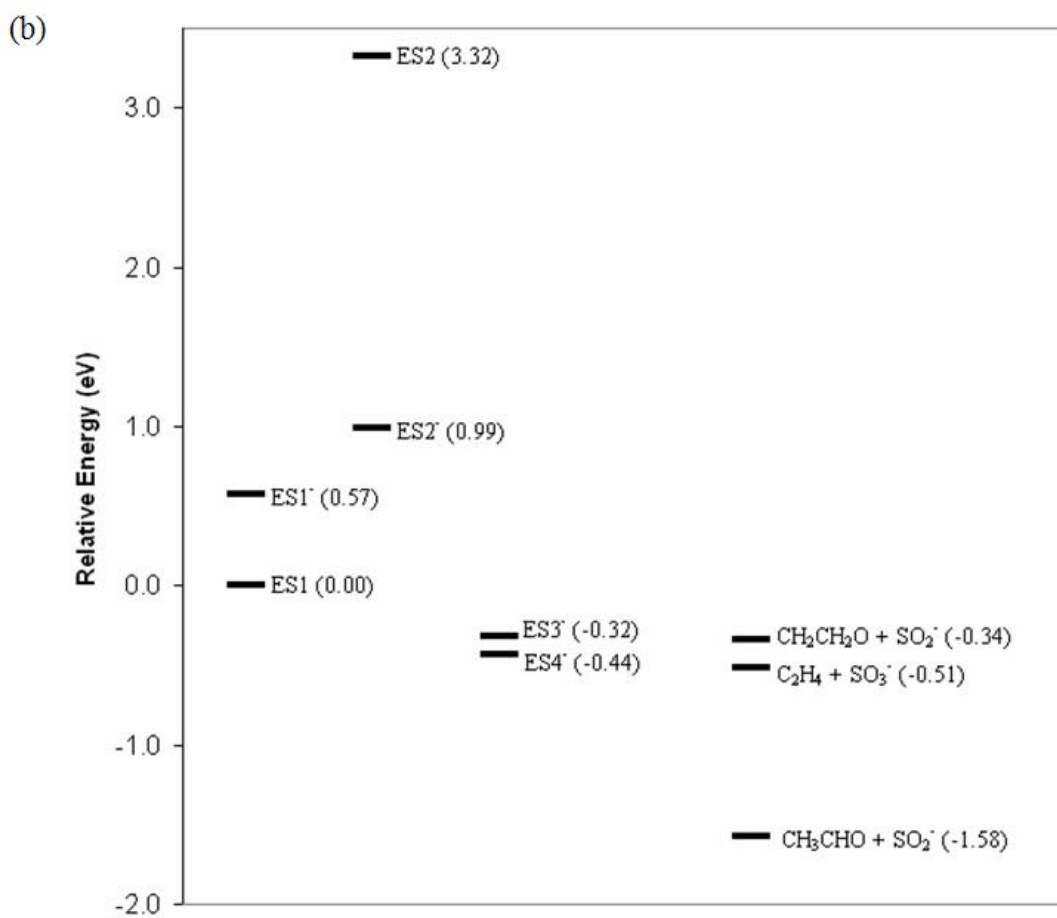
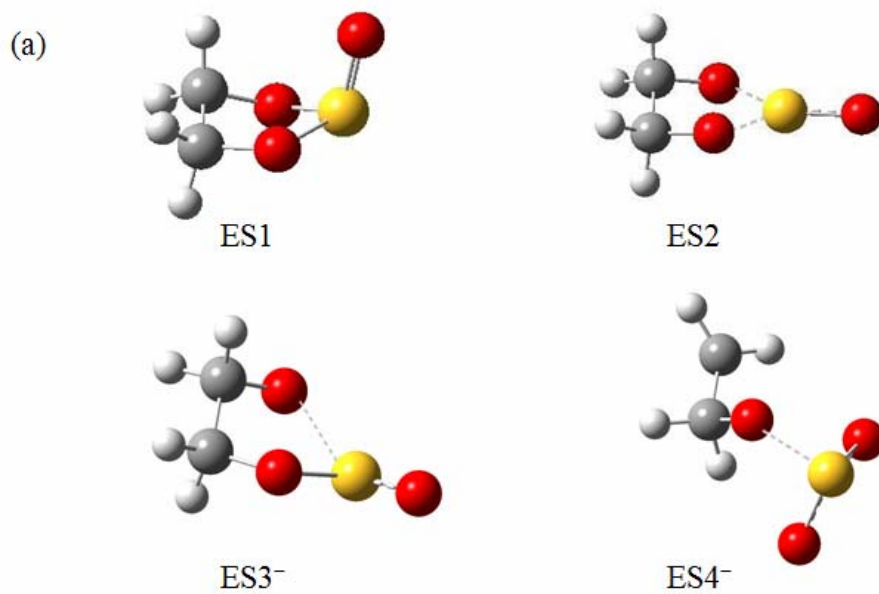


Figure 12. (a) Structures and (b) their relative energies (in parentheses) compared to the neutral ethylene sulfite (ES1 in this figure). Energies have been corrected for vibrational zero-point energy.

In other cases of RET to valence-type anions, e.g., nitromethane, the RET occurs over a very wide range of n^* . However the peak near $n^*=13.5$ for ES is quite narrow, which indicates that the anion results from only a narrow range of initial electron energies. A possible explanation for this behavior comes from previous studies of RET in the hydrogen iodide molecule.⁶⁴ RET in HI shows the I^- ion over a broad region of n , however, for $n<13$ the HI^- ion is also observed. HI^- is predicted to have a bound state at large inter-nuclear separation⁶⁵ and prompted Carman⁶⁴ to suggest that the RET forms HI^- in extended bond length. We propose therefore that part of the anion signal observed in the RET experiments on ES is due to highly distorted long-lived ES^- molecules, specifically, $ES3^-$ and $ES4^-$. The absence of a second RET peak in the case of ethylene carbonate is apparently the consequence of the lack of accessible highly distorted anion.

Since these experiments were carried out under seeded nozzle-jet expansion conditions one might ask if the second unexplained peak could result from the presence of dimer molecules in the beam. Although there were no signals corresponding to that of the dimer mass, the dipole-bound anion could result from dissociative attachment of the dimer leading to a monomer dipole-bound anion. In order to consider this possibility further, the dipole moments of two possible dimer configurations were calculated. The linear dimer is found to possess a dipole moment of 7.9 D. However, the dimer in which the monomer dipoles are opposed (i.e., with no net dipole moment) is over 3 kcal/mol more stable. These calculations indicate that dimers are not responsible for the second peak in this case, however, a complete search for all of the possible dimer structures was not carried out.

The results of the DEA experiments are displayed in Figure 13 and Figure 14. Figure 13 shows the relative dissociative electron attachment cross sections for the ions observed from ES. Electron attachment to form SF_6^- is also shown for comparison. The SO_2^- ion is by far the most

predominant ion formed from electron attachment to ES, although SO_3^- , SO^- , and $(\text{ES-H})^-$ are also formed in much smaller quantities. Shown in Figure 14 are the SO_2^- ions formed from DEA to ES using the trochoidal electron monochromator (TEM). SF_6^- is again shown for comparison. The higher resolution afforded by the TEM is evidenced by the narrower peak exhibited by SF_6^- . Additional structure (possibly due to partially resolved vibrational states) at higher energy can also be seen in SO_2^- using the TEM mode.

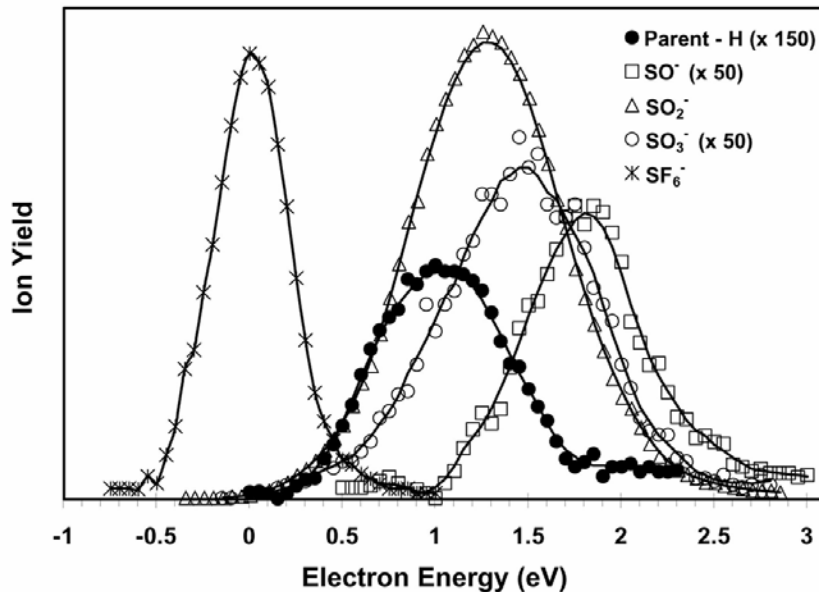


Figure 13. Relative dissociative electron attachment cross sections for the ions created from electron attachment to ES. SF_6^- is included as a reference.

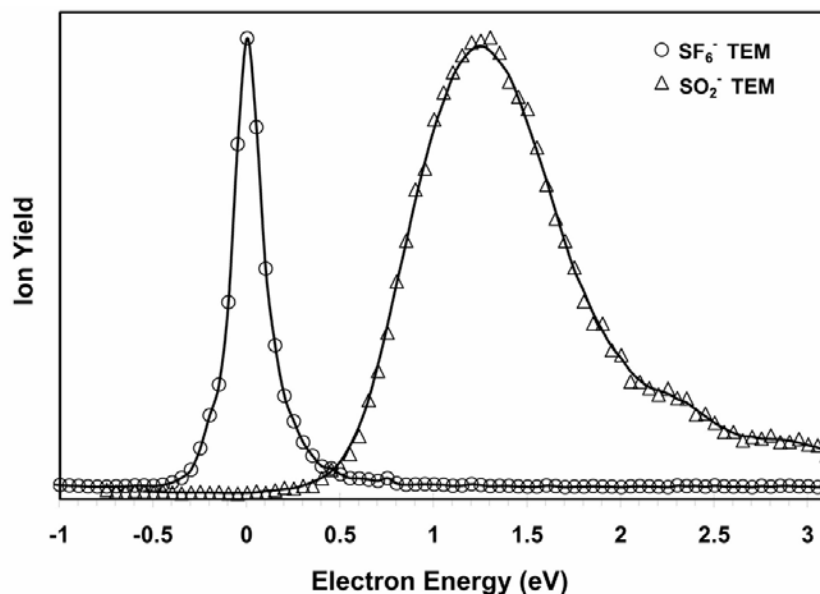


Figure 14. Relative dissociative electron attachment cross sections for SO_2^- ions created from electron attachment to ES using a TEM. SF_6^- is included as a reference.

4.5 CONCLUSIONS

RET and DEA measurements have been used to study anion formation in ethylene sulfite. The RET measurements provide evidence for two anion formation processes, one leading to a dipole-bound anion and the other to the formation of one or more highly distorted valence-type anions. The DEA measurements reveal that the main dissociative process leads to SO_2^- . Formation of SO_3^- , SO^- , and $(\text{ES-H})^-$ is also observed, but these channels are much less important than SO_2^- formation. Electronic structure calculations provide evidence for two stable valence-type $\text{C}_2\text{H}_4\text{SO}_3^-$ anions each of which results from cleavage of one bond of ES^- . Upon breaking of a second bond these isomers can give rise to the SO_2^- , SO_3^- , or SO^- ions. The $\text{C}_2\text{H}_4\text{SO}_3^-$ valence-

type anions are believed to be responsible for the second ($n^*=13.5$) peak seen in the RET measurements.

Finally, these results suggest a potentially important contribution to our general understanding of electron attachment to molecules. It is generally accepted that electron attachment to a molecule occurs through one of four possible mechanisms: (1) shape resonance, (2) electronically excited Feshbach resonance, (3) nuclear excited Feshbach resonance, or (4) radiative attachment. The resonance processes can also lead to dissociation of the transient anion into fragment anions (DEA) depending upon the lifetime of the intermediate resonance state as well as the energetics involved. The lifetime of nuclear excited Feshbach resonances depends upon the number of degrees of freedom, electron affinity, and total internal energy of the anion upon formation as well as the phase space available for decay (i.e., electron energy of the autodetaching electron and the density of rovibrational states in the resulting neutral).⁶⁶ These lifetimes have been measured to be greater than milliseconds for large molecules. Electron attachment processes in which there is partial bond breakage (i.e., distonic anion formation) can lead to very long lifetimes that will require a modification of the simple detailed balance argument employed previously to describe such nuclear excited Feshbach resonances.⁶⁶ In the case studied here the free electron attachment promotes the breaking of one ring bond giving an acyclic anion. Autodetachment would occur when the broken bond is reformed which may be a significant time period. We choose to call this process incomplete dissociative electron attachment (IDEA).

Incomplete dissociative electron attachment leading to an anion with the parent ion mass was not detected under free electron attachment conditions. A likely explanation for this observation is that the slow collision provided by the RET process and the positive Rb^+ ion plays

a role in the formation process. Citing again the case of RET between Rydberg atoms and HI resulting in the formation of greatly extended HI^- ions: the collision ion pair provides the stabilizing body leaving the stable HI^- ion with large internuclear separation.⁶⁴ Such stabilization may not be necessary for large molecules. Such an extreme but interesting and important example of IDEA for a large molecule has been discussed previously. The group of Sanche⁶⁷ have recently reported single strand breaks in the DNA super molecule which are believed to be induced by low energy (0–4 eV) electrons. These authors argue that such "partial" dissociation occurs through negative ion shape resonances. Further theoretical considerations may provide evidence for other such cases.

Acknowledgment

This research was carried out with the support of the National Science Foundation.

**PART II: VIBRATIONAL SPECTRA AND ENERGETICS OF SMALL WATER
CLUSTERS**

5.0 INTRODUCTION

Water clusters have attracted the attention of many experimental and theoretical groups especially after the development of brilliant experimental techniques allowing for the creation, and mass selection of both neutral and anionic molecular clusters. The interest in those species has been boosted further by the fact that nowadays, accurate vibrational spectra can be obtained, giving us valuable structural information.

Molecular clusters are the bridges between single molecules for which very accurate quantum mechanical calculations are possible and the bulk phase of matter which currently can only be treated with classical or semi-classical models, inevitably bringing together lots of approximations. Neutral water clusters are important in our quest for understanding the behavior of bulk water, which is one of the most fundamental and crucial substances affecting living organisms. There is a tremendous amount of work done and being done on water clusters, aiming to enhance our knowledge of the solvation phenomenon which is not only an important aspect of laboratory experiments, but is also a vital biological process. Negatively charged water clusters on the other hand are important tools for studying electron solvation, a phenomenon that was discovered more than a century ago and is still waiting for complete explanation. Electron transfer through water (maybe even water clusters) embedded in the pockets of proteins is another vital process that can be studied more accurately with smaller model systems, i.e. water clusters. The following chapters investigate structural, energetic, and spectroscopic features of small neutral and anionic water clusters.

6.0 THE ROLE OF ANHARMONICITY AND HIGH-ORDER ELECTRON CORRELATION EFFECTS ON THE VIBRATIONAL FREQUENCIES OF WATER CLUSTERS

6.1 INTRODUCTION

Infrared spectroscopy has proven to be especially valuable tool for elucidating the structure of H-bonded clusters.⁶⁸⁻⁸² In general, assignments have been made based on comparison of the measured spectra with spectra calculated in the harmonic approximation.⁸³⁻⁹⁰ However, such an approach may be inadequate in the case that anharmonic corrections to the frequencies are large.⁹¹⁻⁹³ A further complication, which appears not to be as widely appreciated, is that the electronic structure methods generally employed - DFT or MP2 - tend to give H-bonded OH stretch frequencies that are too red-shifted,⁹⁴ even after correcting the frequencies by the usual scaling factors.

In the present work the anharmonic frequencies for $(\text{H}_2\text{O})_n$, $n = 1-6$, are calculated at the Becke3LYP⁹⁵ (for $n = 1-6$) and at the MP2 (for $n = 1-5$) levels of theory. For the $n = 3-5$ clusters, only the cyclic structures, believed to correspond to the global potential energy minima are considered, while for the $(\text{H}_2\text{O})_6$ cluster, four low-energy isomers are studied. The anharmonicity corrections to the harmonic frequencies are calculated using second-order vibrational perturbation theory (VPT2).⁹⁶⁻¹⁰¹ This approach requires the cubic and a subset of the

quartic force constants, that can be readily evaluated on a fast single-processor computer at the MP2 level of theory for clusters up to about $(\text{H}_2\text{O})_5$ in size and at the DFT level for clusters up to about $(\text{H}_2\text{O})_7$ in size when employing the aug-cc-pVDZ basis set.²⁹ The effect of higher-order electron correlation on the harmonic frequencies is examined by means of QCISD¹⁰² calculations for the $n = 1-4$ clusters.

The vibrational zero-point energies from these calculations were reported before.⁹⁴ Here we focus on the individual vibrational frequencies with an emphasis on anharmonicity shifts.

6.2 METHODOLOGY

For each cluster of interest the geometry was first optimized at the Becke3LYP (or MP2) level of theory using tight convergence criteria. The resulting optimized geometries were used in the subsequent evaluation of the harmonic force field and the calculation of the third and fourth derivatives of the energies with respect to displacements of the atoms along the normal modes. The anharmonicity corrections were calculated using the VPT2 approach as implemented by Barone¹⁰³ in the Gaussian 03 package.⁵⁹ In the Becke3LYP calculations, the “ultrafine” grid (*i.e.*, 99 radial shells, 590 angular points per shell) was employed to minimize numerical errors.

For the water monomer, the calculations were performed with each of the aug-cc-pVNZ basis sets,²⁹ where $N = (\text{D}, \text{T}, \text{Q}, \text{and } 5)$, while for the dimer the largest basis set employed was aug-cc-pVQZ, permitting us to determine the sensitivity of the harmonic and anharmonic frequencies to the flexibility of the atomic basis set. For the water trimer, basis sets as large as aug-cc-pVTZ were employed, while for the larger clusters, only the aug-cc-pVDZ basis set was used.

6.3 RESULTS

Table 5 through Table 9 summarize the calculated frequencies and the anharmonic corrections to the harmonic fundamentals of $(\text{H}_2\text{O})_n$, $n = 1-5$, at the various levels of theory (See Appendix B for the $(\text{H}_2\text{O})_6$ results). Where available, the experimental anharmonic frequencies are included for comparison. Table 10 examines the contribution of high-order electron correlation effects to the harmonic vibrational frequencies, and Table 11 reports the changes in the OO distances associated with averaging over the vibrational zero-point levels.

Table 5. Calculated vibrational frequencies of H_2O^a

| | HARMONIC | | | | | | | | Expt. ^b |
|---|-------------------------|-------|-------|-------|-------|-------|-------|-------|--------------------|
| | MP2 | | | | B3LYP | | | | |
| | aVDZ | aVTZ | aVQZ | aV5Z | aVDZ | aVTZ | aVQZ | aV5Z | |
| 1 | 3938 | 3948 | 3966 | 3969 | 3904 | 3899 | 3906 | 3909 | |
| 2 | 3803 | 3822 | 3840 | 3843 | 3795 | 3797 | 3805 | 3807 | |
| 3 | 1622 | 1628 | 1632 | 1632 | 1619 | 1627 | 1629 | 1629 | |
| | ANHARMONIC ^c | | | | | | | | |
| 1 | 3744 | 3767 | 3781 | 3784 | 3713 | 3715 | 3721 | 3722 | 3756 |
| | (194) | (181) | (185) | (185) | (191) | (184) | (185) | (187) | |
| 2 | 3621 | 3653 | 3667 | 3669 | 3615 | 3626 | 3632 | 3634 | 3657 |
| | (182) | (169) | (173) | (174) | (180) | (171) | (173) | (173) | |
| 3 | 1573 | 1578 | 1580 | 1579 | 1567 | 1574 | 1576 | 1576 | 1595 |
| | (49) | (50) | (52) | (53) | (52) | (53) | (53) | (53) | |

^a aVDZ, aVTZ, aVQZ, and aV5Z denote the aug-cc-pVDZ, aug-cc-pVTZ, aug-cc-pVQZ, and aug-cc-pV5Z basis sets, respectively. ^b From Ref. 76. ^c Anharmonicity corrections are given in parentheses.

Table 6. Calculated anharmonic vibrational frequencies^a of (H₂O)₂^b

| | MP2 | | | B3LYP | | | Expt. |
|----|------------|------------|-------------------|------------|------------|------------|---------------------|
| | aVDZ | aVTZ | aVQZ ^c | aVDZ | aVTZ | aVQZ | |
| 1 | 3737 (188) | 3753 (182) | (186) | 3710 (185) | 3711 (179) | 3718 (179) | 3745 ^d |
| 2 | 3722 (182) | 3745 (170) | (173) | 3696 (178) | 3697 (173) | 3705 (173) | 3735 ^e |
| 3 | 3615 (181) | 3648 (166) | (171) | 3617 (172) | 3627 (164) | 3634 (165) | 3660±5 ^e |
| 4 | 3554 (150) | 3583 (136) | (142) | 3531 (141) | 3542 (133) | 3548 (138) | 3601 ^e |
| 5 | 1592 (51) | 1595 (55) | (56) | 1585 (52) | 1592 (55) | 1595 (54) | 1611 ^f |
| 6 | 1580 (44) | 1585 (44) | (47) | 1576 (41) | 1583 (45) | 1586 (44) | 1593 ^f |
| 7 | 505 (134) | 502 (128) | (118) | 507 (127) | 499 (126) | 506 (118) | 520 ^g |
| 8 | 309 (49) | 310 (50) | (52) | 322 (38) | 287 (75) | 306 (54) | 290 ^f |
| 9 | 148 (36) | 138 (46) | (44) | 137 (47) | 117 (70) | 144 (43) | 108 ^h |
| 10 | 106 (45) | 114 (41) | (47) | 132 (25) | 102 (55) | 124 (33) | 103 ^h |
| 11 | 112 (36) | 113 (34) | (36) | 103 (53) | 117 (38) | 145 (10) | 103 ^h |
| 12 | 60 (67) | 60 (67) | (62) | 69 (61) | 37 (93) | 79 (50) | 87 ^h |

^a Anharmonicity corrections are given in parentheses. ^b aVDZ and aVTZ denote the aug-cc-pVDZ and aug-cc-pVTZ basis sets, respectively. ^c Compiled from Ref. 104. ^d Reference 105. ^e Reference 76. ^f In Ar matrix, Ref. 106. ^g In N₂ matrix, Ref. 106. ^h Reference 107.

Table 7. Calculated anharmonic vibrational frequencies^a of (H₂O)₃^b

| | MP2 | | B3LYP | | | |
|----|------|-------|-------|-------|------|-------|
| | aVDZ | | aVDZ | | aVTZ | |
| 1 | 3710 | (186) | 3690 | (180) | 3689 | (178) |
| 2 | 3707 | (187) | 3680 | (189) | 3687 | (179) |
| 3 | 3701 | (189) | 3684 | (181) | 3687 | (175) |
| 4 | 3475 | (166) | 3438 | (155) | 3452 | (147) |
| 5 | 3464 | (169) | 3424 | (159) | 3440 | (149) |
| 6 | 3419 | (156) | 3378 | (142) | 3395 | (132) |
| 7 | 1589 | (69) | 1590 | (58) | 1595 | (66) |
| 8 | 1592 | (42) | 1587 | (40) | 1595 | (44) |
| 9 | 1591 | (40) | 1581 | (43) | 1589 | (47) |
| 10 | 731 | (127) | 755 | (125) | 727 | (148) |
| 11 | 557 | (106) | 580 | (97) | 585 | (87) |
| 12 | 398 | (170) | 441 | (147) | 476 | (108) |
| 13 | 358 | (83) | 385 | (71) | 386 | (69) |
| 14 | 297 | (52) | 312 | (52) | 294 | (73) |
| 15 | 272 | (68) | 286 | (67) | 292 | (63) |
| 16 | 161 | (72) | 193 | (48) | 197 | (52) |
| 17 | 187 | (30) | 184 | (32) | 182 | (33) |
| 18 | 156 | (36) | 150 | (48) | 155 | (53) |
| 19 | 154 | (30) | 155 | (32) | 144 | (50) |
| 20 | 128 | (44) | 139 | (41) | 154 | (28) |
| 21 | 88 | (68) | 135 | (34) | 147 | (29) |

^a Anharmonicity corrections are given in parentheses; aVDZ and aVTZ denote the aug-cc-pVDZ and aug-cc-pVTZ basis sets, respectively. ^b Experimentally observed frequencies (in cm⁻¹): 3725 (free OH stretch), 3530 (bonded OH stretch), 1608, 569, 311, 170, 151, in Ne matrix.⁸²

Table 8. Calculated vibrational frequencies^a of (H₂O)₄^b

| | MP2 | | B3LYP | |
|--------|------|-------|-------|-------|
| 1 | 3693 | (193) | 3675 | (190) |
| 2, 3 | 3694 | (191) | 3680 | (184) |
| 4 | 3692 | (192) | 3674 | (189) |
| 5 | 3349 | (175) | 3287 | (173) |
| 6,7 | 3316 | (170) | 3255 | (166) |
| 8 | 3265 | (131) | 3147 | (173) |
| 9 | 1630 | (51) | 1619 | (53) |
| 10, 11 | 1616 | (35) | 1614 | (28) |
| 12 | 1595 | (41) | 1567 | (59) |
| 13 | 833 | (157) | 856 | (145) |
| 14, 15 | 718 | (101) | 739 | (96) |
| 16 | 695 | (53) | 717 | (48) |
| 17 | 411 | (37) | 406 | (56) |
| 18 | 411 | (37) | 407 | (54) |
| 19 | 383 | (48) | 396 | (51) |
| 20 | 344 | (56) | 352 | (59) |
| 21 | 242 | (46) | 247 | (51) |
| 22 | 232 | (27) | 237 | (25) |
| 23 | 221 | (31) | 219 | (37) |
| 24 | 221 | (31) | 221 | (35) |
| 25 | 200 | (35) | 209 | (36) |
| 26 | 200 | (35) | 210 | (35) |
| 27 | 184 | (25) | 187 | (29) |
| 28 | 180 | (19) | 185 | (26) |
| 29 | 71 | (8) | 80 | (7) |
| 30 | 45 | (5) | 50 | (3) |

^a Anharmonicity corrections are given in parentheses; all results were obtained with the aug-cc-pVDZ basis set. ^b Experimentally observed frequencies (in cm⁻¹): 3714 cm⁻¹ (free OH stretch), 3416 cm⁻¹ (bonded OH stretch), from Ref. 76; 690, 669, 222, 216, from Ref. 82.

Table 9. Calculated vibrational frequencies^a of (H₂O)₅^b

| | MP2 | | B3LYP | |
|----|------|-------|-------|-------|
| 1 | 3701 | (187) | 3679 | (191) |
| 2 | 3698 | (189) | 3690 | (178) |
| 3 | 3696 | (191) | 3692 | (174) |
| 4 | 3687 | (198) | 3683 | (181) |
| 5 | 3691 | (191) | 3684 | (179) |
| 6 | 3324 | (170) | 3259 | (167) |
| 7 | 3313 | (173) | 3246 | (172) |
| 8 | 3282 | (160) | 3258 | (111) |
| 9 | 3275 | (159) | 3228 | (133) |
| 10 | 3168 | (186) | 3048 | (221) |
| 11 | 1634 | (55) | 1629 | (52) |
| 12 | 1627 | (54) | 1617 | (54) |
| 13 | 1617 | (43) | 1599 | (53) |
| 14 | 1582 | (70) | 1595 | (46) |
| 15 | 1581 | (59) | 1585 | (44) |
| 16 | 846 | (138) | 874 | (120) |
| 17 | 767 | (114) | 791 | (104) |
| 18 | 746 | (120) | 759 | (115) |
| 19 | 715 | (72) | 747 | (56) |
| 20 | 694 | (27) | 687 | (45) |
| 21 | 470 | (43) | 476 | (59) |
| 22 | 378 | (89) | 437 | (42) |
| 23 | 419 | (34) | 421 | (45) |
| 24 | 372 | (57) | 395 | (46) |
| 25 | 365 | (45) | 399 | (28) |
| 26 | 265 | (37) | 275 | (33) |
| 27 | 255 | (44) | 271 | (33) |
| 28 | 247 | (49) | 248 | (53) |
| 29 | 210 | (56) | 206 | (63) |
| 30 | 204 | (36) | 216 | (28) |
| 31 | 204 | (32) | 215 | (26) |
| 32 | 160 | (68) | 161 | (71) |
| 33 | 124 | (76) | 128 | (75) |
| 34 | 122 | (71) | 101 | (91) |
| 35 | 157 | (24) | 162 | (21) |
| 36 | 42 | (23) | 59 | (14) |
| 37 | 48 | (14) | 58 | (11) |
| 38 | 29 | (13) | 43 | (2) |
| 39 | 7 | (17) | -4 | (30) |

^a Anharmonicity corrections are given in parentheses; all results were obtained with the aug-cc-pVDZ basis set. ^b Experimentally observed frequencies: 3714 cm⁻¹ (free OH stretch), 3360 cm⁻¹ (bonded OH stretch).⁷⁶

Table 10. Contributions of anharmonicity and higher-order correlation corrections to the frequency shifts^a (cm⁻¹) of the single-donor OH stretch vibrations of the (H₂O)_n, n = 2–4, clusters^b

| Cluster ^c | aug-cc-pVDZ | | | Est. ^d | Expt. ^e |
|----------------------|-------------|------------|-----------------|-------------------|--------------------|
| | MP2 Harm | MP2 Anharm | QCISD Harm | | |
| W ₂ | -167 | -129 | -121 (-130) | -83 | -106 |
| W ₃ | -230 | -208 | -167 (-176) | -145 | -174 |
| | -238 | -219 | -174 (-183) | -155 | |
| | -296 | -264 | -217 (-233) | -185 | |
| W ₄ | -347 | -334 | -253 (-265) | -240 | -291 |
| | -385[2] | -367 [2] | -281 (-297) [2] | -263 [2] | |
| | -475 | -418 | -350 (-372) | -293 | |

^a The shifts are with respect to the average of the two stretching frequencies of the water monomer. ^b Numbers in parentheses are from MP2 calculations using the QCISD geometry. ^c W₂, W₃, and W₄ stand for the water dimer, trimer, and tetramer, respectively. ^d The estimated frequency shifts were obtained using the aug-cc-pVDZ basis set and the following assumption : shift (Est.) = shift (MP2-Anharm) + shift (QCISD-Harm) – shift (MP2-Harm). ^e From Ref. 76.

Table 11. Changes in the OO distances (Å) of the (H₂O)_n, n = 2–6, clusters due to vibrational averaging (ΔR_{OO})^a

| | | | | | | | | | |
|----------------------------------------|------|------|------|------|------|------|------|------|------|
| (H ₂ O) ₂ | .059 | | | | | | | | |
| (H ₂ O) ₃ | .046 | .046 | .047 | | | | | | |
| (H ₂ O) ₄ | .030 | .030 | .030 | .030 | | | | | |
| (H ₂ O) ₅ | .027 | .028 | .026 | .026 | .023 | | | | |
| (H ₂ O) ₆ -chair | .019 | .019 | .019 | .019 | .019 | .019 | | | |
| (H ₂ O) ₆ -book | .062 | .032 | .023 | .030 | .019 | .028 | .019 | | |
| (H ₂ O) ₆ -cage | .022 | .025 | .023 | .026 | .032 | .050 | .084 | .059 | |
| (H ₂ O) ₆ -prism | .020 | .035 | .036 | .018 | .051 | .045 | .020 | .142 | .102 |

^a Results obtained at MP2/aug-cc-pVDZ level for (H₂O)_n, n = 2–5 and Becke3LYP/aug-cc-pVDZ level for n = 6.

For the clusters up to the pentamer in size, the anharmonicity corrections to the frequencies were calculated using both the MP2 and Becke3LYP electronic structure methods.

Overall the anharmonic corrections calculated using these two approaches are quite close. The largest difference is 49 cm^{-1} , which occurs for the anharmonic correction associated with one of the single-donor OH stretch vibrations of $(\text{H}_2\text{O})_5$. Similarly, the corrections for the lowest frequency single-donor OH stretching vibrations of $(\text{H}_2\text{O})_4$ differ by 42 cm^{-1} with the two methods. This discrepancy appears to be due to a limitation of the procedure for dealing with the occurrence of nearly degenerate zeroth-order fundamentals and combination states (*e.g.*, Fermi-resonances). Nevertheless, for the majority of the stretching and bending modes that are generally those characterized in jet experiments, the difference between the anharmonicity corrections obtained using MP2 and Becke3LYP are quite small.

The calculations on the water monomer and dimer reveal that the anharmonic corrections to the frequencies are also relatively insensitive to the basis set employed in most cases. For the OH stretch vibrations the MP2 anharmonicity corrections change by up to 10 cm^{-1} as the basis set is enlarged. However, since these changes are relatively small compared to the total anharmonic corrections for these modes and since they are similar in the monomer, it appears to be justified to use the aug-cc-pVDZ basis set for calculating the anharmonicity corrections to the frequencies of the larger clusters. In addition, in the water monomer case, the anharmonicity corrections from the aug-cc-pVQZ basis set fall in between the corrections from the aug-cc-pVDZ and aug-cc-pVTZ basis sets (Table 5), suggesting that the series probably converges in that range, which gives us even more confidence in using only the aug-cc-pVDZ basis set for calculating the frequency shifts in the larger water clusters. The case is similar with the water dimer OH stretch vibrations, where again the anharmonicity corrections from the aug-cc-pVQZ basis set fall in between the results from aug-cc-pVDZ and the aug-cc-pVTZ basis sets.

We note however, that in the Becke3LYP results for the water dimer, although there is a good agreement between the anharmonicity corrections for the bending mode frequencies between the smaller two basis sets, and slightly better agreement (compared to the corresponding MP2 results) in the corrections to the OH stretching frequencies, the difference in the anharmonicity corrections for the lowest five intermolecular frequencies range from 15 to 37 cm^{-1} . In DFT methods, the grid used in the numerical quadrature introduces an additional error besides the errors due to problems related to the convergence of SCF and due to the coupling between the modes. As a result, for low-frequency modes exploring flat potential energy surfaces, this may lead to a greater basis set sensitivity of the Becke3LYP method in the numerical evaluations of the cubic and quartic force constants. This problem is apparent in the case of the water pentamer cluster (Table 9), where there is a very good agreement between the harmonic frequencies obtained with the MP2 and the Becke3LYP methods for the lowest frequency normal mode, whereas the latter method yields a negative value for the anharmonic frequency (-4 cm^{-1}). However the magnitude of this imaginary frequency can be considered to be practically zero (the corresponding MP2 value is 7 cm^{-1}) and is not a major point of concern for the reliability of the method or a significant source of error in the anharmonicity corrections to the zero-point energies. Similarly, we obtain one small imaginary anharmonic frequency for the prism isomer of the water hexamer cluster (See Appendix B). Different step-size in the numerical evaluation of the cubic and quartic force constants in the DFT calculations may be needed for such low-frequency modes. (The step-size used in this work was the program's default step-size of 0.025 \AA .) Nevertheless, Becke3LYP seems to be a promising tool for interpreting spectra of larger water clusters since - as mentioned above - the experiments on these, usually probe the OH stretching and the HOH bending frequency regions.

The calculations, both MP2 and Becke3LYP, including anharmonicity corrections, tend to underestimate H-bonded OH stretching frequencies, as compared to experiment. This is actually a consequence of the tendency of the Becke3LYP and MP2 procedures to underestimate the OO distances between H-bonded water molecules and to overestimate the elongation of the associated OH bonds, which leads to overestimated red shifts of the H-bonded OH stretch vibrations in both the harmonic and anharmonic approximations, compared to those that would be obtained upon inclusion of high-order electron correlation effects.

Table 10 reports the shifts in the harmonic frequencies of the single-donor OH stretch vibrations of the $(\text{H}_2\text{O})_n$, $n = 2-4$, clusters as calculated in the MP2 and QCISD approximations. The shifts are reported relative to the mean of the symmetric and asymmetric stretch vibrations of the water monomer at the same level of theory. The redshifts of the single-donor OH stretch vibrations calculated using the QCISD method are smaller than the corresponding MP2 values by 46 cm^{-1} in $(\text{H}_2\text{O})_2$, 63 to 79 cm^{-1} in $(\text{H}_2\text{O})_3$, and 94 to 125 cm^{-1} in $(\text{H}_2\text{O})_4$. Thus, not only there is a tendency of the MP2 and Becke3LYP methods to exaggerate the redshifts of the frequencies associated with the H-bonded OH groups, but also the errors tend to grow as the hydrogen-bonded network becomes more extended.

As mentioned above, the differences between the MP2 and the QCISD values of the OH stretch frequencies are primarily due to the differences in the geometries obtained with these two methods. Indeed, the harmonic OH stretch frequencies calculated at the MP2 level using QCISD geometries are nearly identical to those calculated using the QCISD method together with QCISD geometries (see Table 10).

Table 10 also reports the frequency shifts for the single-donor OH stretch vibrations obtained by assuming that the contributions of high-order electron correlation effects to the

harmonic frequencies and of vibrational anharmonicity calculated at the MP2 level are additive (the “*Est.*” column). This approach gives shifts (and vibrational frequencies) in close agreement with those measured experimentally. Finally, the results summarized in Table 10 suggest that, the effects of high-order electron correlation and anharmonicity on the frequencies of H-bonded OH groups can, to a good approximation, be accounted for by reducing the harmonic frequency shifts obtained at the MP2 level by about 37%. This scaling was tested only on the (H₂O)₂- (H₂O)₄ clusters, where all H-bonded OH groups are associated with single-donor water molecules. It is possible that a different scaling factor would be required for the frequencies of vibrations associated with double-donor water molecules.

In the cyclic water clusters, the average OO distances between H-bonded water molecules decrease with increasing cluster size as a result of the increasing importance of the induction interactions.⁷² In Table 11 we report the changes in the OO distances (ΔR_{OO}) of adjacent oxygen atoms resulting from vibrational averaging. These ΔR_{OO} values also tend to get smaller with increasing size of the cyclic clusters. However for the cage, prism and book isomers of the water hexamer, the average ΔR_{OO} values are much larger than that (0.019 Å) of the chair isomer, with individual ΔR_{OO} values being as large as 0.142 Å. In all cases the large ΔR_{OO} values are associated with double-donor water molecules. This is also true for the book isomer, where the only ΔR_{OO} value (*i.e.* 0.062 Å) that is much larger than all others in that cluster, involves an oxygen atom in a double-donor water molecule.

6.4 CONCLUSIONS

The harmonic and anharmonic frequencies of water clusters up through the hexamer in size have been calculated perturbatively using the Becke3LYP and the MP2 electronic structure methods.

By focusing on the frequency shifts, which enables one to “isolate” the changes induced by the H-bonding environment, it is seen that both inclusion of anharmonicity corrections and the inclusion of high-order electron correlation effects lead to decreases in the redshifts of the OH stretch vibrations of donor OH groups, with the latter being more important. The shifts obtained by assuming that these two corrections are additive, are close to those deduced from experimental vibrational spectra. Further, to a good approximation, the effects of high-order correlation and anharmonicity on the OH stretch frequencies associated with H-bonded OH groups can be estimated by reducing the MP2-level frequencies by 37%.

The present study demonstrates that it may be possible to obtain MP2-quality anharmonicity corrections for the OH stretching and HOH bending frequencies of small water clusters, using much less computationally demanding DFT methods and not so large basis sets (such as aug-cc-pVDZ). These, combined with harmonic frequencies from methods including higher order electron correlation effects (such as QCISD), result in fairly accurate estimates of the experimental vibrational frequencies of such systems.

7.0 ON THE CONTRIBUTION OF VIBRATIONAL ANHARMONICITY TO THE BINDING ENERGIES OF WATER CLUSTERS

This work was published as

Diri, K.; Myshakin, E. M.; Jordan, K. D. *J. Phys. Chem. A* **2005**, *109*, 4005.

7.1 ABSTRACT

The second-order vibrational perturbation theory method has been used together with the B3LYP and MP2 electronic structure methods to investigate the effects of anharmonicity on the vibrational zero-point energy (ZPE) contributions to the binding energies of $(\text{H}_2\text{O})_n$, $n = 2 - 6$, clusters. For the low-lying isomers of $(\text{H}_2\text{O})_6$ the anharmonicity correction to the binding energy is calculated to range from -248 to -355 cm^{-1} . It is also demonstrated that while high-order electron correlation effects are important for the individual vibrational frequencies, they are relatively unimportant for the net ZPE contributions to the binding energies of water clusters.

7.2 INTRODUCTION

It has long been appreciated that vibrational anharmonicity is important in water clusters and other H-bonded systems.^{76,80,84,91,92,108-130} For example, anharmonicity is important for accounting in a quantitative manner for the spectral shifts in the OH stretch vibrations in going from an isolated water monomer to the H-bonded environments of the monomers in a water cluster, and for the appearance of various overtone and combination bands in the vibrational spectra of the clusters.^{81,90,93,131} Anharmonicity also makes important contribution to the vibrational zero-point energies, for example contributing about 0.23 kcal/mol to the dissociation energy (D_0) of $(\text{H}_2\text{O})_2$.¹²¹

One of the major challenges in experimental and theoretical studies of water clusters is the rapid growth in the number of possible isomers with increasing number of water monomers.¹³² For example, $(\text{H}_2\text{O})_6$ has been predicted to have four isomers lying within 0.2 kcal/mol of the global potential energy minimum¹³³ and 23 isomers lying within 2 kcal/mol of the global minimum.¹³⁴ In such a case, the relative stabilities of the various isomers could be significantly altered by anharmonicity corrections to the ZPEs. Clary and Gregory have concluded that the energy ordering of the low-lying isomers of $(\text{H}_2\text{O})_6$ is altered upon inclusion of corrections for ZPE calculated including vibrational anharmonicity.^{109,135} However, these authors did not separate the harmonic from anharmonic contributions to the ZPEs, so the importance of the anharmonicity corrections for the relative energies is not clear. We note also that Losada et al. have argued that since the number of the low frequency OH flipping modes changes from one isomer of $(\text{H}_2\text{O})_6$ to another, these highly anharmonic vibrations could play an important role in determining the relative stabilities of the low-energy isomers.¹³³

In spite of the obvious importance of vibrational anharmonicity on the properties of water clusters, few of the theoretical studies of these clusters have included anharmonicity effects. Moreover, those studies that have included vibrational anharmonicity have employed approximations that introduce considerable uncertainty in the magnitudes of the calculated anharmonicity contributions. For example, the diffusion Monte Carlo calculations of Gregory and Clary^{109,135} were carried out assuming rigid water monomers and employing a modified version of the ASP water model¹³⁶ for describing the intermolecular interactions. Thus, the resulting vibrational ZPEs have errors due to the neglect of intramolecular degrees of freedom as well as to the limitations of the water model.

In recent years, the vibrational SCF (VSCF) method¹³⁷⁻¹⁴¹ and the second-order vibrational perturbation theory method (VPT2)⁹⁶⁻¹⁰¹ have been coupled with electronic structure codes, allowing for the calculation of anharmonic vibrational frequencies and vibrational ZPEs using ab initio potential energy surfaces. These approaches do not require the use of rigid monomers and avoid other problems associated with model potentials. The vibrational SCF method has been applied in conjunction with ab initio or density functional electronic structure methods to the water dimer,¹¹² but, due to the steep computational cost, this approach has not been applied to clusters as large as (H₂O)₆. As implemented by Chaban et al.,¹⁴¹ a VSCF calculation on a single isomer of (H₂O)₆ would require nearly 290,000 energy evaluations when using 16 grid points, which is computationally prohibitive with reasonably large basis sets. (We note, however, that Gordon and co-workers have recently introduced variants of the VSCF method that reduce the computational effort by about an order of magnitude.¹⁴²) The VPT2 method is much less computationally demanding, and, at the time we initiated this study, had not

been applied to water clusters. However, Bouteiller et al. have recently published a paper in which they employed the VPT2 method to calculate frequencies of the water dimer.¹⁴³

The VPT2 method is analogous to the MP2 method for electronic structure calculations, with the harmonic approximation being used to generate the zeroth-order vibrational wave functions and energies needed for the perturbation corrections involving the cubic force constants and semi-diagonal quartic force constants. As implemented by Barone et al.¹⁴⁴ and incorporated in the Gaussian 03 code,⁵⁹ the necessary cubic and quartic force constants are calculated by numerical differentiation of the analytical Hessians. For (H₂O)₆, a VPT2 calculation requires evaluating 98 Hessians to obtain the necessary cubic and quartic force constants. This requires about two orders of magnitude less computational time than would vibrational SCF calculations, as implemented by Chaban et al.

In the present study we apply the vibrational perturbation theory method to the (H₂O)_n, n = 1 - 6, clusters. For the n = 2 - 5 clusters only the lowest-energy isomers are considered, while for (H₂O)₆ the lowest energy chair, cage, prism and book isomers^{85,133,145-147} (see Figure 15) are considered. In the figures and tables, the (H₂O)_n isomers are referred to as W_n for short. The anharmonicity corrections were calculated using the Becke3LYP⁹⁵ method for all clusters considered and using the MP2 method for the clusters up to n = 4 in size. The aug-cc-pVDZ²⁹ basis set was employed. For the monomer and dimer, calculations are also performed with the larger aug-cc-pVTZ²⁹ basis set. We focus here attention on the vibrational zero-point energies; the trends in the vibrational frequencies will be considered in a separate publication.¹⁴⁸

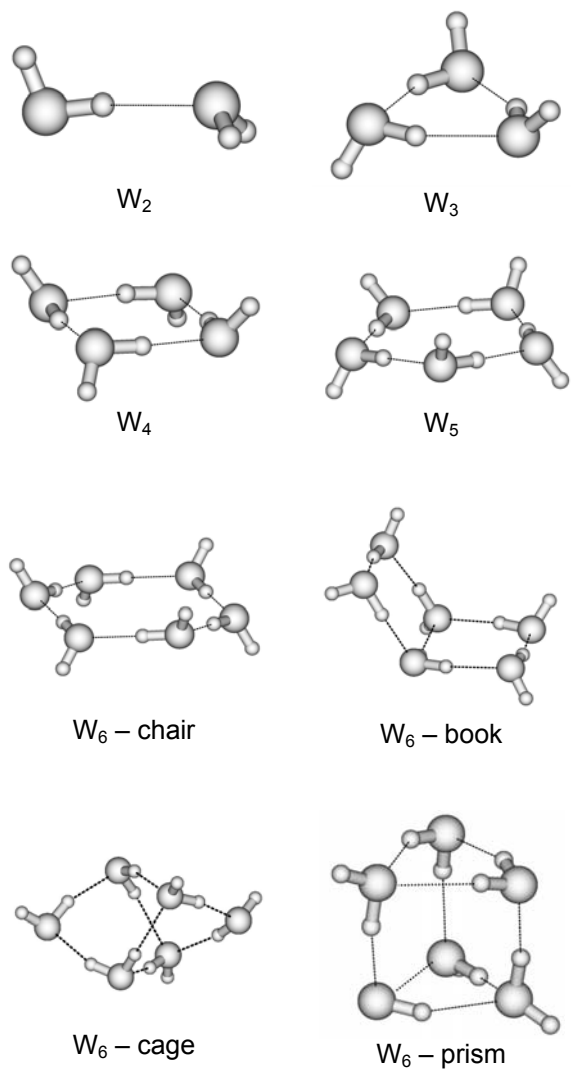


Figure 15. Water clusters studied in this work.

7.3 METHODOLOGY

All calculations were performed using the Gaussian 03 program.⁵⁹ The geometries were optimized using the “tight” criterion, and the Becke3LYP calculations were carried out using the ultrafine grid. The Hessians were calculated analytically, and a step size of 0.01 bohr was used for the numerical differentiations to produce the required third and fourth derivatives.

In applying vibrational perturbation theory to polyatomic systems it is essential to have a suitable strategy for dealing with Fermi resonances. Barone’s VPT2 code screens for Fermi resonances and treats them via a degenerate perturbation strategy proposed by Martin et al.¹⁴⁹ A second issue that arises in applying the VPT2 approach to water clusters is that it is unable to treat shifts in frequencies due to tunneling between local minima separated by small barriers as occurs, for example, upon flipping the H atoms of free OH of water clusters. As shown by Losada and Leutwyler,¹⁵⁰ tunneling associated with the OH flipping degrees of freedom can lead to large reductions in the associated vibrational transition energies, but is much less important for the ZPEs, the primary quantities of interest here.

7.4 RESULTS

Although the focus of this study is on vibrational ZPEs, it is instructive to compare in the case of (H₂O)₂ the calculated and experimentally observed anharmonic vibrational frequencies (Table 12). Overall, the Becke3LYP and MP2 anharmonic frequencies are in fairly good agreement, although the OH stretch frequencies are 21-48 cm⁻¹ lower at the Becke3LYP/aug-cc-pVTZ level.

For the most part these differences are also found for the harmonic frequencies, with the result that anharmonicity corrections are comparable in the Becke3LYP and MP2 approximations. The average absolute difference between the calculated (MP2/aug-cc-pVTZ) and measured anharmonic frequencies for the OH stretch and HOH bending vibrations is only 12 cm^{-1} . For the intermolecular vibrations the average difference between theory and experiment is only 19 cm^{-1} , but it should be noted that there is considerable uncertainty in the experimental frequencies of some of these modes.

Table 12. Harmonic and Anharmonic Vibrational Frequencies and Zero-Point Energies (cm⁻¹) of (H₂O)₂

| | calculated ^a | | | | | | | | experimental anharmonic |
|-----|-------------------------|-------|-------|-------|------------|------|-------|------|----------------------------|
| | harmonic | | | | anharmonic | | | | |
| | MP2 | | B3LYP | | MP2 | | B3LYP | | |
| | aVDZ | aVTZ | aVDZ | aVTZ | aVDZ | aVTZ | aVDZ | aVTZ | |
| | 3925 | 3935 | 3895 | 3890 | 3737 | 3753 | 3710 | 3711 | 3745 ^b |
| | 3904 | 3915 | 3874 | 3870 | 3722 | 3745 | 3696 | 3697 | 3735 ^c |
| | 3796 | 3814 | 3789 | 3791 | 3615 | 3648 | 3617 | 3627 | 3660±5 ^c |
| | 3704 | 3719 | 3672 | 3675 | 3554 | 3583 | 3531 | 3542 | 3601 ^c |
| | 1643 | 1650 | 1637 | 1647 | 1592 | 1595 | 1585 | 1592 | 1611 ^d |
| | 1624 | 1629 | 1617 | 1628 | 1580 | 1585 | 1576 | 1583 | 1593 ^d |
| | 639 | 630 | 634 | 625 | 505 | 502 | 507 | 499 | 520 ^e |
| | 358 | 360 | 360 | 362 | 309 | 310 | 322 | 287 | 290 ^d |
| | 184 | 184 | 184 | 187 | 148 | 138 | 137 | 117 | 108 ^f |
| | 151 | 155 | 157 | 157 | 106 | 114 | 132 | 102 | 103 ^f |
| | 148 | 147 | 156 | 155 | 112 | 113 | 103 | 117 | 103 ^f |
| | 127 | 127 | 130 | 130 | 60 | 60 | 69 | 37 | 87 ^f |
| ZPE | 10101 | 10133 | 10053 | 10059 | 9860 | 9898 | 9820 | 9806 | |

^a aVDZ and aVTZ denote aug-cc-pVDZ and aug-cc-pVTZ, respectively. ^b Reference 105. ^c Reference 76. ^d In Ar matrix, Reference 106. ^e In N₂ matrix, Reference 106. ^f Reference 107.

From Table 12 it can also be seen that with the exception of the OH stretch vibrations, the frequencies, both harmonic and anharmonic, calculated with the aug-cc-pVDZ and aug-cc-pVTZ basis sets agree to within 10 cm^{-1} . The sensitivity of the frequencies to the basis set is greater for the OH stretch vibrations with the frequency differences being as large as 18 cm^{-1} in the harmonic approximation and 33 cm^{-1} in the anharmonic approximation. However, as noted below, the basis set dependence is much less important for the anharmonicity contributions to the binding energy.

Table 13 and Table 14 report for the $n = 2 - 6$ clusters the calculated harmonic and anharmonic ZPEs, as well as the ZPE contributions to the cluster binding energies, calculated by subtracting n times the ZPE of the monomer from the ZPE of the $(\text{H}_2\text{O})_n$ cluster of interest. For $(\text{H}_2\text{O})_2$, the ZPE contribution to the binding energy is calculated at the MP2/aug-cc-pVDZ level to be 738 cm^{-1} in the harmonic approximation and 649 cm^{-1} when allowing for vibrational anharmonicity. These values are reduced by only 3 and 6 cm^{-1} , respectively, upon adoption of the aug-cc-pVTZ basis set. The corresponding ZPE contributions to the binding energy at the Becke3LYP/aug-cc-pVDZ level, 735 and 652 cm^{-1} , are close to the MP2 values. The calculated anharmonicity contributions to the binding energy of $(\text{H}_2\text{O})_2$ (89 and 83 cm^{-1} at the MP2/aug-cc-pVDZ and B3LYP/aug-cc-pVDZ levels, respectively) are in excellent agreement with a prior estimate¹²¹ (80 cm^{-1}) of this quantity.

Table 13. Harmonic and Anharmonic ZPEs and ZPE Contributions to the Binding Energies (cm^{-1}) of the $(\text{H}_2\text{O})_n$, $n = 1 - 6$, Clusters Calculated at the B3LYP/aug-cc-pVDZ Level of Theory^a

| | W ₁ | W ₂ | W ₃ | W ₄ | W ₅ | W ₆ chair | W ₆ book | W ₆ cage | W ₆ prism |
|--------------------------------|----------------|----------------|----------------|----------------|----------------|-------------------------|------------------------|------------------------|-------------------------|
| ZPE | | | | | | | | | |
| harm. | 4659 | 10053 | 15855 | 21503 | 26893 | 32316 | 32553 | 32669 | 32715 |
| anh.-corr. ^a | -75 | -233 | -346 | -464 | -612 | -730 | -699 | -771 | -805 |
| Total | 4584 | 9820 | 15509 | 21039 | 26281 | 31586 | 31854 | 31898 | 31910 |
| ZPE contrib. to D ₀ | | | | | | | | | |
| harm. | - | 735 | 1879 | 2867 | 3599 | 4363 | 4600 | 4716 | 4762 |
| anh.-corr. ^a | - | -83 | -121 | -163 | -236 | -279 | -248 | -321 | -355 |
| Total | - | 652 | 1758 | 2704 | 3363 | 4084 | 4352 | 4395 | 4407 |

^a anh.-corr. denotes the anharmonicity correction to the vibrational ZPE and to the ZPE contribution to D₀.

Table 14. Harmonic and Anharmonic ZPEs and ZPE Contributions to the Binding Energies (cm^{-1}) of the $(\text{H}_2\text{O})_n$, $n = 1 - 6$, Clusters Calculated at the MP2/aug-cc-pVDZ Level of Theory^a

| | W ₁ | W ₂ | W ₃ | W ₄ | W ₅ | W ₆ chair | W ₆ book | W ₆ cage | W ₆ prism |
|--------------------------------|----------------|----------------|----------------|----------------|----------------|-------------------------|------------------------|------------------------|-------------------------|
| ZPE | | | | | | | | | |
| harm. | 4682 | 10101 | 15913 | 21607 | 27056 | 32520 | 32731 | 32864 | 32933 |
| anh.-corr. ^b | -76 | -241 | -374 | -470 | -612 | -730 | -699 | -771 | -805 |
| total | 4606 | 9860 | 15539 | 21137 | 26444 | 31790 | 32032 | 32093 | 32128 |
| ZPE contrib. to D ₀ | | | | | | | | | |
| harm. | - | 738 | 1868 | 2881 | 3648 | 4430 | 4642 | 4774 | 4843 |
| anh.-corr. ^b | - | -89 | -146 | -166 | -236 | -279 | -248 | -321 | -355 |
| total | - | 649 | 1722 | 2715 | 3412 | 4151 | 4394 | 4453 | 4488 |

^a For the $n = 5$ and 6 clusters, the anharmonicity corrections are from Becke3LYP/aug-cc-pVDZ calculations. ^b anh.-corr. denotes the anharmonicity correction to the vibrational ZPE and to the ZPE contribution to D₀.

Figure 16 plots for the $n = 2 - 6$ clusters the calculated harmonic and anharmonic ZPE contributions per monomer to the binding energies. The two curves are roughly parallel, with the difference ranging from 42 to 59 cm^{-1} per monomer (see Table 15). For the four $(\text{H}_2\text{O})_6$ isomers considered, the calculated anharmonicity corrections to the binding energies range from

-248 cm^{-1} (book) to -355 cm^{-1} (prism). Thus, vibrational anharmonicity changes the relative energies of these isomers by up to 107 cm^{-1} (0.3 kcal/mol).

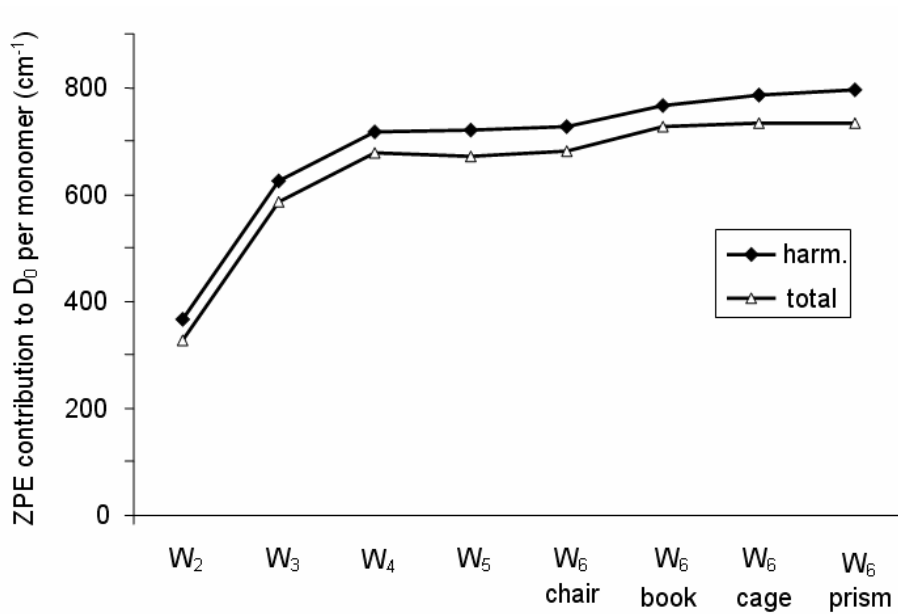


Figure 16. Vibrational ZPE contributions per monomer (cm^{-1}) to the dissociation energies of the $(\text{H}_2\text{O})_n$, $n = 2 - 6$, clusters.

Table 15. Vibrational ZPE Contributions (cm^{-1}) to the Binding Energies Reported per Monomer and Calculated at the B3LYP/aug-cc-pVDZ Level of Theory.

| | W ₂ | W ₃ | W ₄ | W ₅ | W ₆ chair | W ₆ book | W ₆ cage | W ₆ prism |
|-------|----------------|----------------|----------------|----------------|-------------------------|------------------------|------------------------|-------------------------|
| harm. | 368 | 626 | 717 | 720 | 727 | 767 | 786 | 794 |
| anh. | -42 | -40 | -41 | -47 | -46 | -42 | -53 | -59 |
| total | 326 | 586 | 676 | 673 | 681 | 725 | 733 | 735 |

Calculations at the MP2/aug-cc-pVTZ//MP2/aug-cc-pVDZ level of theory including corrections for BSSE and vibrational ZPEs, calculated in the harmonic approximation, give relative energies of 0.00, 0.02, 0.05 and 0.15 kcal/mol for the chair, cage, book and prism isomers of the water hexamer, respectively.¹³³ When these results are combined with the anharmonicity corrections calculated here, we find that the cage isomer is predicted to be the most stable, followed by the prism (+0.04 kcal/mol), chair (+0.10 kcal/mol) and book (+0.24 kcal/mol). Obviously, when dealing with isomers this close in energy, the calculated energy ordering cannot be taken as definitive.

We next consider the contributions of various types of vibrations to the ZPEs of the water clusters. Table 16 decomposes the calculated harmonic ZPE contributions to the binding energies into contributions from the OH stretch, HOH bend, and intermolecular degrees of freedom. Here we focus on the harmonic results because the anharmonic ZPE corrections do not depend on the frequency values alone.¹⁵¹ As expected, the most important class of vibrations for the ZPE contributions to the binding energies is the intermolecular vibrations. However, the contributions due to the OH stretch degrees of freedom are also sizable, being 11-24% as large as the contributions due to intermolecular vibrations in magnitude. The ZPE contributions due to the HOH bending vibrations are about an order of magnitude smaller still. Whereas the ZPE contributions from the intermolecular vibrations and the intramolecular bending vibrations make positive contributions to D_0 , the net ZPE contributions due to the OH stretching degrees of freedom make negative contributions to D_0 .

Table 16. ZPE Contributions (cm^{-1}) of Various Classes of Vibrations to the Binding Energies of the $(\text{H}_2\text{O})_n$, $n = 2 - 6$, Clusters Calculated in the Harmonic Approximation at the B3LYP/aug-cc-pVDZ Level.

| | W_2 | W_3 | W_4 | W_5 | W_6 chair | W_6 book | W_6 cage | W_6 prism |
|----------------------|-------|-------|-------|-------|----------------|---------------|---------------|----------------|
| OH stretch | -84 | -398 | -859 | -1160 | -1410 | -1405 | -1324 | -1259 |
| bending modes | 9 | 22 | 53 | 90 | 104 | 105 | 119 | 130 |
| intermolecular modes | 811 | 2256 | 3673 | 4669 | 5669 | 5901 | 5921 | 5891 |
| total | 735 | 1879 | 2867 | 3599 | 4363 | 4600 | 4716 | 4762 |

Both the B3LYP and MP2 methods give OO distances too short and single- and double-donor OH bond lengths too long compared to those from calculations including high-order electron correlation effects. These geometrical errors translate into errors in the calculated vibrational frequencies. This leads naturally to the question as to whether the limitations of these theoretical methods have significant consequences for the ZPE contributions to the binding energies. To examine this issue, we have optimized the geometries and calculated the harmonic frequencies for the $(\text{H}_2\text{O})_n$, $n = 2 - 4$, clusters at the QCISD¹⁰²/aug-cc-pVDZ level of theory. The ZPE contributions due to both the OH stretch and the intermolecular vibrations are significantly altered in going from the MP2 (or B3LYP) to the QCISD level of theory (Table 17). However, the net ZPEs are essentially unchanged upon the inclusion of high-order correlation effects. Thus, we conclude that both the B3LYP and MP2 methods are suitable for calculating the contributions of vibrational ZPE to the binding energies of water clusters.

Table 17. ZPE Contributions (cm^{-1}) of Various Classes of Vibrations to the Binding Energies of the $(\text{H}_2\text{O})_n$, $n = 2 - 4$, Clusters Calculated in the Harmonic Approximation at the QCISD/aug-cc-pVDZ Level^a

| | W_2 | W_3 | W_4 |
|----------------------|----------------|-------------------|-------------------|
| OH stretch | -49 (-84, -76) | -239 (-398, -347) | -544 (-859, -766) |
| bending modes | 11 (9, 11) | 27 (22, 28) | 62 (53, 65) |
| intermolecular modes | 776 (811, 803) | 2091 (2256, 2187) | 3400 (3673, 3582) |
| total | 737 (735, 738) | 1879 (1879, 1868) | 2919 (2876, 2881) |

^a Becke3LYP/aug-cc-pVDZ and MP2/aug-cc-pVDZ results are reported in parentheses, with the Becke3LYP results being given first.

7.5 CONCLUSIONS

The VPT2 method has been combined with the Becke3LYP and MP2 electronic structure methods to calculate anharmonic contributions to the ZPEs of the $(\text{H}_2\text{O})_n$, $n = 1 - 6$, clusters. The anharmonic contribution to the ZPE correction to the binding energy is calculated to be -83 , -121 , -163 , and -236 cm^{-1} for $(\text{H}_2\text{O})_2$, $(\text{H}_2\text{O})_3$, $(\text{H}_2\text{O})_4$, and $(\text{H}_2\text{O})_5$, respectively. For the four low-energy isomers considered, the anharmonic contribution to the ZPE correction to the binding energy of $(\text{H}_2\text{O})_6$ ranges from -248 to -355 cm^{-1} , being larger in magnitude for the cage and prism than for the chair and book isomers. Allowing for the effects of vibrational anharmonicity the most stable isomer of $(\text{H}_2\text{O})_6$ is predicted to be the cage isomer, followed by the prism, chair, and book isomers, in order of increasing energy, with all four isomers lying within 0.2 kcal/mol of one another. To date the cage, chair, and book isomers have been observed experimentally, the cage in the microwave experiments of Liu et al.,^{72,152} the chair in the Helium droplet experiments of Nauta et al.,⁷⁷ and the book isomer in the IR studies of Steinbach et al.¹⁵³ and Diken et al.⁹⁰

High-order correlation effects, while important for the frequencies of individual vibrational modes, are found to be relatively unimportant for the net vibrational zero-point energies. In other words, the success of the Becke3LYP and MP2 methods for calculating the vibrational ZPEs is a consequence of a near cancellation of errors. The origin of this cancellation is well understood in that these theoretical methods underestimate the frequencies of the OH groups engaged in H-bonding and tend to overestimate the frequencies of the intermolecular vibrations. The present study also reveals that there are sizable differences between the ZPE contributions to the binding energies calculated considering only the intermolecular degrees of freedom and those calculated including all degrees of freedom. This suggests that rigid monomer water models are of limited use for calculation of ZPE contributions to the binding energies of water clusters.

Acknowledgement. This research was carried out with the support of grant CHE-0078528 from the National Science Foundation. We acknowledge valuable discussions with Prof. V. Barone about the vibrational perturbation theory method.

8.0 ISOLATION AND SPECTROSCOPIC CHARACTERIZATION OF A NEW HIGH ELECTRON BINDING ENERGY ISOMER OF $(\text{H}_2\text{O})_7^-$

Manuscript in preparation

Joseph R. Roscioli, Nathan I. Hammer, Mark A. Johnson, Kadir Diri, and Kenneth D. Jordan

8.1 INTRODUCTION

There has been a recent resurgence of interest in the negatively charged water clusters, largely driven by the observation that their optical spectrum¹⁵⁴⁻¹⁵⁶ and relaxation dynamics¹⁵⁷⁻¹⁵⁹ are similar to those of the bulk hydrated electron,¹⁶⁰⁻¹⁶⁶ a species whose behavior has presented one of the long standing challenges for contemporary chemical physics. The clusters thus provide relevant model systems which are sufficiently small that they can be addressed in the “supermolecular” regime using advanced electronic structure methods. The $(\text{H}_2\text{O})_n^-$ clusters occur with three distinct groups of electron binding energies over a large range of clusters, denoted I, II, and III in decreasing order of their electron binding energies.¹⁶⁷⁻¹⁶⁹ In the cases of the hexamer and octamer anions, we have previously correlated differences in the vertical electron detachment energies (VDEs) exhibited by the two more strongly binding isomers (I and II) to their distinct electron binding motifs at the molecular level, deduced from their patterns of vibrational bands obtained with predissociation spectroscopy.^{170,171} The form (I) that most

strongly binds the electron yields a unique vibrational band in the HOH bending region that is red-shifted by about 70 cm^{-1} relative to the ν_2 band in the isolated water molecule. This feature is associated with the water molecule that most strongly interacts with the excess electron as indicated in Figure 17,^{170,172,173} which is attached to the network with an unusual double H-bond acceptor (AA) motif such that both of its hydrogen atoms point toward the excess electron cloud. The lower VDE isomer (II) does not display this spectral feature, yielding instead bands more consistent with those expected for predominately neutral water networks. It is anticipated, of course, that as the cluster size increases, the number of isomers will rapidly increase to the point that one will only be able to group the resulting structures according to average properties. Here we extend this study to the heptamer anion, where we vary the extent of Ar solvation to empirically change the distribution of isomers prepared by the ion source. We will show that the heptamer anion already presents a complicated situation in which several isomers are at play. Most importantly, we report the observation of a new type that displays even higher VDE than previously reported for the class I isomers, which were thought to represent the highest binding isomer class. We consider several scenarios for the structural assignment of this isomer, with the aid of electronic structure calculations.

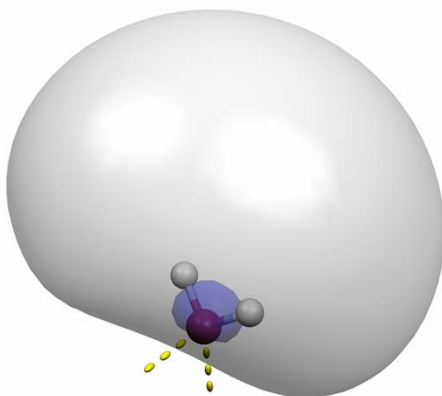
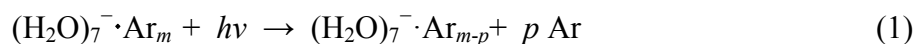


Figure 17. Acceptor-acceptor (AA) binding motif of the isomer I variants of $(\text{H}_2\text{O})_n^-$. In this scheme, a single water molecule serves as the binding site for an excess electron, pointing both free hydrogens into the electron's diffuse orbital. This AA molecule is easily revealed in infrared spectra by the presence of its very red-shifted ($>50 \text{ cm}^{-1}$) HOH bend.

8.2 EXPERIMENTAL

Vibrational spectra were acquired by predissociation or electron autodetachment of size-selected $(\text{H}_2\text{O})_7^- \cdot \text{Ar}_m$ ($m = 0 - 10$) complexes, with predissociation:¹⁷⁴



being used to obtain the spectra of the $m = 2-10$ clusters and electron autodetachment:[#23]



being required to obtain the spectra of the $m = 0$ and 1 clusters. The $(\text{H}_2\text{O})_7^- \cdot \text{Ar}_m$ ($m = 0 - 10$) cluster ions were generated by slow secondary electron attachment to argon-solvated neutral water clusters, where the slow electrons were prepared by ionizing a pulsed nozzle (Parker-Hannefin) expansion with a 1 keV counterpropagating electron beam. The expansion was

formed by expanding 4 atm Ar carrier gas, saturated with water vapor over a reservoir held at 2°C, through a 0.5 mm diameter orifice. The clusters were irradiated with a table-top IR laser source (Laser Vision) in both the 3100 – 3600 and 1400 – 1800 cm^{-1} regions, the lower energy region being generated by parametric conversion in AgGaSe_2 .¹⁷⁵ Photofragmentation occurs with Ar losses expected for an effective binding energy of 400 cm^{-1}/Ar (e.g., loss of 4 Ar atoms at $h\nu = 1600 \text{ cm}^{-1}$). The reported spectra result from the addition of approximately 10 individual scans and are corrected for laser pulse energy changes over the scan range, with the results presented as photoproduct yield normalized to the energy/pulse. For photoelectron spectra, photodetachment was carried out with the doubled fundamental beam from a Nd:YAG laser (532 nm) and the resulting photoelectrons were analyzed with a field-free, time-of-flight photoelectron spectrometer.^{168,174,176} Photoelectron spectra typically result from 50,000 shots, and were obtained with the laser polarization oriented along the electron flight axis.

8.3 THEORETICAL

From the theoretical work of Kim and coworkers it is known that $(\text{H}_2\text{O})_7^-$ has a large number of low energy isomers,¹⁷⁷ and our recent Parallel Tempering Monte Carlo (PTMC) simulations using an electron-water pseudo-potential^{22,178,179} which accounts for polarization and dispersion interactions between the excess electron and the water molecules through Drude oscillators (from now on referred as the Drude model) have uncovered many additional low-energy structures.¹⁸⁰ All these structures were optimized with the MP2 and the Becke3LYP methods, together with the 6-31(1+,3+)G* basis set which was obtained from the standard 6-31G++G* by adding two extra diffuse functions on each H atom.¹⁸¹ The geometrical structures of these isomers are

depicted in Figure 18 (the structures labeled with “*” were discovered in this work, while the rest of the isomers were found previously by Kim et al.¹⁷⁷). For each optimized structure, the harmonic vibrational frequencies and the energy of the neutral molecule were calculated. The differences of the MP2 energies of the anions and neutrals were used to give theoretical estimates of the VDEs. For selected isomers, VDEs were also calculated at the CCSD/6-31(1+,3+)G* level of theory using the MP2 geometries and also using the Drude model.

The vibrational frequencies of each isomer were calculated with both the MP2 and the Becke3LYP methods again using the 6-31(1+,3+)G* basis set. The choice of this basis set was stimulated by the remarkable agreement between the scaled Becke3LYP/6-31(1+,3+)G* and experimental frequencies of the (H₂O)₄⁻, (H₂O)₅⁻, and (H₂O)₆⁻ clusters in the OH stretch region. Similar results were recently obtained by Hammer et al. using the 6-311++G** (sp) basis set.¹⁷³ In the HOH bending region on the other hand, the MP2 method combined with the 6-31(1+,3+)G* basis set gives slightly better results than the corresponding Becke3LYP values compared to experiment. Therefore, in the present study we use the MP2/6-31(1+,3+)G* frequencies to compare them against the experimental results in the bending frequency region of (H₂O)₇⁻ whereas for the OH stretching frequency region, we adopt the Becke3LYP/6-31(1+,3+)G* procedure. Scaling factors for the basis sets were chosen such that they give the best overall agreement with experiment.

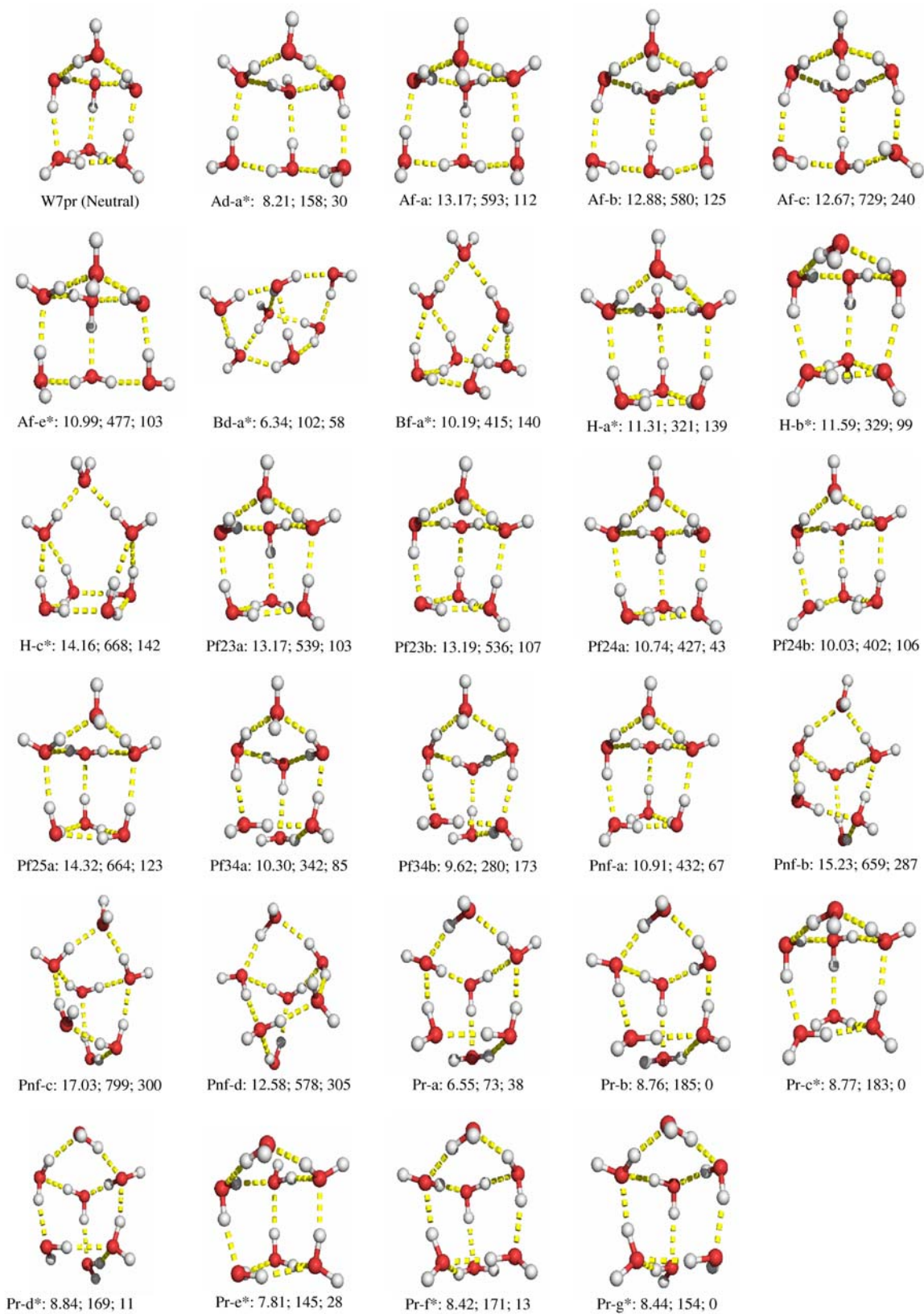


Figure 18. The calculated most stable 28 possible structures of $(\text{H}_2\text{O})_7$.

The Gaussian 03⁵⁹ suite of programs was used for all electronic structure calculations. The Becke3LYP calculations were performed using the “fine” grid implemented the program (*i.e.* 75 radial shells and 302 angular points per shell, resulting in about 7000 points per atom). This type of grid was found to give practically the same harmonic frequencies as the larger “ultrafine” grid (*i.e.*, 99 radial shells, 590 angular points per shell) in test calculations.

Studies on the water hexamer anion have shown that a small number of Ar atoms does not significantly perturb the frequencies of that cluster.⁷ This effect was also tested and confirmed in our calculations on $(\text{H}_2\text{O})_7^-$, as well as in recent calculations on $(\text{H}_2\text{O})_4^-$ by Herbert et al.¹⁸²

8.4 RESULTS AND DISCUSSION

8.4.1 Photoelectron spectra: Ar dependence of the isomer distribution

Figure 19 presents the evolution of the photoelectron spectra of the $(\text{H}_2\text{O})_7^- \cdot \text{Ar}_m$ clusters for $m = 0 - 10$, with the expected locations of the type I and II isomers being indicated by the dashed vertical lines as labeled at the top of the figure. Both type I and II isomers are found to have significant population for the $m = 0$ cluster. However, the contribution of the type II form is greatly reduced upon addition of one or more Ar atoms, which is quite different from the behavior displayed by the $(\text{H}_2\text{O})_6^-$ cluster, for which isomer II gradually gave way to I at about $m = 5$. Even more surprising is the appearance of a new band (labeled I' in Figure 19) that emerges in the spectra of the $(\text{H}_2\text{O})_7^- \cdot \text{Ar}_m$, $m \geq 5$ clusters, with a VDE about 0.15 eV greater than that of

isomer I. The growth of I' is accompanied by deletion of I, suggesting that two distinct $(\text{H}_2\text{O})_7^-$ species are interconverting, analogous to the behavior in the larger ($m > 11$) size regime where there is a transition between forms I and II. However, there are no prior reports of interconversion between a type I species and another isomer of a $(\text{H}_2\text{O})_n^-$ cluster with even higher electron binding energy, which raises the question of the structural difference between I and I'. To address this question, we turn to theoretical predictions of the cluster structures, and then determine which of these are at play in our ion ensemble by analysis of their vibrational spectra.

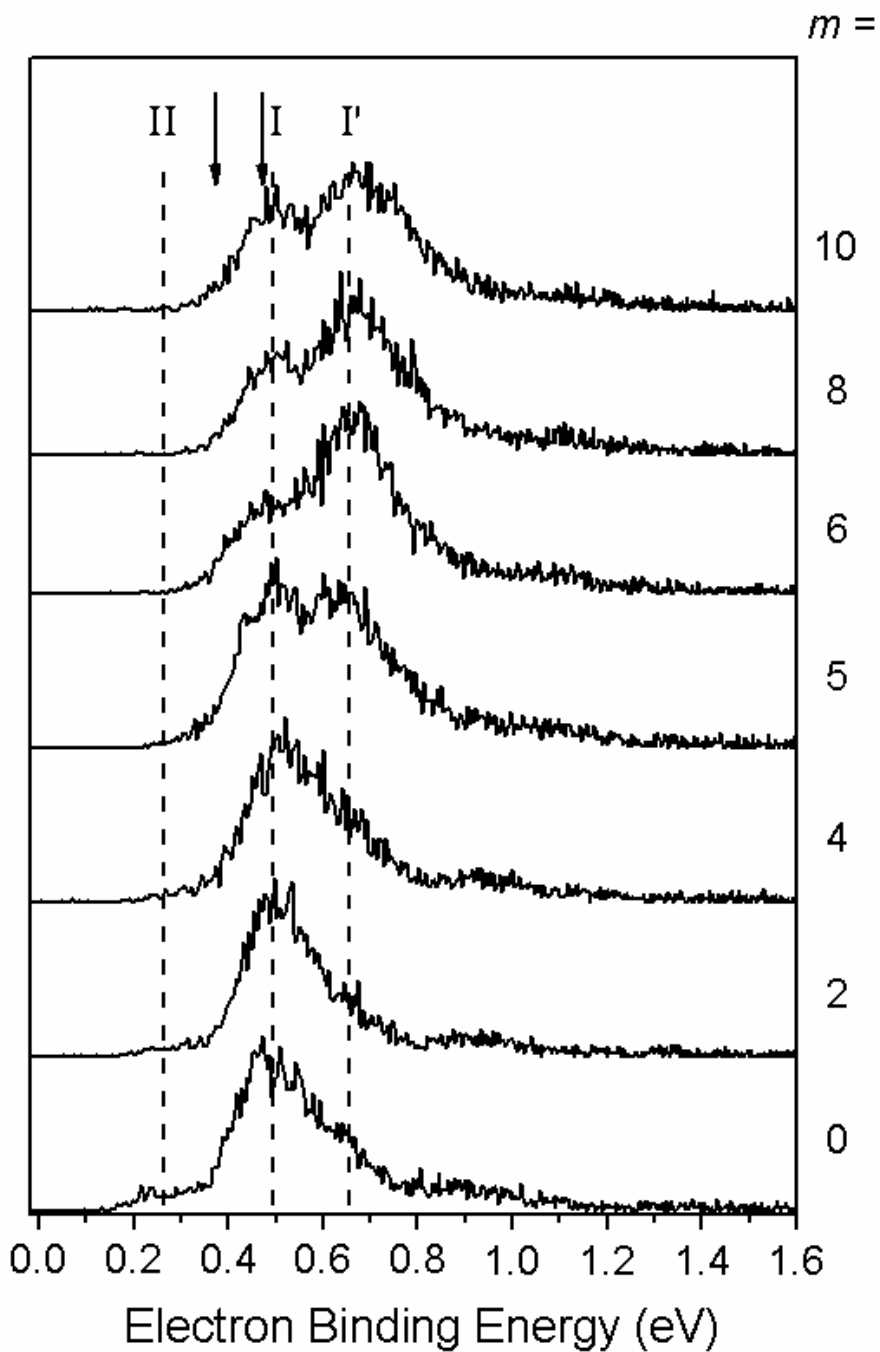


Figure 19. Photoelectron spectra of the $(\text{H}_2\text{O})_7^- \text{Ar}_m$ ($m = 0-10$) species. Expected electron binding energies of isomers I and II, along with the emergence of a new, higher-binding isomer (I'), are indicated by the dashed lines. The arrows indicates the energy of the infrared bleaching laser used to selectively remove isomers II and I from the population (0.372 and 0.471 eV, respectively).

8.4.2 Theoretical expectations

Table 1 summarizes the relative energies, VDEs, and dipole moments of the isomers considered, together with the corresponding values from CCSD(T) and Drude model calculations. Calculated VDEs of the various $(\text{H}_2\text{O})_7^-$ isomers range from 0.1 to 0.8 eV, with the electron binding energy correlating fairly closely with the dipole moment of the associated neutral cluster (See also Figure 20). All isomers with a calculated VDE over 0.35 eV contain a double-acceptor (AA) monomer. The most stable AA-type anion (Pf24a) is calculated to be 43 meV less stable than the most stable non-AA isomers (Pr-b, Pr-c*, and Pr-g*) in the MP2/6-31(1+,3+)G* calculations, while this energy difference is reduced to 26 meV upon inclusion of higher order electron correlation through the CCSD(T) calculations. Corrections for vibrational zero-point energies further reduce this difference by 20 meV and make both isomers almost isonergetic. In addition to these, Table 21 suggests that calculations with a larger basis set actually stabilize the AA type clusters with respect to isomer Pr-b. For example, the energy difference between Pr-b and Pf24a is reduced by 9 meV when the larger aug-cc-pVDZ (2s2p,1s) basis set is used. The exponents of the supplemental diffuse basis functions are summarized in Table 18:

Table 18. The exponents of the supplemental set of diffuse functions for the basis sets used.

| Atom | Function type | aug-cc-pVDZ (2s2p,1s) | 6-31(1+,3+)G* |
|------|---------------|-----------------------|---------------|
| O | s | 0.00987000 | |
| | s | 0.00123375 | |
| | p | 0.00857000 | |
| | p | 0.00107125 | |
| H | s | 0.00371750 | 0.012 |
| | s | | 0.004 |

If the effects of using a larger basis set, higher order electron correlation, and adding the zero point energies are assumed to be uncoupled and additive, then isomer Pf24a becomes more stable than Pr-b (by 3 meV). We note however that all these effects may not be completely separate from each other and that the level of accuracy involved in the calculations does not permit us to unambiguously assign the global minimum. Geometry optimizations followed by frequency calculations at higher level (such as CCSD(T)) with larger basis sets are needed to obtain a better ordering of the relative energies, however this is not of great importance for this particular study. On the other hand, of greater importance are the VDEs, for which the smaller basis set gives results that are very close to the ones obtained with the larger basis set (Table 19 and Table 21). This is presumably due to cancellation of errors that arise by the fact that the calculations with the smaller basis set do not describe the neutral clusters as accurately as the calculations with the larger basis set (as evidenced by the overestimated dipole moments) which compensates for the inadequate “diffuseness” of the basis set. All these results in better match between the experimental vibrational spectra and the spectra calculated with the 6-31(1+,3+)G* basis set (with both MP2 and Becke3LYP methods).

Table 19. Relative energies, VDEs, and dipole moments of the isomers considered, calculated at the MP2 and CCSD(T) levels of theory utilizing the 6-31(1+,3+)G* basis set, and with the Drude model.^a

| | MP2 | | | CCSD(T) ^b | | Drude Model ^c | | | | |
|-------|-----|------------------------|---------|----------------------|------------------------|--------------------------|-----|-----|-----|---------|
| | VDE | Rel Stab. ^d | μ^e | VDE | Rel Stab. ^d | Energy ^f | KT | PT2 | CI | μ^e |
| Ad-a* | 158 | 74 | 8.21 | 191 | 39 | 60 | 40 | 89 | 174 | 6.94 |
| Af-a | 593 | 155 | 13.17 | 630 | 91 | 64 | 246 | 436 | 540 | 11.29 |
| Af-b | 580 | 168 | 12.88 | | | 68 | 237 | 424 | 531 | 11.02 |
| Af-c | 729 | 284 | 12.67 | | | 183 | 263 | 481 | 603 | 10.82 |
| Af-e* | 477 | 146 | 10.99 | | | 89 | 177 | 341 | 444 | 9.55 |
| Bd-a* | 102 | 101 | 6.34 | 134 | 56 | 106 | 19 | 50 | 130 | 5.39 |
| Bf-a* | 415 | 184 | 10.19 | | | | | | | |
| H-a* | 321 | 183 | 11.31 | 365 | 114 | 89 | 124 | 240 | 359 | 9.60 |
| H-b* | 329 | 143 | 11.59 | | | 123 | 129 | 247 | 359 | 9.88 |
| H-c* | 668 | 186 | 14.16 | | | | | | | |
| Pf23a | 539 | 147 | 13.17 | | | 86 | 225 | 404 | 511 | 11.32 |
| Pf23b | 536 | 151 | 13.19 | | | 92 | 223 | 401 | 506 | 11.35 |
| Pf24a | 427 | 87 | 10.74 | 465 | 23 | 83 | 151 | 296 | 394 | 9.29 |
| Pf24b | 402 | 150 | 10.03 | | | 125 | 136 | 276 | 376 | 8.69 |
| Pf25a | 664 | 167 | 14.32 | 701 | 89 | 95 | 296 | 506 | 606 | 12.47 |
| Pf34a | 342 | 128 | 10.30 | 381 | 65 | 92 | 112 | 226 | 330 | 8.79 |
| Pf34b | 280 | 216 | 9.62 | | | 179 | 80 | 170 | 270 | 8.14 |
| Pnf-a | 432 | 111 | 10.91 | 470 | 49 | 74 | 153 | 298 | 397 | 9.39 |
| Pnf-b | 659 | 331 | 15.23 | 697 | 251 | 205 | 301 | 506 | 613 | 13.11 |
| Pnf-c | 799 | 344 | 17.03 | | | 244 | 382 | 619 | 722 | 14.81 |
| Pnf-d | 578 | 349 | 12.58 | | | 231 | 233 | 423 | 537 | 10.80 |
| Pr-a | 73 | 81 | 6.55 | 105 | 41 | 116 | 14 | 35 | 108 | 5.59 |
| Pr-b | 185 | 44 | 8.76 | 221 | -3 | 48 | 53 | 116 | 213 | 7.36 |
| Pr-c* | 183 | 44 | 8.77 | 219 | -3 | 44 | 54 | 117 | 214 | 7.39 |
| Pr-d* | 169 | 55 | 8.84 | 204 | 9 | 91 | 49 | 104 | 197 | 7.50 |
| Pr-e* | 145 | 71 | 7.81 | 182 | 23 | 93 | 35 | 81 | 174 | 6.62 |
| Pr-f* | 171 | 57 | 8.42 | 207 | 10 | 73 | 47 | 104 | 200 | 7.09 |
| Pr-g* | 154 | 44 | 8.44 | | | | | | | |

^a All energies are in meV. ^b MP2 geometries were used. ^c MP2 geometries were used, however the monomer geometries were fixed to the values in the Dang-Chan model. ^d Relative Stability defined as: E(anion) – E(of the neutral global minimum). ^e Dipole moment of the corresponding neutral at the anion geometry in units of Debye. ^f Energy of Pr-c* is set to match the MP2 Rel. Stab.value (44 meV).

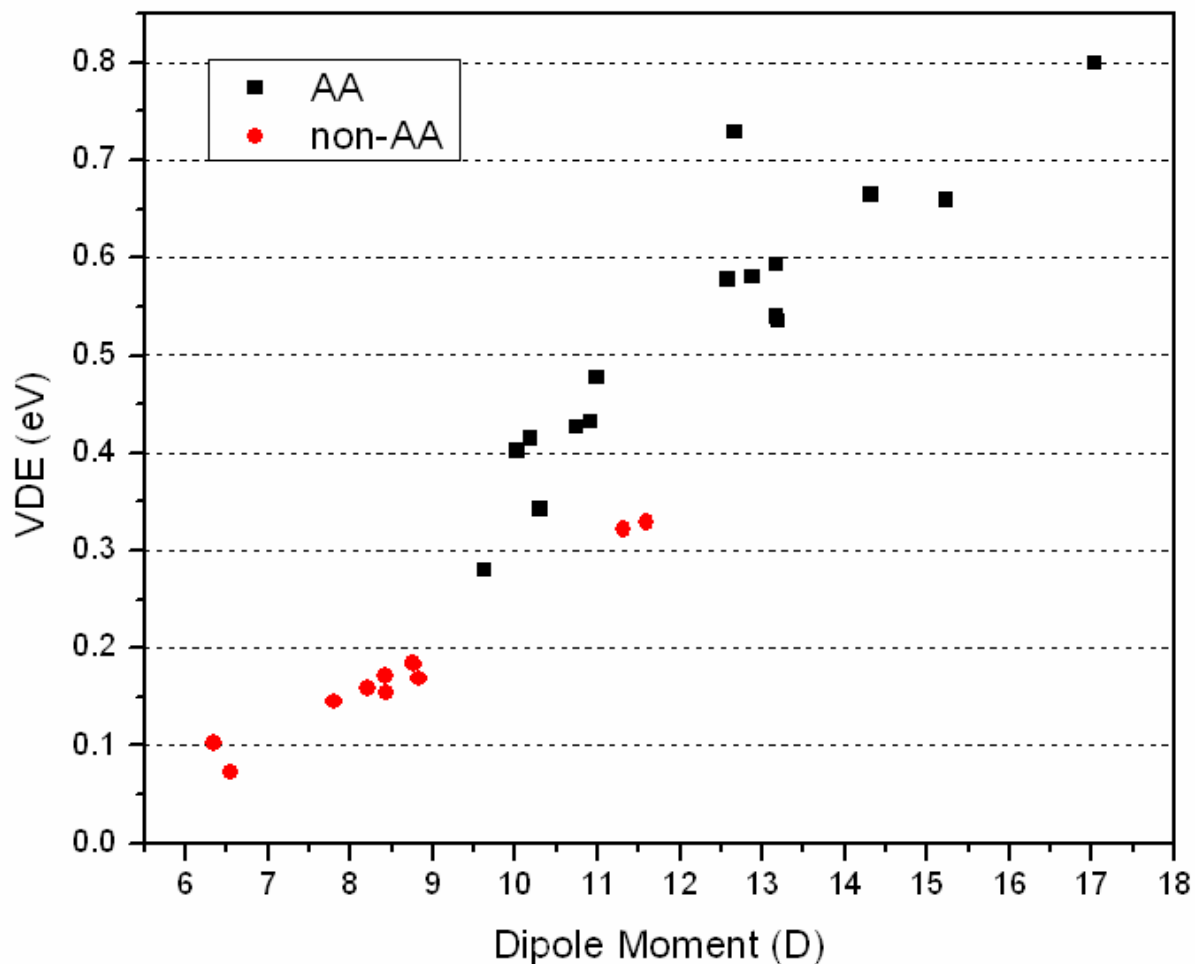


Figure 20. Calculated vertical detachment energies (VDE) of the $(\text{H}_2\text{O})_7^-$ structures shown in Figure 18, plotted as a function of the dipole moments of their neutral scaffolds. The dramatic separation of the AA and non-AA type binding motifs qualitatively supports the structural assignments of isomers I and II for $(\text{H}_2\text{O})_7^-$.

Table 20. Relative zero point energies (meV) of selected isomers calculated using the 6-31(1+,3+)G* basis

| | set. | |
|-------|------|-----------|
| | MP2 | Becke3LYP |
| Af-a | -36 | -36 |
| H-a | -10 | 0 |
| Pf24a | -20 | -18 |
| Pnfa | -21 | -25 |
| Pr-b | 0 | 0 |

Table 21. Relative energies, VDEs, and dipole moments of selected isomers, calculated at the MP2/aug-cc-pVDZ (2s2p,1s) level of theory.^a

| | VDE | Rel Stab. ^b | μ^c |
|-------|-----|------------------------|---------|
| Af-a | 556 | 99 | 11.86 |
| afa2 | 440 | 109 | 10.03 |
| Pf24a | 391 | 61 | 9.85 |
| Pnfa | 406 | 75 | 10.07 |
| Pr-b | 156 | 26 | 7.73 |

^a All energies are in meV. ^b Relative Stability defined as: $E(\text{anion}) - E(\text{of the neutral global minimum})$. ^c Dipole moment of the corresponding neutral at the anion geometry in units of Debye.

The presence of an AA electron binding site is actually straightforward to address experimentally, as previous vibrational studies of the $(\text{H}_2\text{O})_n^-$, ($n = 3 - 6$) ions have shown that the AA water molecule yields a clear signature band in the bending region located about 80 cm^{-1} below the frequency of the bend in the free water molecule, and in a region free from bands found in the small neutral water clusters. We therefore carried out a survey of the bending spectra with the results presented in the next section.

8.4.3 Evolution of the HOH bending spectra with argon

Figure 21 presents the argon dependence of the $(\text{H}_2\text{O})_7^- \cdot \text{Ar}_m$ HOH bending spectra, with the location of the AA band indicated in the top trace. Note that the AA signature band is prominent at all Ar cluster sizes, and that this feature splits into a closely spaced doublet in the spectra of the $m = 9$ and 10 clusters. In addition, there is a weaker band with an intermediate red-shift indicated by the asterisk, which interestingly disappears around $m = 5$, the same size range where

new features (labeled α , β and γ) appear in the higher energy region. Note that these spectral changes occur at the same number of Ar atoms where the photoelectron spectra reveal the emergence of the new high binding isomer (I'). The feature designated by the * occurs in the vicinity of the bending vibration associated with isomer II in recent studies of the $n = 6$ and 8 clusters,^{170,183} but the isomer II band in the PES is already quite small at $m = 1$, and is further diminished with increasing Ar solvation. The Ar-dependent vibrational spectra thus suggest that structural changes with increasing number of Ar atoms are occurring that are not anticipated by their photoelectron spectra. To sort out which vibrational features are associated with the different electron binding classes, we next turn to a photoselection technique that isolates predissociation spectra arising from particular electron binding energy species.

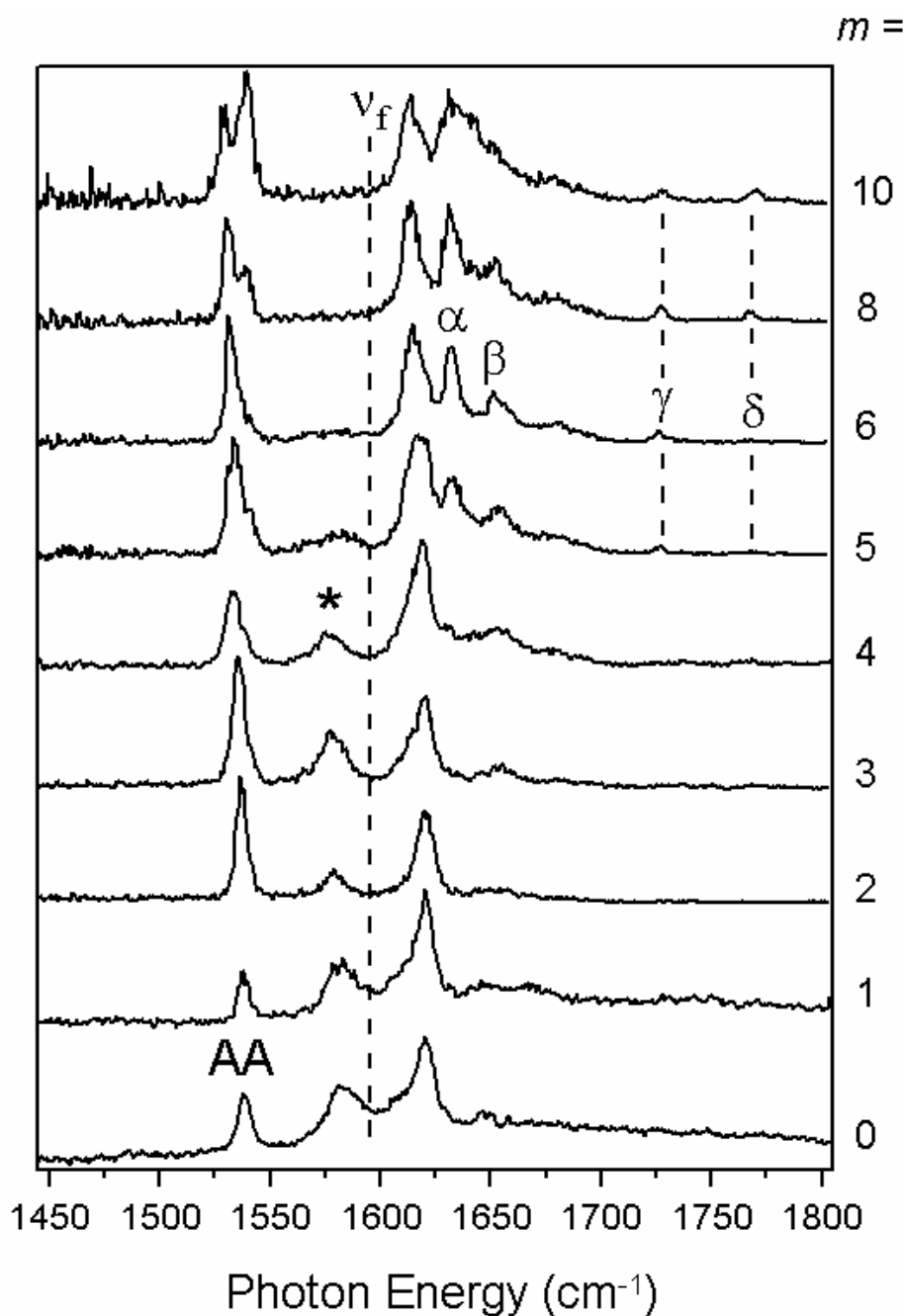


Figure 21. Infrared spectra of $(\text{H}_2\text{O})_7^- \cdot \text{Ar}_m$ ($m = 0-10$) in the HOH bending region. The red-shifted bend at $\sim 1535 \text{ cm}^{-1}$ indicates the existence of the AA binding motif throughout the $m = 0-10$ series. The bending vibrational frequency of a free H_2O molecule is represented by the dashed line at 1595 cm^{-1} . Features labeled α , β , γ , and δ , whose presence coincides with the emergence of a new peak in the photoelectron spectrum (see Figure 19) between $m = 4$ and 6, suggest that this new peak is created by a $(\text{H}_2\text{O})_7^-$ isomer which is structurally different than isomer I.

8.4.4 Isomer-specific predissociation spectra using VDE-dependent photodepletion

We recently demonstrated that the isomers with low electron binding energy can be very efficiently and selectively removed from the $(\text{H}_2\text{O})_n^-$ ion ensemble through low energy photodetachment in a saturated regime. This requires first intersecting the ion packet with a tunable infrared photodetachment laser just before the ions are excited with a (second) predissociation laser scanned through the vibrational spectrum. In this arrangement, sequentially tuning the photodetachment laser energy to higher energies progressively removes low electron binding species from the ensemble.

8.4.5 Isolation of the isomer II spectrum

Figure 22 illustrates the application of the isomer photoselection scheme to the $n = 7$, $m = 4$ species. In this case, the photodetachment laser is tuned to 3000 cm^{-1} (0.372 eV), which should deplete only the isomers that contribute to the low-energy photoelectron band labeled as II in Figure 19. In the ensuing discussion we simply refer to isomer II as if it were a single species, although more than one structurally distinct isomer could, in fact, be contributing to the spectroscopic signatures associated with II. Interestingly, the interloper (*) peak is completely removed by the photodetachment laser, establishing that this feature is in fact due to isomer II as anticipated above.

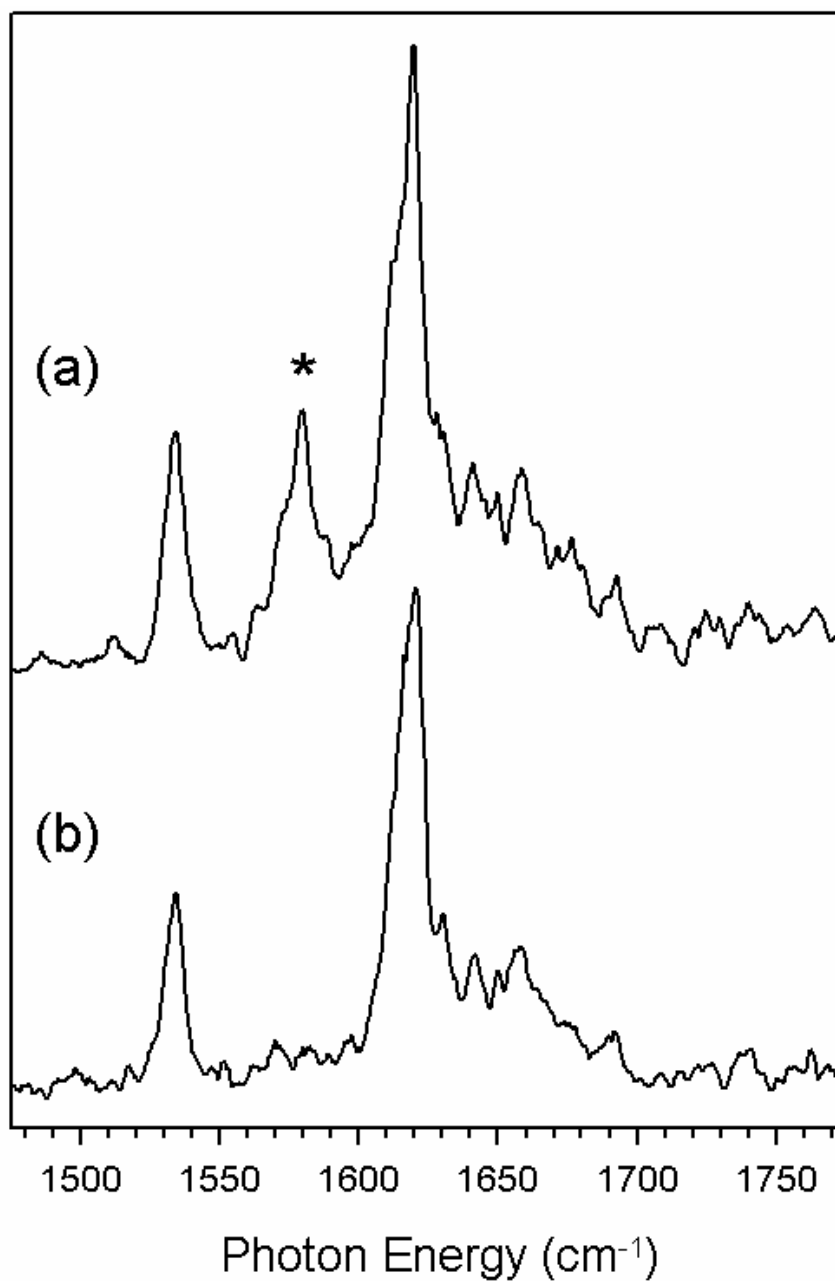


Figure 22. Infrared spectrum of $(\text{H}_2\text{O})_7^- \cdot \text{Ar}_4$ (a) before and (b) after bleaching the ion packet with an infrared laser tuned to 3000 cm^{-1} (0.372 eV). The bleaching laser removes isomer II from the population, leaving only isomer I for interrogation by the second infrared laser. The persistence of the red-shifted HOH bend transition at 1535 cm^{-1} after photobleaching establishes that isomer I exhibits an AA-type electron binding motif.

The contribution of the type II isomer to the heptamer bending spectrum can be isolated by subtracting the laser off-laser on spectra in Figure 22. The resulting pattern is compared in Figure 23 with the corresponding spectra recovered previously for the type II $n = 6$ (scaled from the D₂O spectrum) and $n = 8$ anions.^{170,183} All three spectra display a dominant feature near 1580 cm⁻¹, i.e, which occurs with about half the red-shift (relative to the isolated bend origin in H₂O) that is observed for the sharper AA bands associated with their type I forms.

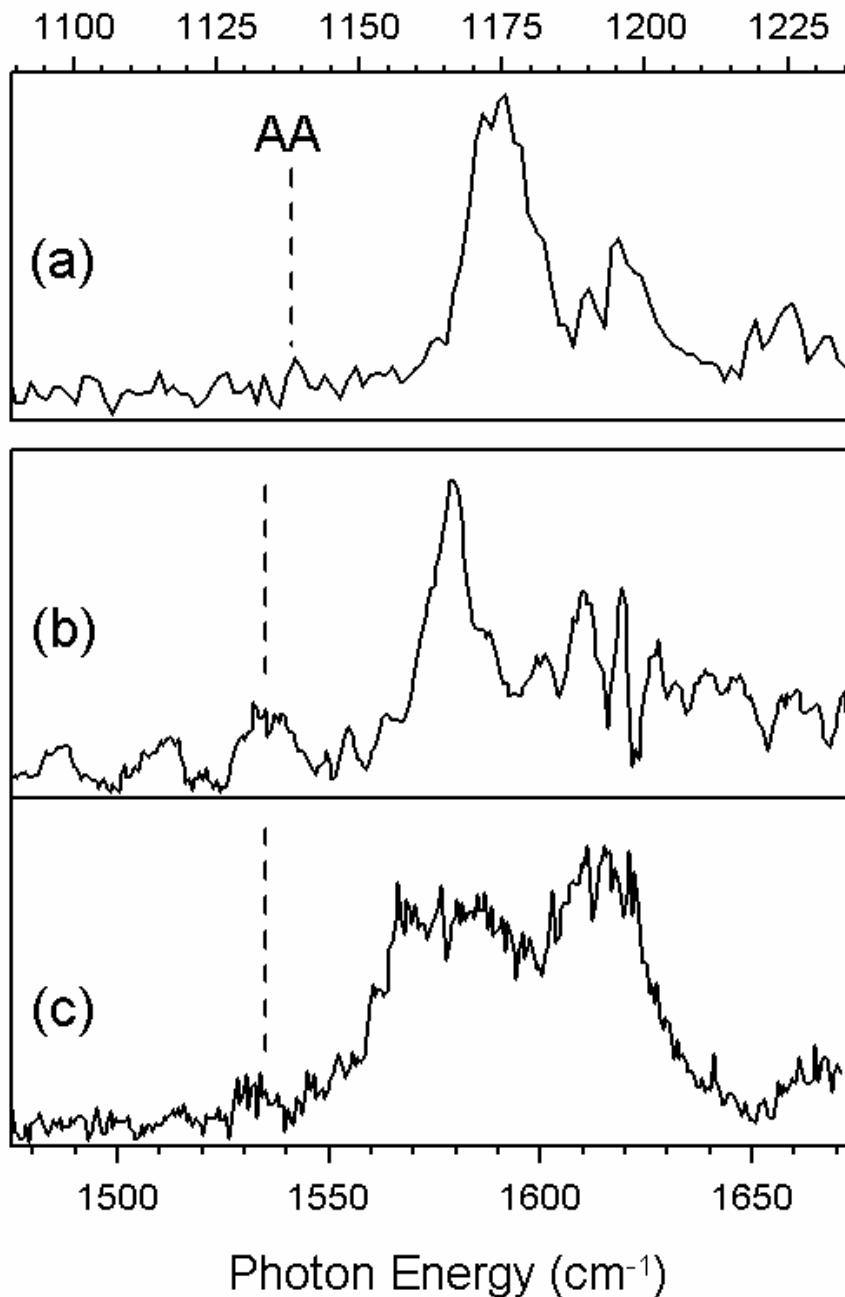


Figure 23. Infrared HOH bending spectrum of the isomer II variant of $(\text{H}_2\text{O})_7^- \cdot \text{Ar}_4$ (trace b), determined by subtraction of trace (b) from trace (a) in Figure 22, shown in comparison with the analogous spectra for $(\text{D}_2\text{O})_6^-$ (trace a) and $(\text{H}_2\text{O})_8^-$ (trace c) species from previous studies.^{170,183} All three species exhibit intensity that is either at or slightly red-shifted from the free H_2O bending frequency (1595 cm^{-1} for H_2O and 1178 cm^{-1} for D_2O), indicative of similar electron binding motifs, in which one or more dangling OH groups serve as the capture point for the excess electron. The dashed line indicates the position of the red-shifted AA band present in isomer I species.

It is noteworthy that, although the photoelectron spectra (Figure 19) seem to indicate that very little of the ensemble is actually present as isomer II, the vibrational spectrum arising from this isomer is a significant fraction ($\sim 10\%$) of the oscillator strength in the bending region. This effect can be rationalized if one considers that the infrared spectra are acquired in a linear action regime as opposed to the saturated regime used to obtain the photoelectron spectrum. Thus, the two observations are consistent if the 1580 cm^{-1} bending vibrational feature associated with type II has a much larger absorption cross section than do the bending vibrations arising from the higher electron binding species. In this regard, it is relevant to note that the low electron binding energy of isomer II places its excited bending energy level quite close to the direct photodetachment continuum. This property, when combined with the fact that the charge distribution of the excess electron is larger in II than in I, likely creates an enhancement mechanism where the vibrational transition moment is amplified by the strong interaction between the bending motion and the more diffuse excess electron wavefunction.¹⁷³

Several of the minimum energy structures recovered in our theoretical survey are consistent with the low VDE and the lack of an AA electron binding site for isomer II. One such structure (designated Pr-b in Figure 18) is included in Figure 24, along with a contour of the excess electron wavefunction and calculated harmonic spectrum in the bending region. This structure indeed displays a very intense transition, with an intermediate red-shift that arises mostly from the vibration of the hydrogen atom most closely contacting the excess electron cloud. This H atom is associated with a water molecule residing in an AAD H-bonding site in the supporting network. However, it is important to note that the electron binding arises from the fact that the cluster has several OH groups aligned in approximately the same direction, resulting in a net dipole moment of about 8.8 D.

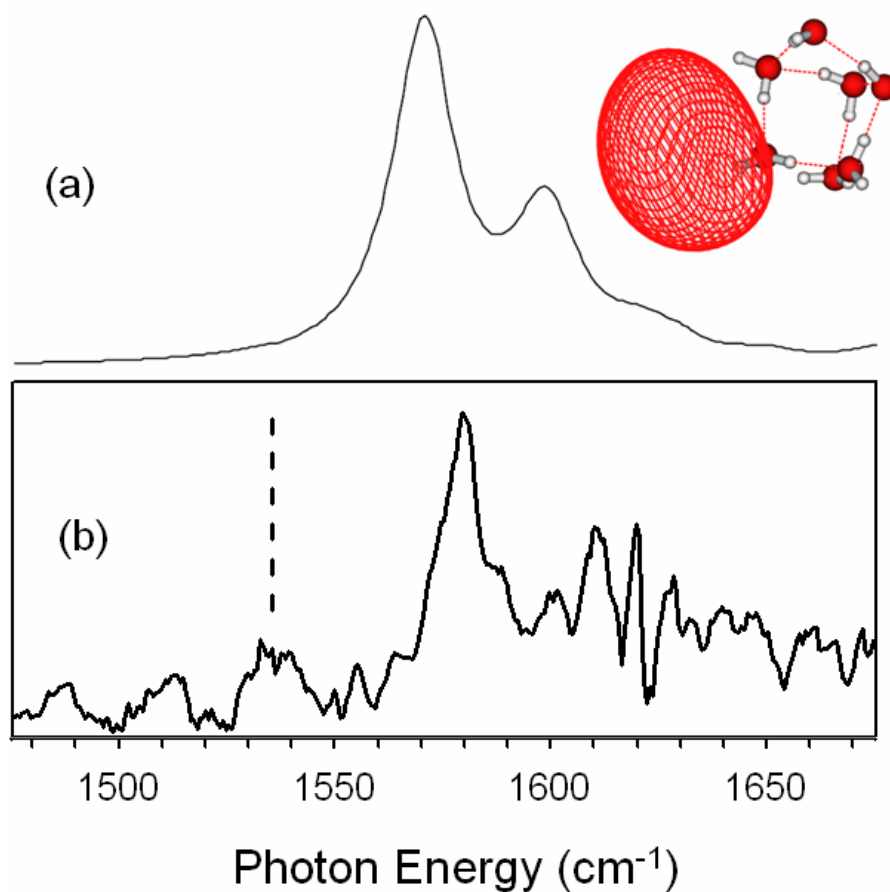


Figure 24. Calculated structure and infrared spectrum of a $(\text{H}_2\text{O})_7^-$ species with a non-AA type electron binding motif (a). The isomer shown is Pr-b, together with the orbital occupied by the excess electron. Vibrational frequencies were calculated at the MP2/6-31(1+,3+)G* level and scaled by 0.93. Peaks were given line widths of 9 cm^{-1} to facilitate comparison with the experimental spectrum (b).

8.4.6 Characterization of the type I and I' isomers in the bending region

The low electron binding energy of the type II species precludes the observation of sharp vibrational transitions in the OH (and OD) stretching region because these features are severely broadened by rapid vibrational autodetachment. Consequently, we had to rely on the bending

region exclusively for its structural characterization. For the I and I' forms, due to their higher electron binding energies, it was possible to measure both HOH bending and OH stretching vibrational spectra. We again used isomer-selective population modulation to selectively remove isomers with smaller VDEs from a mixed ensemble. We consider the spectra in the bending region first.

The bending vibrational spectrum characteristic of the type I isomer was already isolated for $(\text{H}_2\text{O})_7^- \text{Ar}_4$ (Figure 22b) when isomer II was removed by photodepletion. We compare this result with the type I spectra obtained previously for the $n = 6$ and 8 clusters in Figure 25. The bending spectrum of the type I isomer of all three of these clusters is dominated by three strong transitions, the low energy AA feature near 1530 cm^{-1} , an intense feature near 1620 cm^{-1} , just above the bending origin of the isolated water molecule (arrow), and a weaker feature near 1650 cm^{-1} . The two bands lowest in energy have been assigned in the hexamer to a dimer sub-cluster with water molecules in AA and AD H-bonding environments, respectively, forming a pocket that effectively traps the excess electron. Although, the persistence of this spectral signature suggests that this motif is maintained in the higher clusters, the theoretical results, discussed later, indicate that the AA molecule in the type I isomer of $(\text{H}_2\text{O})_7^-$, is actually in a different H-bonding environment.

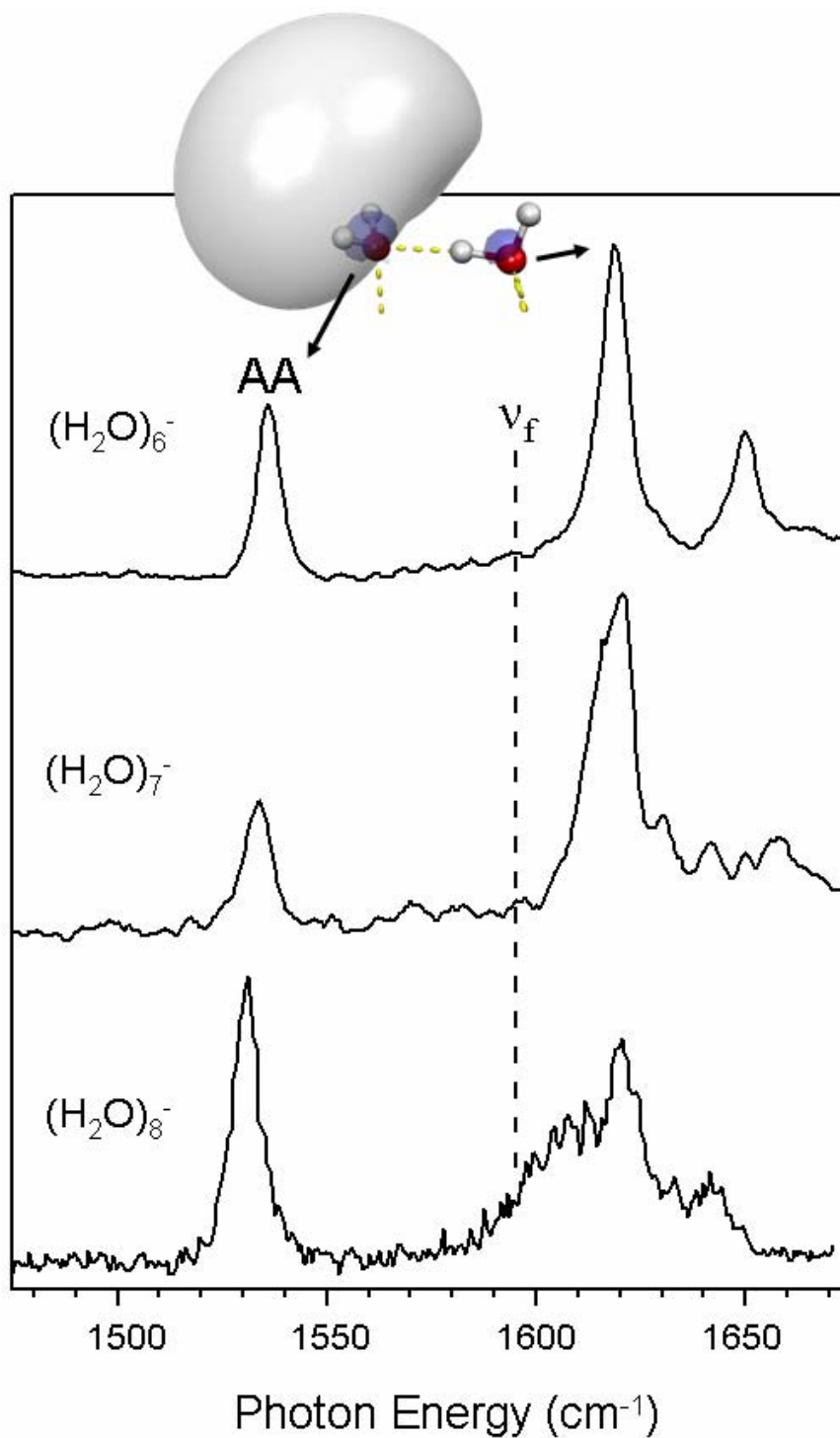


Figure 25. Infrared spectra of the isomer I species for $(\text{H}_2\text{O})_6^-$ (top panel), $(\text{H}_2\text{O})_7^-$ (center panel), and $(\text{H}_2\text{O})_8^-$ (bottom panel). The red-shifted peak at $\sim 1535 \text{ cm}^{-1}$ that is present in all species establishes that isomer I displays the AA-type electron binding motif. The similarity of the spectra in the 1600-1650 cm^{-1} range suggests that the supporting scaffolds of isomer I clusters in this size range share similar structural aspects.

Isolation of the vibrational spectrum of I' was accomplished using photodepletion at 3800 cm^{-1} , with the resulting spectrum in the bending region being displayed in Figure 26 along with that just obtained for type I. Most importantly, the spectrum of this new species also contains the characteristic AA band at 1530 cm^{-1} , with the most pronounced difference between I and I' being the introduction of a new strong band (labeled alpha) just above that arising from the AD water molecule in the hexamer structure.

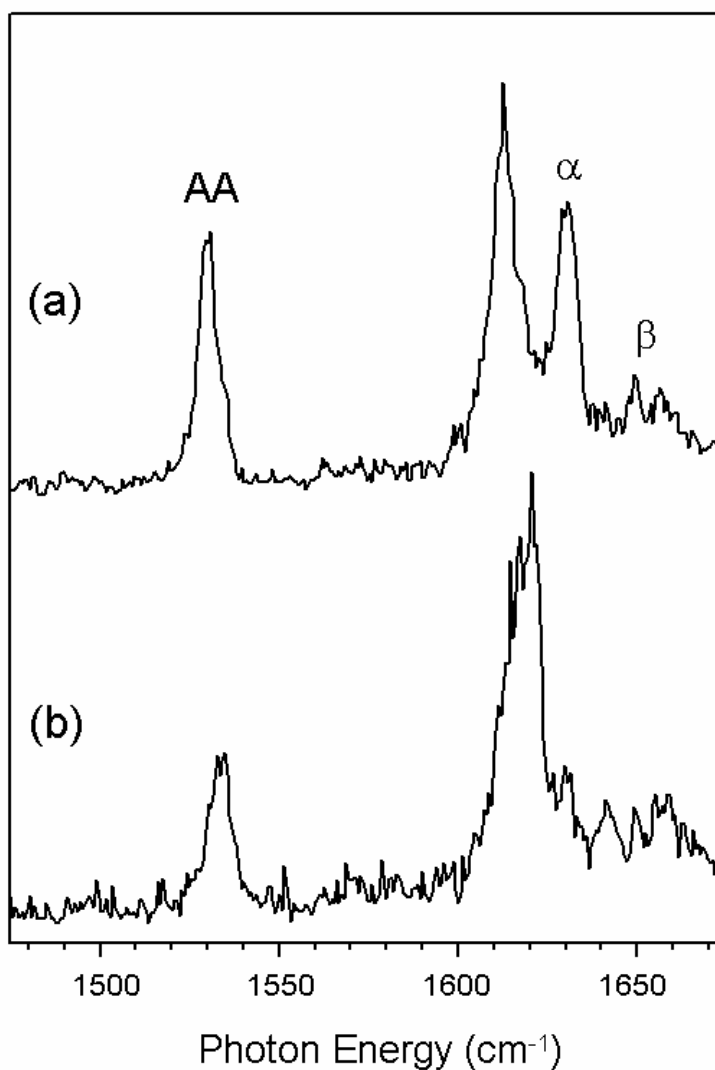


Figure 26. Comparison of the infrared spectra of $(\text{H}_2\text{O})_7^-$ (a) isomer I' and isomer I species in the HOH bending region. The isomer I' spectrum is obtained by photobleaching the ion packet with a laser tuned to 3800 cm^{-1} before interaction with the second infrared laser, thereby removing both isomers I and II from the population.

The calculations predict five isomers with a VDE near that observed for the type I species and six isomers near that observed for the type I' species. Before attempting assignments of these two isomers, we first examine the spectra in the OH stretch region.

8.4.7 Spectra of isomers I and I' in the OH stretching region

To further explore the nature of the H-bonding network in the I and I' isomers, we also measured the vibrational spectra in the OH stretching region with the results summarized in Figure 27. As in the bending spectra, there are significant changes in the pattern of stretching vibrations in the neighborhood of $m = 5$. The nature of this change is interesting in that, although two of the three dominant peaks in the low m spectra appear similar to the dominant doublet in the spectrum of 6(I), additional Ar atoms bring out many more peaks that effectively fill in the gap between the 6(I) doublet. There are also very low energy peaks (A and B) not found in the smaller negatively charged water clusters, and these are significant in that one of them (A at 3130 cm^{-1}) disappears at $m = 5$, and is replaced by a new feature (B) at 3000 cm^{-1} . This switchover is significant because these features are mutually exclusive in the two isomers. That is, when I' becomes evident in the PES, peak A is absent. Consequently, if A is indeed an intrinsic member of the I vibrational pattern, then its absence above $m = 5$ would appear to preclude the presence of I in this range, even though the photoelectron spectra still reveal a low energy shoulder signaling its contribution to the ensemble of ions. One is therefore left with the conclusion that there are at least two different isomeric forms within the photoelectron band nominally catalogued as "isomer I".

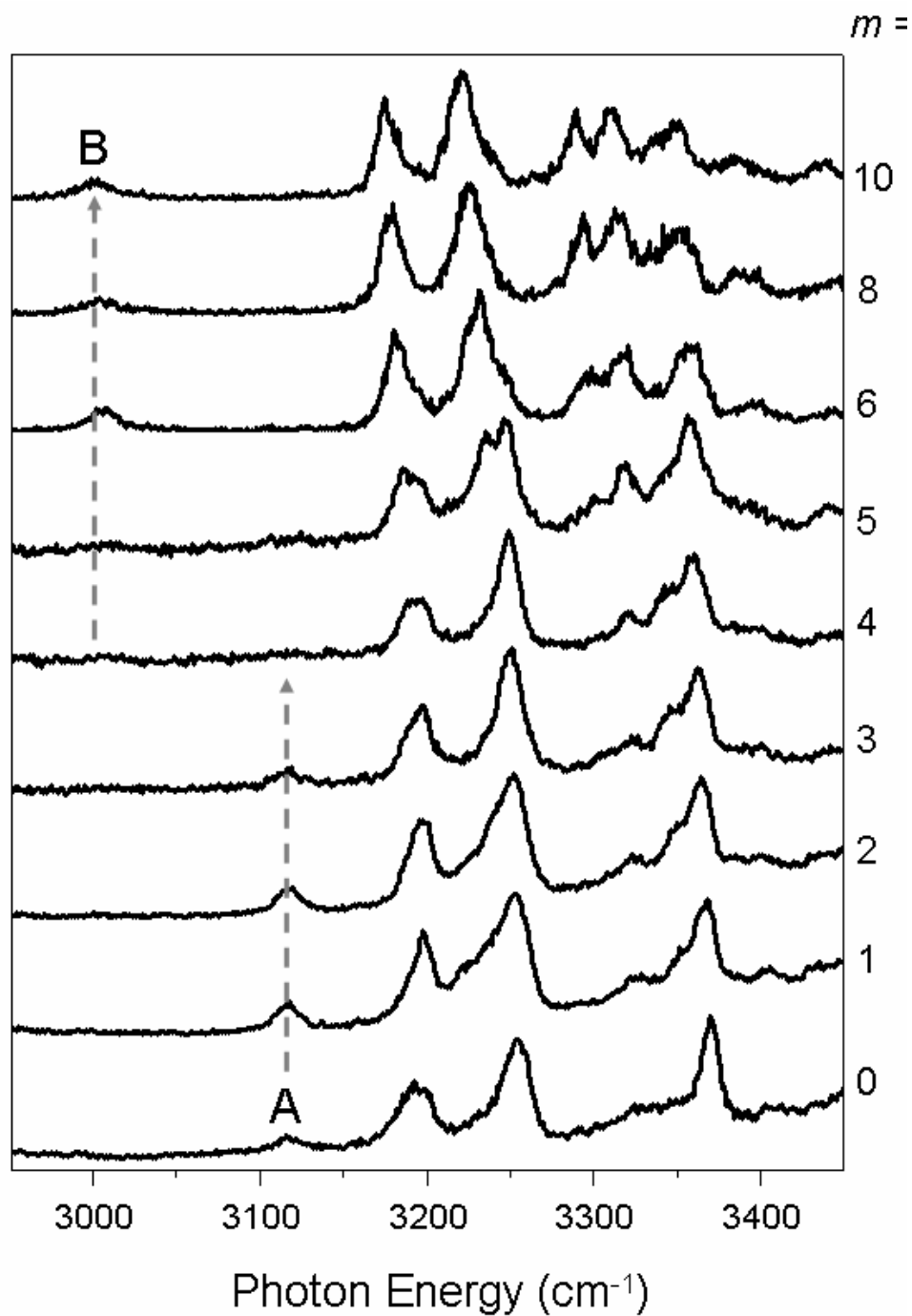


Figure 27. Argon dependence of $(\text{H}_2\text{O})_7^- \cdot \text{Ar}_m$ ($m = 0-10$) in the OH stretching region. The transition from isomer I to I' is most obvious at $m = 5$, where new distinguishable peaks emerge at 3200, 3250, and 3300 cm^{-1} .

With the behavior of the low energy (A and B) transitions in mind, it was of interest to explore whether the contribution from the 0.4 eV (“I”) VDE species for $m > 5$ indeed has the same vibrational pattern as that displayed by the type I isomer observed at low m . Figure 28 presents the response of the $m = 6$ stretching spectrum upon photochemical hole burning at 3800 cm^{-1} (0.47 eV). Interestingly, the depleted peaks representing the I ($m = 6$) contribution are similar to those displayed by I’ with the exception of the peak labeled by C, which is not present in the 0.4 eV binding energy spectrum, and the peak labeled D which is unique to I at high m . This is not the pattern observed at low m , indicating that Ar solvation not only brings in a higher binding species (I’), but also changes type I such that new peaks appear. This reinforces the conclusion based on the behavior of the low energy (A and B) bands, which indicated that the low m type I spectrum does not persist above $m = 5$. Note that such behavior was not observed in the hexamer anion, where Ar solvation (up to $m = 15$) did not fundamentally change the pattern of the vibrational structure of the type I isomer, but rather caused a continuously increasing red-shifting of the same spectral features.

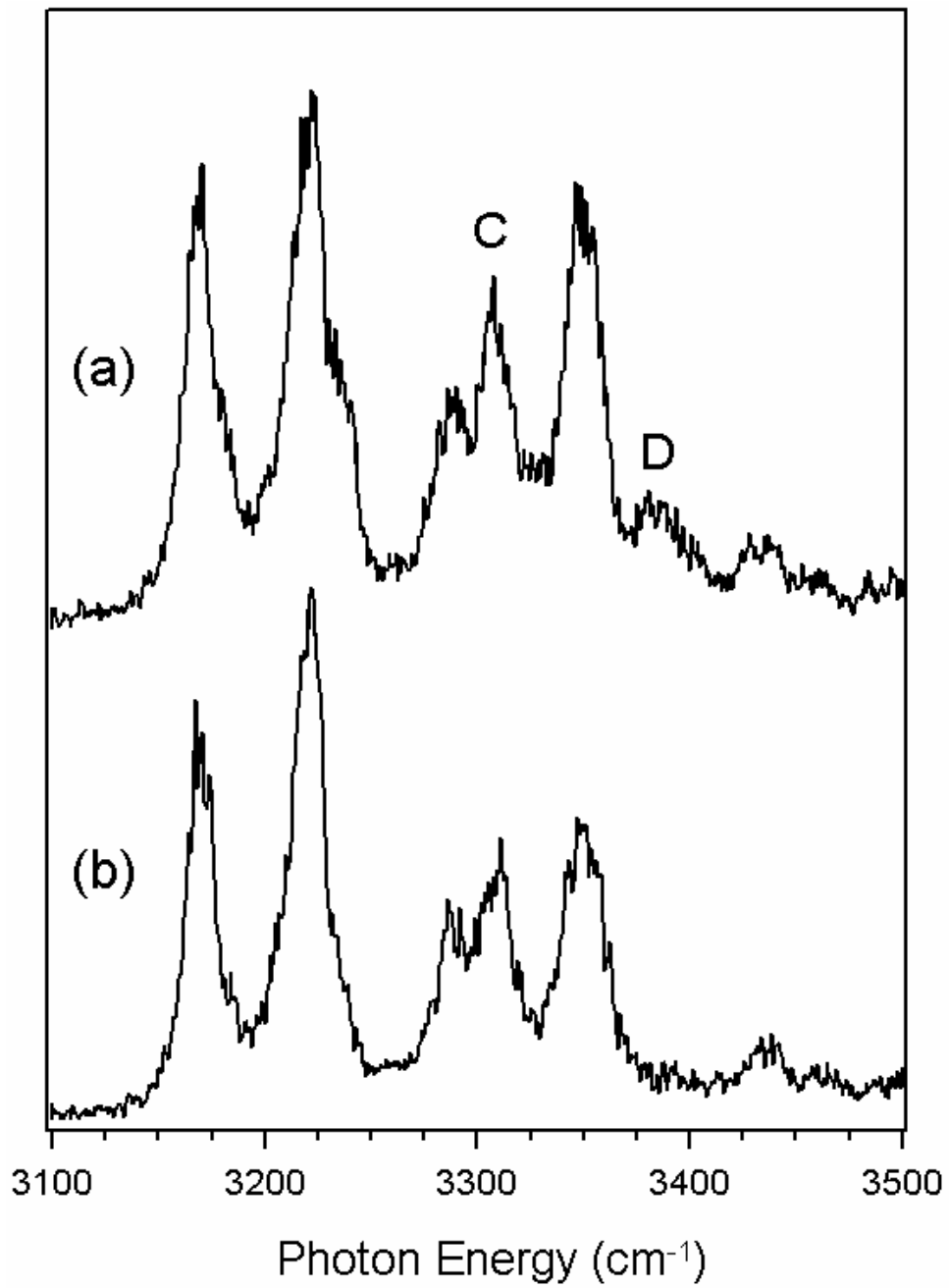


Figure 28. OH stretch region vibrational spectrum of of $(\text{H}_2\text{O})_7^- \text{Ar}_6$ (a) and the spectrum of isomer I' (b) obtained by hole burning at 0.47 eV.

The observation of a unique stretching pattern for the I ($m > 5$) species of course raises the question of whether its bending spectrum is also distinct from that obtained at low m . Unfortunately, we were not able to achieve sufficient signal-to-noise in the burn data at large m to distinguish this pattern from that displayed by I'.

8.5 SUMMARY OF THE M-DEPENDENCE OF THE $(\text{H}_2\text{O})_7^- \text{AR}_M$ SPECTRA: EMERGENCE OF COMPLEXITY

Similar to the situation observed previously for $(\text{H}_2\text{O})_6^-$ and $(\text{H}_2\text{O})_8^-$, the HOH bending spectra of the low VDE isomer II form of $(\text{H}_2\text{O})_7^-$ indicate that this species does not possess a double acceptor (AA) water molecule in the local electron binding motif. The situation with the higher VDE species is more complicated, however, as at least three distinct isomers appear to be at play depending on the number of Ar atoms in the system. Simple behavior is recovered at small size, where the bend and stretch spectra appear quite similar to those recovered by the type I isomer in the hexamer, and this pattern persists until $m = 5$. Unlike the smooth response of the hexamer to Ar solvation, however, an abrupt change occurs above $m = 5$ in the vibrational spectra of $(\text{H}_2\text{O})_7^- \text{Ar}_m$ that is commensurate with the emergence of a new photoelectron band (I') with VDE = 0.6 eV. This new species continues to display the characteristic AA band in the bending region but yields a distinct new feature at higher energy, and its OH stretching spectrum consists of a set of five or so peaks in place of the three that dominated the type I spectrum at low m . The most perplexing aspect of this data set is the observation that, even though the photoelectron band peaking at 0.4 eV persists at all Ar cluster sizes, the vibrational spectra associated with the

nominal type I form also appears to change above $m = 5$ such that it yields more resolved peaks in both the stretch and bend regions, indicating that at least two different isomers are at play.

The complexity displayed by the high electron binding forms of the heptamer anion serves to emphasize that, as the size of a water cluster increases, the number of available isomers increases dramatically. In this context, it is not surprising that structural variations occur within the regimes previously coarsely divided into isomer classes according to overall VDE. It is thus important that even in the face of this complexity, the type I and type II isomers are clearly differentiated by a structural difference according to whether the electron binding site has a water molecule in an AA binding site for the excess electron. It is also of primary interest that, within the higher binding classes, there is a difference in electron binding energy of about 0.2 eV between species (I, I ($m > 5$), and I') that have many vibrational features in common. Thus, very subtle changes in the network arrangement, that preserve many aspects of the local binding environments, can lead to rather large (0.2 eV) changes in the overall electron binding energy.

8.5.1 Theoretical considerations of plausible structures for isomers I, I', and II

Based on comparison of the measured VDEs and the VDEs of the 28 low-energy isomers of $(\text{H}_2\text{O})_7^-$ characterized theoretically, there are four possible candidates for the type II species, and five and six viable candidates for the I and I' species, respectively. Although there is considerable similarity of the calculated vibrational spectra within each of these groups of isomers, comparison of the calculated and experimental spectra does permit us to narrow down the possibilities considerably. In particular, one of the most stable isomers characterized theoretically, Pr-b, appears to be the best match for type II (see Figure 25 above), although we cannot fully rule out the less stable H-a species. In addition, based on the comparison of the

calculated and measured spectra we attribute I ($m < 5$) to isomer Pnf-a and I ($m > 5$) to Pf24a. Although Pnf-a and Pf24a have similar VDEs and spectra in the bending region, the two species have several different features in the OH stretching spectra, which correlate with the experimental data and allow us to assign the peaks in the latter. Figure 29 displays the calculated spectra for Pf24a (top) and Pnf-a (bottom), together with the experimental ones. We note that the strongly red shifted peak B in the experimental spectrum is also present in the calculated spectrum for Pf24a. In addition, peak D (which was assigned to isomer I ($m > 5$) after the hole burning experiment in Figure 28) is apparent in the calculated spectrum of Pf24a. On the other hand, in Pnf-a, the lowest frequency OH transition (A) is less redshifted compared to Pf24a, in agreement with the experiment. Moreover, Pnf-a has the peak labeled “C”, which is missing in Pf24a, but is present in the experimental spectrum.

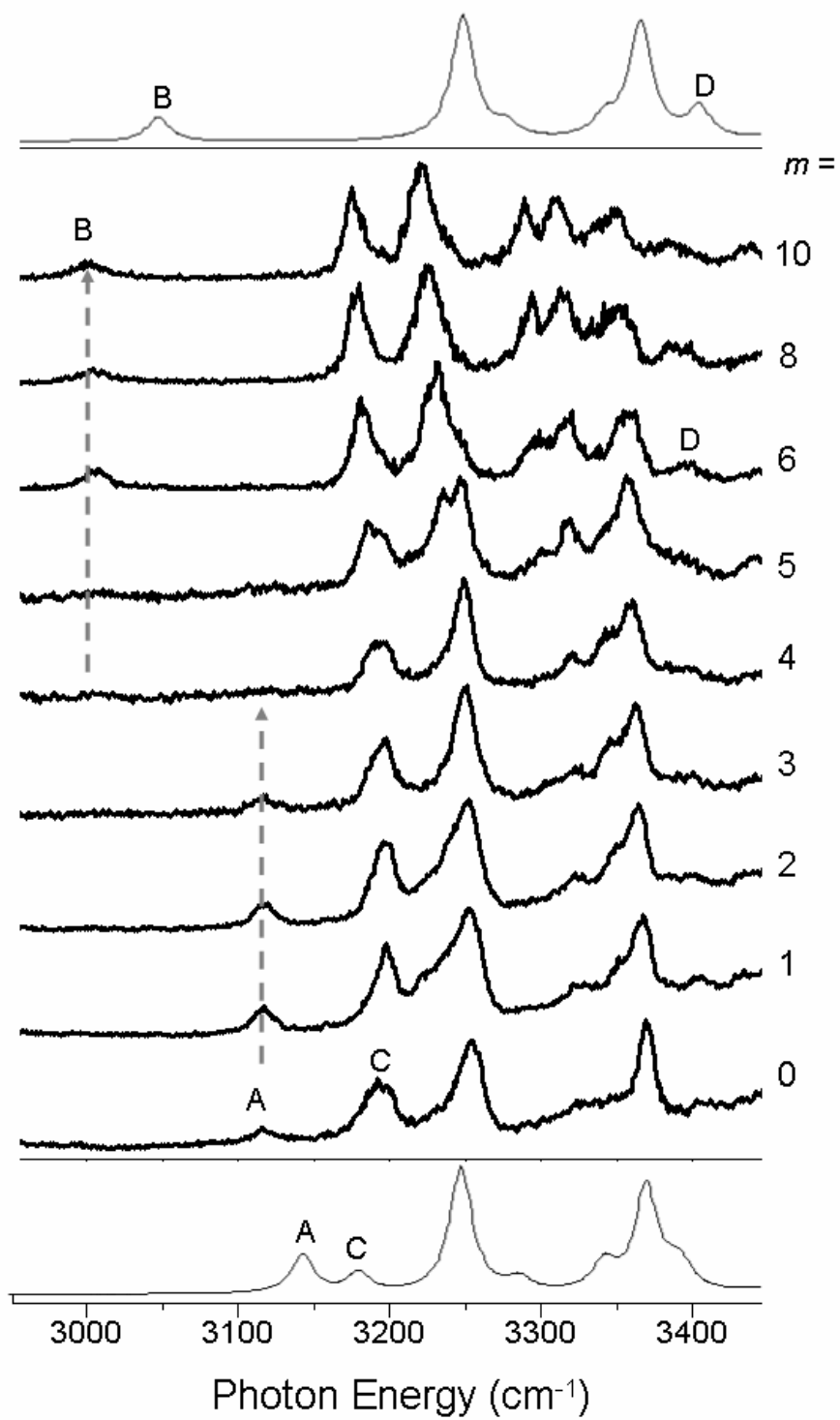


Figure 29. Calculated spectra of Pf24a (top) and Pnf-a (bottom), together with the experimental ones. Note that the experimental spectra here are not those of isolated isomers.

Comparison of the calculation results with experimental photoelectron and vibrational spectra also allows us to narrow down the choices for isomer I' and we assign it to Af-a. Figure 30 shows the bending spectra of the relevant species. The spectrum of Af-a in the bending region matches closely the experimentally observed one. However, the agreement between theory and experiment is less apparent in the OH stretching region. Figure 31 depicts the calculated (b) and experimental (c) spectra of Af-a and isomer I', respectively, in that region. Although the calculated frequencies agree with the experimental ones fairly well, this is not true for the intensities of the peaks. In particular, the strong peaks around 3165 cm^{-1} and 3290 cm^{-1} in the experimental spectrum show up as much less intense absorptions (in the calculated spectrum) relative to the other transitions. This might be attributed to the inadequate accuracy of the method and basis set used, as well as to a failure in the harmonic approximation. Another possibility is that another isomer, such as Af-e*, may be contributing to the spectrum. Indeed, the spectrum in Figure 31 (a) shows a very strong peak for the corresponding low-intensity frequency of the structurally very similar Af-a isomer. As seen in Figure 32, these two isomers differ only by the orientation of one dangling OH bond. Although their relative stabilities are very close to each other (Af-e* being lower in energy by 9 meV at the MP2/6-31(1+,3+)G* level of theory), their VDEs differ significantly. However, the energy at which the hole burning experiment to obtain the spectrum of I' was done (0.47 eV) is very close to the calculated VDE of Af-e* and the latter value is expected to increase significantly at a higher level of theory, which implies that this isomer may still be present in the jet expansion.

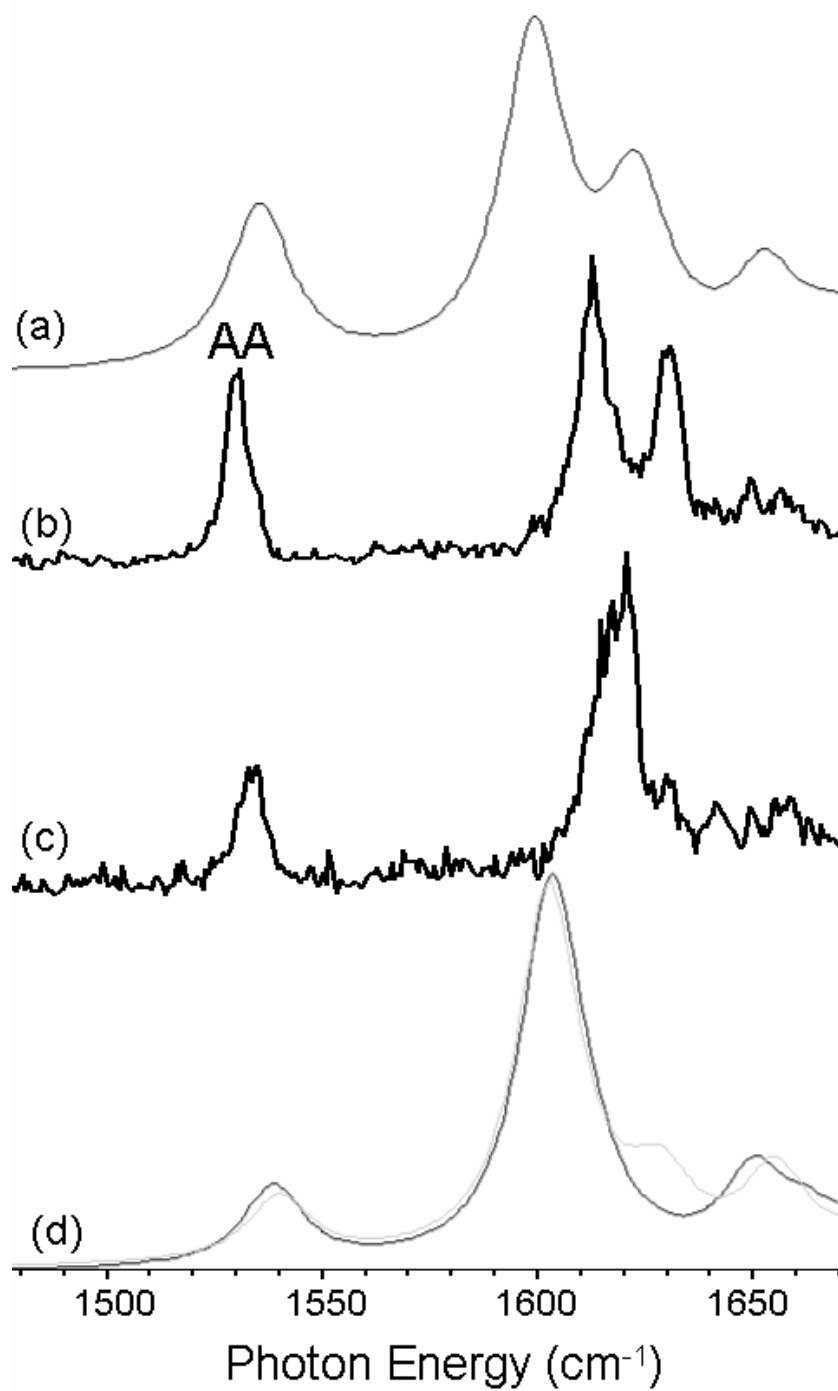


Figure 30. Comparison of isomers I' and I in the HOH bending region. (a) is the calculated spectrum for Af-a, and (b) is the corresponding experimental data. (c) shows the experimental spectrum of isomer I, while (d) depicts the corresponding calculated spectra of I ($m < 5$) and I ($m > 5$) [i.e., Pnf-a (bold) and Pf24a (pale), respectively].

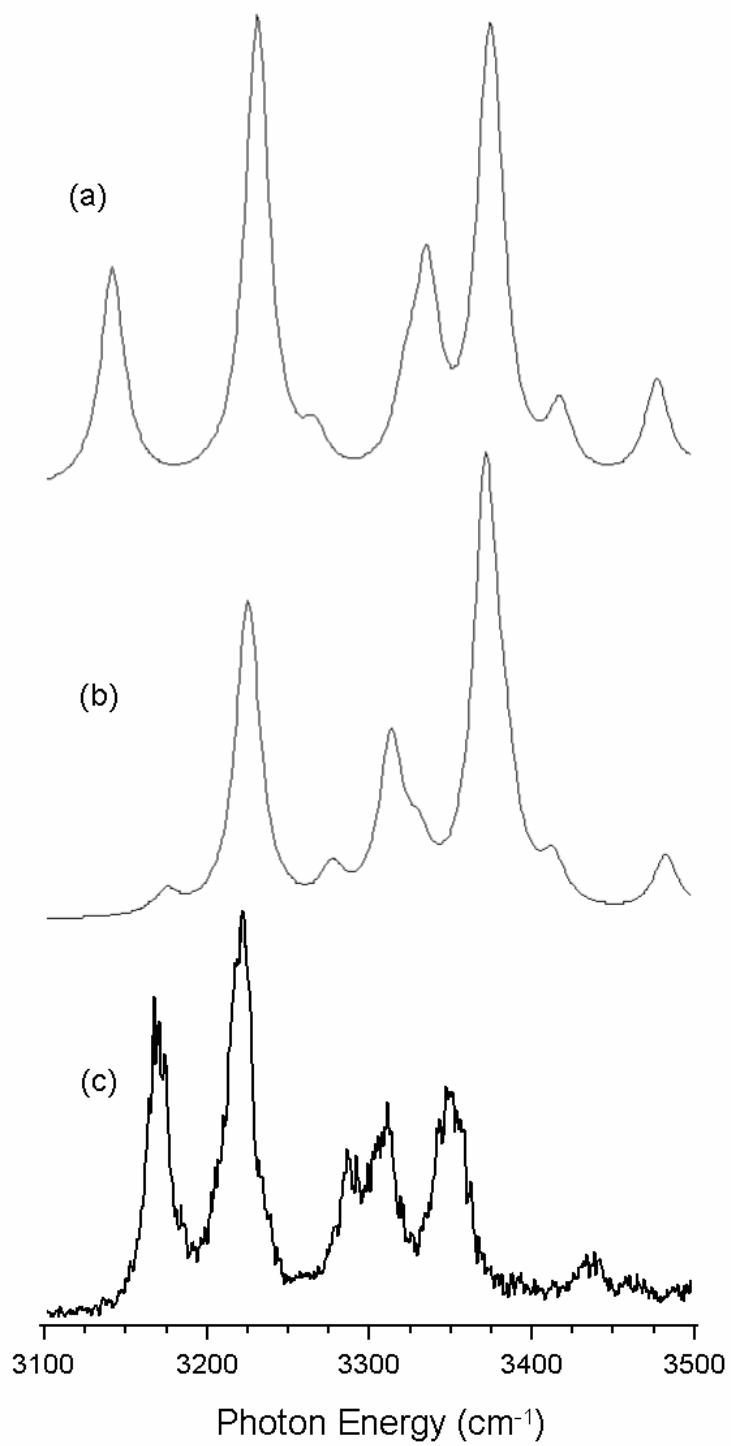


Figure 31. Calculated vibrational spectra of Af-e* (a) and Af-a (b), together with the experimental data from the hole burning experiment at 0.47 eV (c).

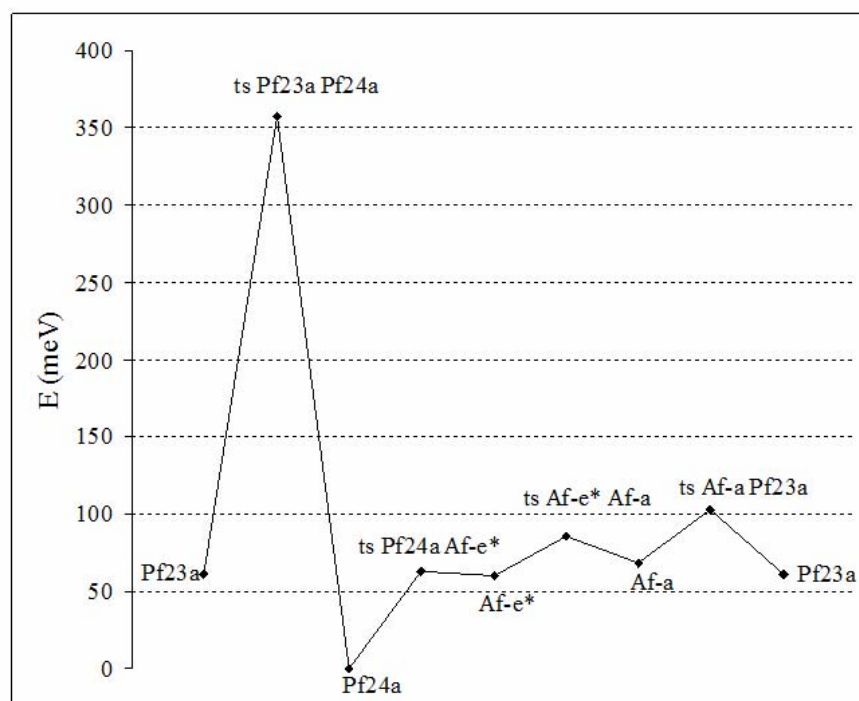
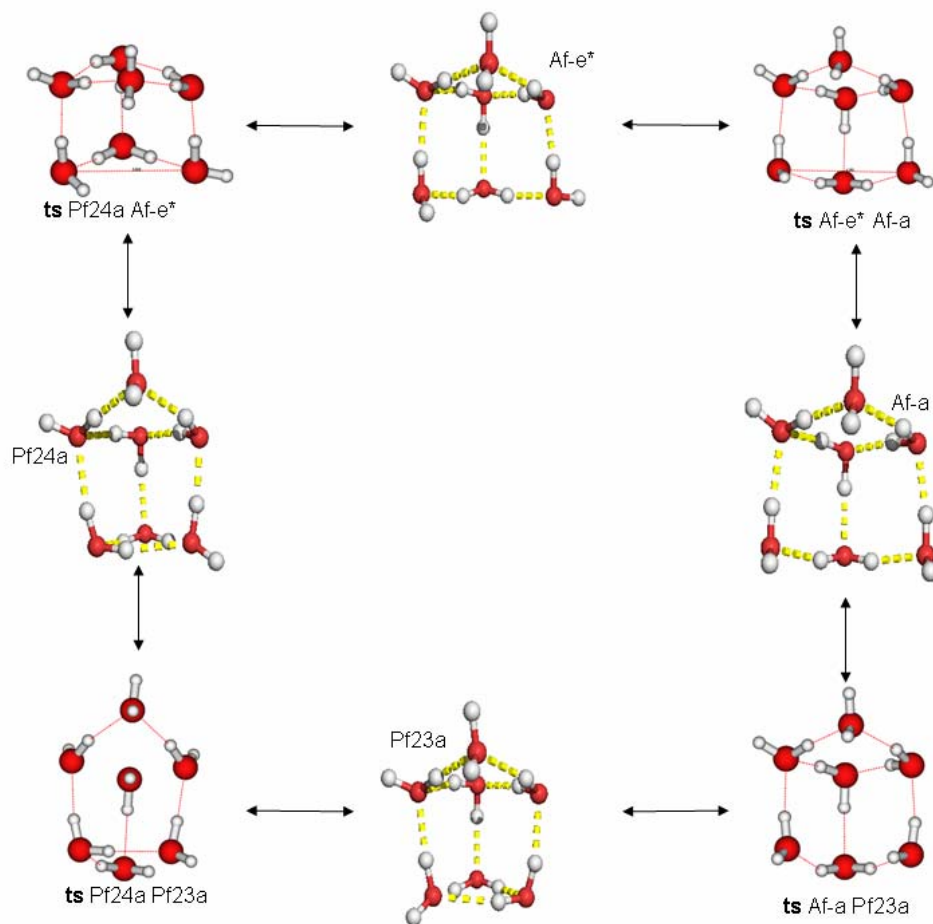


Figure 32. Barriers (meV) for interconversion between selected structures. “ts” denotes a transition state.

Figure 32 also shows the barriers for interconversion between several selected structures. Pf24a and Af-a differ only by one H-bond, i.e., breaking one H-bond in the 3-membered ring in Pf24a converts it to Af-a. However the potential energy surface is more complicated and that conversion goes through isomer Af-e*. The primary difference between Pnf-a and Af-a and Pf24a is that the former has a double donor water in the four membered ring containing the AA water, whereas the latter two clusters have the double donor water in the “base” of the cluster (i.e., in the intact or ruptured 3-membered ring). Pnf-a can be converted to Pf24a through a sequence of donor-acceptor exchanges. It is unlikely that in cold clusters with attached Ar atoms, such an interconversion can occur. It is more likely that the presence of different isomers of $(\text{H}_2\text{O})_7^-$ for different numbers of attached Ar atoms, is a consequence of trapping in different local minima as the clusters are cooled by Ar atom evaporation. However, it is possible that once Af-e* is formed, it can be converted to Pf24a. MP2/6-31(1+,3+)G* calculations predict the barrier for this conversion to be only 3 meV (see Table 22). The barrier for the conversion of Af-a to Af-e* on the other hand is 17 meV at the same level of theory.

Table 22. Relative energies (meV) of the structures shown in Figure 32.

| | |
|----------------|-----|
| Pf23a | 61 |
| ts Pf23a Pf24a | 358 |
| Pf24a | 0 |
| ts Pf24a Af-e* | 63 |
| Af-e* | 60 |
| ts Af-e* Afa | 86 |
| Af-a | 69 |
| ts Af-a Pf23a | 103 |
| Pf23a | 61 |

8.6 RECOMMENDATIONS FOR FURTHER WORK

Although calculations on small anionic water clusters suggest that their vibrational spectra can be tackled qualitatively at a relatively low level of theory, it is apparent that the procedure works due to near cancellation of errors, and involves the use of ambiguous scaling factors for the frequencies. In order to obtain more accurate frequencies, one needs to go beyond the harmonic approximation and the B3LYP or MP2 methods. This however is a computationally prohibitive procedure even for the small water cluster anions. An alternative would be to use the Drude model mentioned above to obtain vibrational frequencies of such clusters. This will require the coupling of the model to a flexible monomer model for neutral water. The Jordan group plans to undertake this task.

Another interesting phenomenon that can be studied using the Drude model is the dynamics in negatively charged water clusters. The model can be used in molecular dynamics simulations, which may provide a valuable insight into the long standing problem of electron solvation.

APPENDIX A

THEORETICAL INVESTIGATION OF THE NEUTRAL PRECURSOR OF $(\text{H}_2\text{O})_6^-$

This work was published as:

Myshakin, E. M.; Diri, K.; Jordan, K. D. *J. Phys. Chem. A* 2004, 108, 6758.

A.1 ABSTRACT

In a recent ingenious experiment Diken et al. (Diken, E. G.; Robertson, W. H.; Johnson, M. A. *J. Phys. Chem. A* **2004**, 108, 64) obtained the vibrational spectrum in the OH stretch region of the neutral $(\text{H}_2\text{O})_6$ precursor to the $(\text{H}_2\text{O})_6^-$ ion. Comparison of the measured spectrum with the calculated harmonic vibrational spectra of various low-energy isomers of $(\text{H}_2\text{O})_6$ led these authors to conclude that the observed spectrum is due to the book isomer, although agreement between theory and experiment is only qualitative. In the present study a hybrid MP2/QCISD method is used to overcome a shortcoming of earlier theoretical calculations of the harmonic spectra of low-energy $(\text{H}_2\text{O})_6$ isomers, and the coupling of the fundamentals with overtones and combination states is accounted for by means of a cubic force-field approximation. The results of

these calculations provide further support for the assignment of the book form of $(\text{H}_2\text{O})_6$ as the precursor of the dominant observed $(\text{H}_2\text{O})_6^-$ isomer.

A.2 INTRODUCTION

Negatively charged water clusters were first observed by Haberland and co-workers in 1984.¹ Since that time there have been numerous experimental²⁻¹⁵ and theoretical studies¹⁵⁻²⁶ of these fascinating species. $(\text{H}_2\text{O})_6^-$, in particular, has attracted considerable attention, in part because it is the smallest water cluster displaying a well-defined vibrational spectrum in the OH stretch region.^{11-13,15} Several different structures have been proposed for $(\text{H}_2\text{O})_6^-$.^{11,15-20} To date, comparison of the vibrational spectra calculated for various $(\text{H}_2\text{O})_6^-$ isomers with the experimentally determined spectrum has not permitted a definitive assignment of the isomer responsible for the spectrum. What is clear from the theoretical studies is that the anion has a geometry appreciably different from that of any of the low-energy forms of the neutral cluster.^{15,19-21} Thus, either the electron-capture process is accompanied by a substantial rearrangement of the H-bonding network or it involves a high-energy isomer of the neutral cluster.

Recently, Johnson and co-workers have carried out a novel experiment allowing them to obtain the vibrational spectrum of the neutral $(\text{H}_2\text{O})_6$ cluster that is responsible for the observed $(\text{H}_2\text{O})_6^-$ spectrum.²⁷ This was accomplished by monitoring the formation of $(\text{H}_2\text{O})_6^-$ upon IR absorption by $(\text{H}_2\text{O})_6\text{Ar}_{10-12}$ followed by electron capture. Comparison of the calculated harmonic spectra for various low-energy isomers of the neutral $(\text{H}_2\text{O})_6$ cluster with the measured spectrum revealed that the best agreement was with the spectrum calculated for the book form of

(H₂O)₆. However, there are significant differences between the calculated and measured spectra, even after scaling the calculated harmonic frequencies to account approximately for anharmonicity effects. There are two major sources of error in calculations of the vibrational frequencies of various isomers of (H₂O)₆ carried out to date, namely, the use of the normal-mode approximation and the neglect of high-order electron correlation effects. With regards to the latter, both the MP2 and density functional methods, e.g., Becke3LYP,^{28,29} that have been used in earlier theoretical studies of (H₂O)₆, tend to overestimate the elongation of OH bonds engaged in H-bonding, causing too large a red shift in the associated vibrational frequencies.^{15,30,31} The remedy to this problem is well-understood, namely, to optimize the geometries and to calculate the vibrational frequencies using a method such as coupled-cluster theory that recovers high-order correlation effects.³¹ However, such calculations with suitably flexible basis sets would be computationally prohibitive for a cluster of the size of (H₂O)₆.

In the present study, we use a hybrid MP2/QCISD³² approach to calculate the harmonic vibrational spectra of the lowest energy ring, cage, prism, and book isomers of (H₂O)₆. These isomers, which are depicted in Figure 1, are known from prior theoretical studies³³⁻³⁶ to be close in energy. The hybrid MP2/QCISD approach is used to overcome the problems associated with the use of MP2 or DFT geometries for calculating frequencies. In addition, the effects of vibrational anharmonicity, specifically the coupling of the fundamentals with overtones and combination states, are calculated using a cubic force field. Comparison of the calculated and measured²⁷ spectra allows us to conclude unambiguously that the book isomer of (H₂O)₆ is the precursor of the dominant form of (H₂O)₆⁻. We conclude by discussing the implications of these results for the formation of (H₂O)₆⁻.

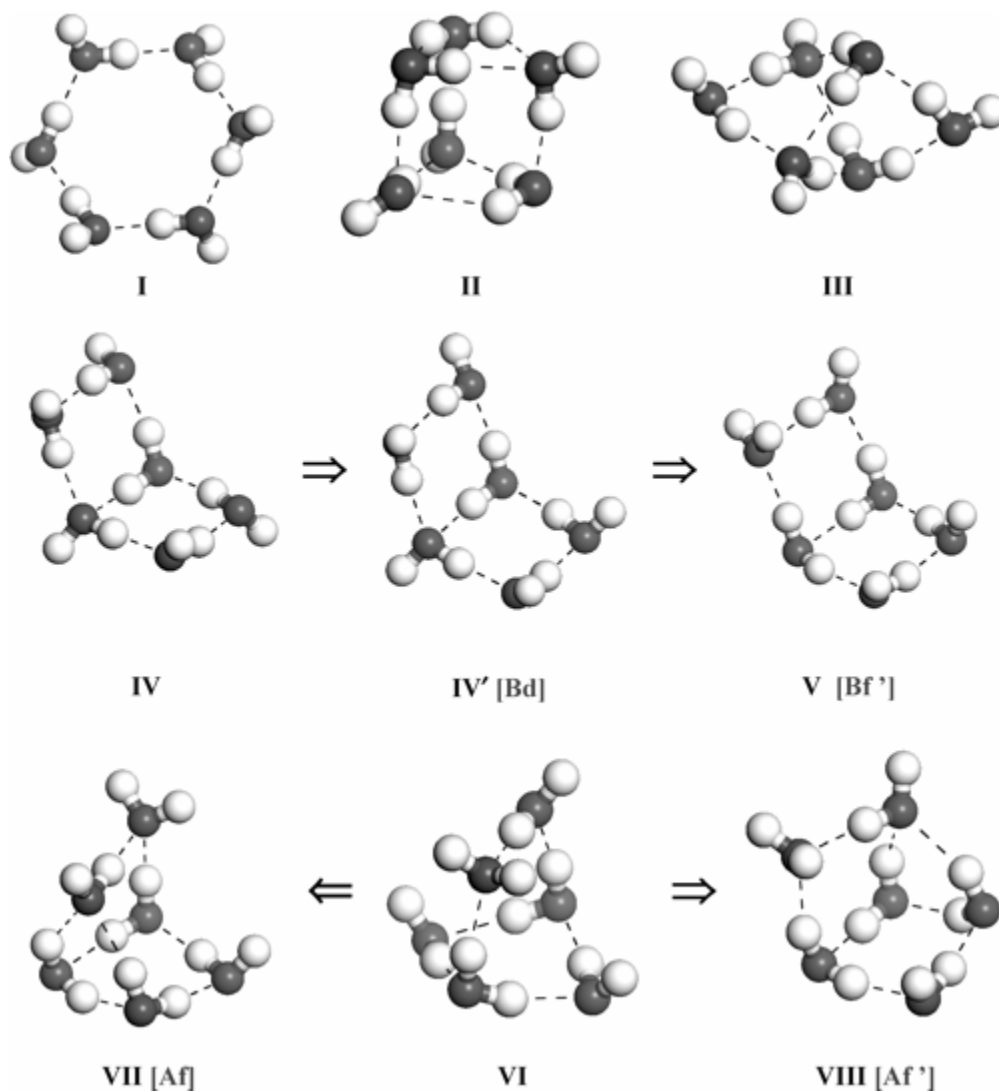


Figure 1. Low-energy isomers of $(\text{H}_2\text{O})_6$ and $(\text{H}_2\text{O})_6^-$ considered in this study. Structures I-IV correspond, respectively, to the lowest energy ring, prism, cage, and book forms of neutral $(\text{H}_2\text{O})_6$. IV' and V-VIII are local minima of the anion. The arrows indicate a possible pathway for proceeding from the neutral book to the most stable forms of the anion (VII and VIII). V can rearrange to VIII either by direct means or via intermediate VI. IV' differs from IV only with respect to the flip of one of the free OH groups. This flip is accompanied by an increase in the dipole moment and, hence, by increased electron binding.

A.3 METHODOLOGY

In the present approach the QCISD procedure,³² which is closely related to the coupled-cluster singles-plus-doubles (CCSD) method, was used to optimize the geometries of the lowest energy ring, cage, book, and prism isomers of $(\text{H}_2\text{O})_6$. The resulting geometries were then used to calculate the harmonic vibrational frequencies using the MP2 method. Hereafter, this will be referred to as the MP2/QCISD method. A detailed study of the $(\text{H}_2\text{O})_n$, $n = 2-4$, clusters has shown that this approach gives vibrational frequencies and intensities for the OH stretch vibrations very close to those obtained from calculations in which the QCISD method is used for both the geometry optimizations and the vibrational frequency calculations.³¹ The 6-31+G[2d,p]^{37,38} basis set was used for the majority of the calculations on the neutral clusters. To establish that this basis set is suitable for calculating the structures and the harmonic vibrational spectra, in the case of the cage isomer the calculations were also carried out with the more flexible aug-cc-pVDZ^{39,40} basis set. The Gaussian 03⁴¹ program suite was used for the calculations.

To account for "near-degeneracy" mixing of the OH stretch with combination and overtone bands, the cubic force constants were calculated at the Becke3LYP level. (Studies of smaller water clusters have shown that there is fairly good agreement between the cubic couplings calculated in the Becke3LYP and MP2 approximations.³¹) The Hamiltonian allowing for cubic couplings was constructed by combining the MP2/QCISD fundamental frequencies and Becke3LYP cubic force constants, with the former being scaled to allow for "diagonal" anharmonicities and the latter to compensate for the tendency of the cubic-force field method to overestimate the couplings.⁴²⁻⁴⁴ The vibrational spectra were calculated variationally using this Hamiltonian and bases consisting of the OH stretch fundamentals and all combination and

overtone states that fall within 600 cm^{-1} of the OH stretch fundamentals.^{42,43} The intensities of the various transitions were assumed to derive from the OH stretch normal modes, and the dipole moments were assumed to vary linearly with the OH stretch coordinates. All calculated vibrational lines were given Gaussian line shapes with 7 cm^{-1} half-widths to facilitate comparison with experiment.

In addition to presenting new theoretical results for the vibrational spectra of various isomers of the neutral $(\text{H}_2\text{O})_6$ cluster, we also examine pathways for rearrangement of the neutral book isomer to the most stable form of the anion. These calculations were carried out at the Becke3LYP level using the 6-311++G**(sp) basis set, formed by adding on the O atoms extra diffuse sp Gaussian functions⁴⁵ to the 6-311++G** basis set.^{46,47}

A.4 RESULTS

Rotational constants have been determined experimentally for the cage isomer of $(\text{H}_2\text{O})_6$,^{48,49} making this a valuable system for judging the reliability of various theoretical methods for predicting the geometries of H-bonded clusters. Our QCISD/6-31+G[2d,p] and QCISD/aug-cc-pVDZ calculations for this isomer give rotational constants of 2183, 1139, and 1065 MHz, and 2186, 1123, and 1077 MHz, respectively. These two sets of rotational constants are in close agreement with one another and with experiment (2162, 1129, and 1067 MHz), thereby establishing the suitability of the 6-31+G[2d,p] basis set for calculating the geometries of the clusters. In contrast, the rotational constants associated with the MP2/aug-cc-pVDZ-optimized geometry, 2240, 1151, and 1104 MHz, are in much poorer agreement with experiment.⁵⁰

The calculated harmonic spectra in the OH stretch region for the book, ring, cage, and prism isomers of $(\text{H}_2\text{O})_6$ are reproduced in Figure 2 together with the experimental spectrum measured by Diken et al.²⁷ The calculated OH stretch frequencies have been reduced by a factor of 0.942 to correct in an approximate manner for vibrational anharmonicity. Overall, the calculated harmonic spectrum for the book isomer is in the best agreement with the measured spectrum, as was concluded previously by Diken et al.²⁷ Moreover, the agreement between theory and experiment is significantly better than when using the harmonic spectrum calculated using the MP2 method (in which the same approach is used to optimize the geometry and to calculate the frequencies).

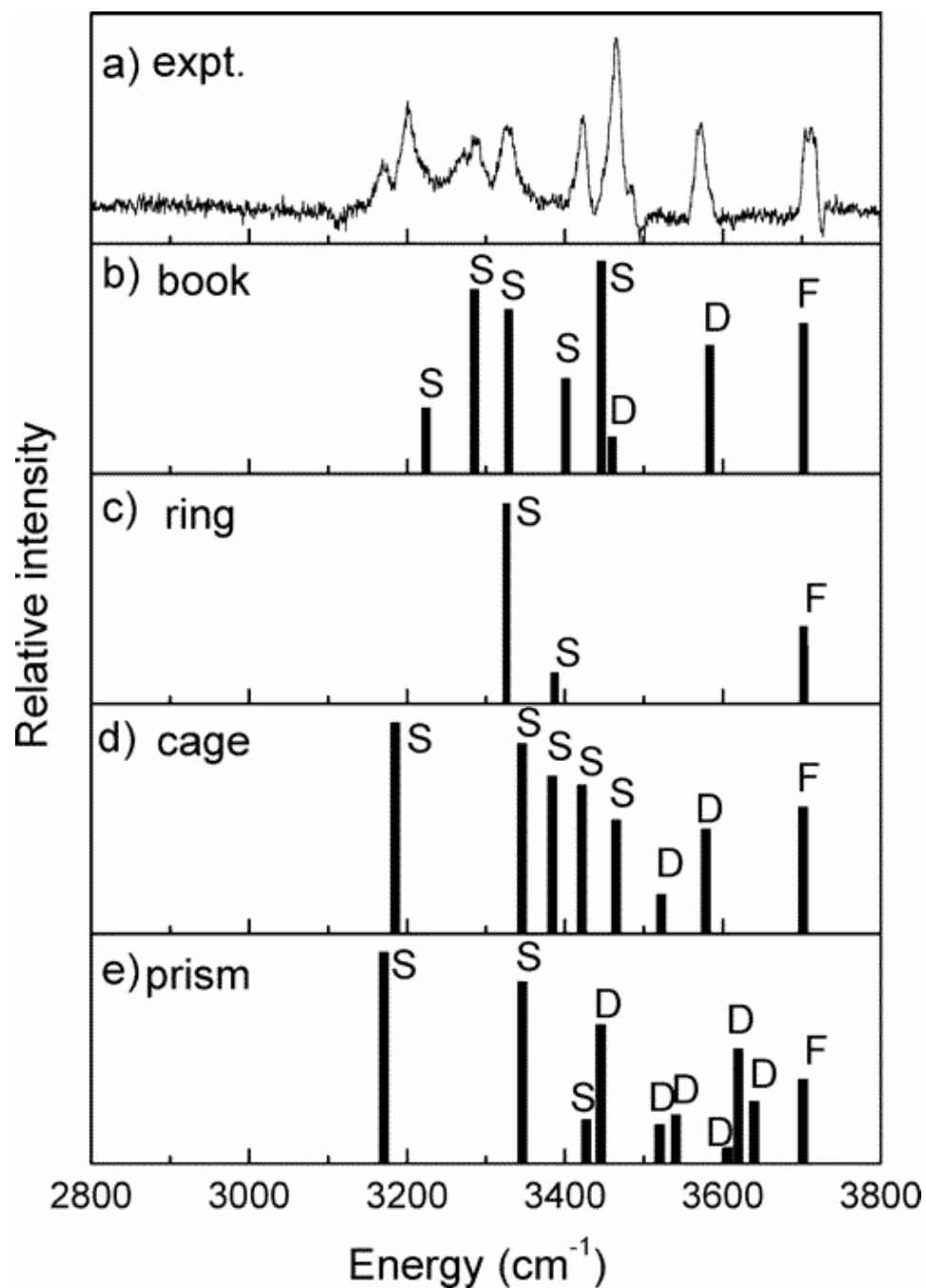


Figure 2. Vibrational spectra of the $(\text{H}_2\text{O})_6$ cluster in the OH stretch region. The experimental spectrum (a) results from $(\text{H}_2\text{O})_6\text{Ar}_{10-12}$ clusters that are precursors of $(\text{H}_2\text{O})_6^-$ (reproduced from ref 27). The theoretical spectra for the book (b), ring (c), cage (d), and prism (e) isomers were obtained in the harmonic approximation from MP2 calculations using QCISD geometries. The calculated frequencies have been scaled by 0.942. F and S denote, respectively, transitions associated with free and donor OH groups of single-donor water molecules, and D denotes transitions associated with double-donor water molecules.

Comparison of the calculated and experimental spectra allows us to conclude that the line observed near 3720 cm^{-1} is due to the five free OH stretch vibrations, those near 3450 and 3470 cm^{-1} are due to the OH stretch vibrations of the double-donor water, and the two lines near 3410 cm^{-1} are due to single-donor OH stretch vibrations. Nonetheless, there remains the problem that the experimental spectrum has five peaks between 3170 and 3330 cm^{-1} , whereas the calculated harmonic spectrum has only three single-donor OH stretch transitions in this range. This is not an unexpected result, since clusters containing water molecules often display extra structure in this region as a result of mixing of H-O-H bend overtones with the OH stretch fundamentals.^{51,52}

Figure 3 displays the vibrational spectra for the book, ring, cage, and prism isomers of $(\text{H}_2\text{O})_6$ calculated by allowing for mixing of the OH stretch fundamentals with overtones and combination states. The experimental spectrum is reproduced for comparison. In calculating these spectra, the frequencies of the OH stretch fundamentals were reduced by 0.942 , with this scale factor being determined by comparing the average of the OH stretch frequencies calculated in the harmonic and anharmonic approximations and using the Becke3LYP level of theory.³¹ For the other classes of vibrations (H-O-H bend, OH wag, intermolecular stretch) the MP2/QCISD harmonic frequencies were scaled by the factors needed to bring their average into agreement with the average of the anharmonic frequencies from the Becke3LYP calculations. The anharmonic frequencies used for determining the scaling factors were obtained using the second-order perturbative approach⁵³ implemented in Gaussian 03⁴¹ and will be reported in ref 31. In generating the theoretical spectrum reported in Figure 3, the cubic force constants were reduced by 15% to compensate for the tendency of the unscaled force constants to overestimate the couplings.⁴²⁻⁴⁴ However, it should be noted that this scaling does not significantly alter the appearance of the calculated spectra.

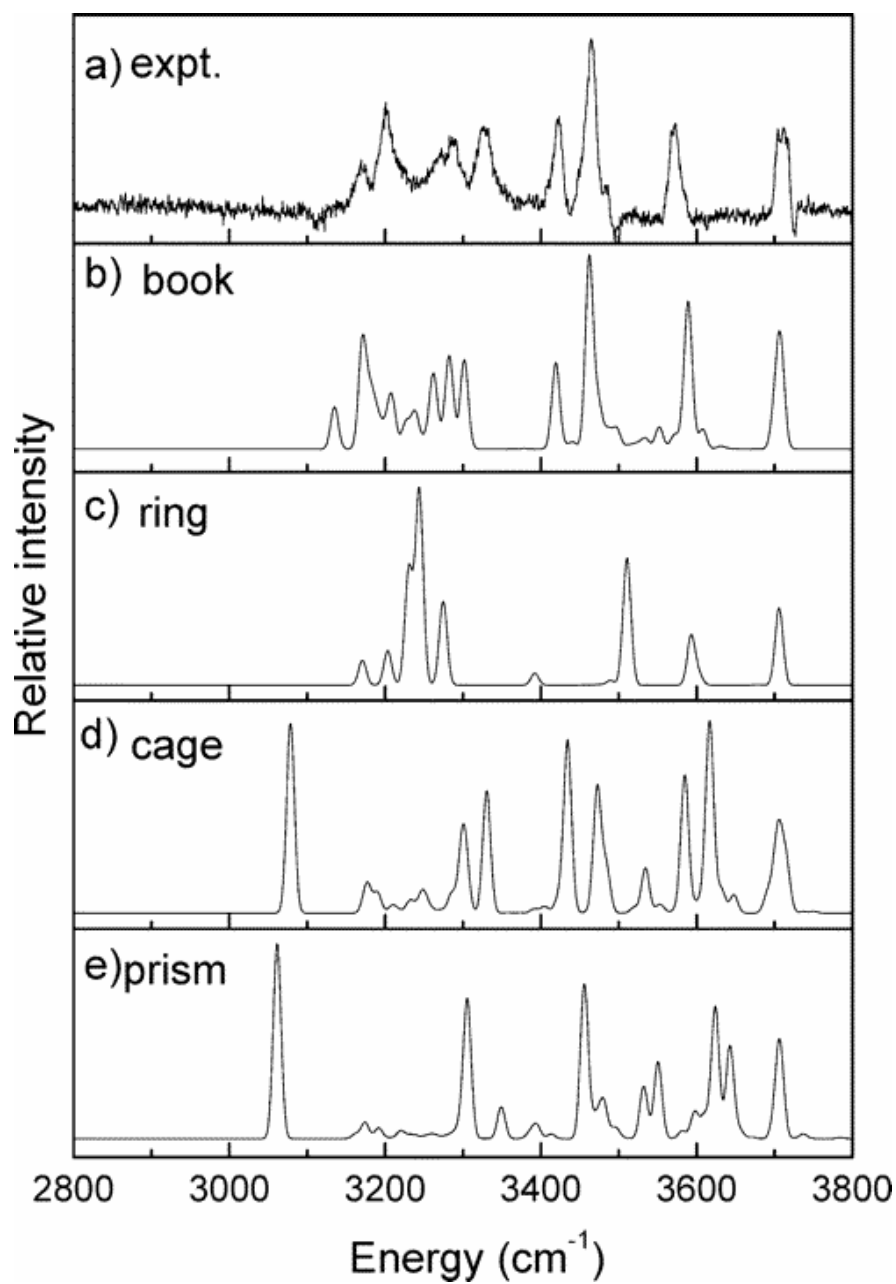


Figure 3. Vibrational spectra of the $(\text{H}_2\text{O})_6$ cluster in the OH stretch region. The experimental spectrum (a) results from $(\text{H}_2\text{O})_6\text{Ar}_{10-12}$ clusters that serve as the precursor to $(\text{H}_2\text{O})_6^+$ (reproduced from ref 27). The simulated spectra for the book (b), ring (c), cage (d), and prism (e) isomers were calculated by allowing for near-degeneracy mixing of the OH stretch fundamentals with various overtones and combination states. The frequencies of the fundamentals were scaled as discussed in the text. The cubic force constants were reduced by 15%.

By far the best agreement between the calculated spectra reported in Figure 3 and the experimental spectrum is for the book isomer. The four intense transitions observed between 3420 and 3720 cm^{-1} are closely reproduced by the calculations. Moreover, the calculated spectrum of the book isomer displays considerable structure due to overtones and combination bands in the 3170-3330 cm^{-1} region, in agreement with experiment. Given the sensitivity of the spectral features in this region to the energy spacings between the unmixed fundamentals and the overtones and combination states, the agreement between theory (book isomer) and experiment is quite satisfying. In light of these results, we conclude that the book form of $(\text{H}_2\text{O})_6$ is the precursor for the dominant experimentally observed isomer of $(\text{H}_2\text{O})_6^-$, i.e., that which has a vertical detachment energy of 0.42 $\text{eV}^{2,6}$ and for which the vibrational spectrum in the OH stretch region was measured by Ayotte et al.¹⁵

A.5 IMPLICATIONS FOR ANION FORMATION

Two recent theoretical studies have identified **VII**, depicted in Figure 1, as the most stable form of $(\text{H}_2\text{O})_6^-$.^{19,21} One of these, by Kim et al.,¹⁹ proposed that **VII** is the isomer responsible for the vibrational spectrum of $(\text{H}_2\text{O})_6^-$ measured by Ayotte et al.,¹⁵ although, in our opinion, the agreement between their calculated (Becke3LYP) vibrational spectrum of this isomer and that measured is not close enough for an unambiguous assignment. The inability to account for the spectrum in a quantitative manner at the Becke3LYP level is not surprising, since this approach (at least when used with a flexible basis set) considerably overbinds the excess electron¹⁵ and also suffers from the problem (mentioned above) of exaggerating red shifts associated with the OH stretch vibration of the H-bonded OH groups. We have calculated the

vibrational spectrum of **VII** using the MP2 approximation, which shares with the B3LYP method the tendency to overestimate the bond lengths of OH groups engaged in H-bonding but, in contrast to the B3LYP method, considerably underestimates the binding of the excess electron. The resulting spectrum is in poorer agreement with the experimental spectrum for the anion than is that calculated using the Becke3LYP method. It is well-established that high-level electronic structure methods such as CCSD(T) are required to accurately describe the binding of an excess electron to clusters such as $(\text{H}_2\text{O})_6$.⁵⁴⁻⁵⁶ As a result, we believe that a definitive identification of the observed anionic isomer based on comparison of calculated and observed vibrational spectra would require optimizing the geometries and calculating the vibrational spectra of the various low-energy isomers of the anion at the CCSD(T) level, a computationally daunting task, particularly given the large basis set required.

In the absence of a definitive assignment of the structure of the $(\text{H}_2\text{O})_6^-$ anion based on comparison of calculated and measured vibrational spectra, it is useful to consider whether there is an energetically accessible pathway leading from the book form of the neutral cluster (**IV**) to the most stable (**VII**) isomer of the anion. Pathways for interconversion of several of the relevant low-energy minima of $(\text{H}_2\text{O})_6^-$ have been mapped out at the Becke3LYP/6-311++G**(sp) level of theory by Kim et al.⁴⁵ For our current purpose, the most important finding of ref 45 is that the overall barrier for interconversion of the anion from **IV'** (**Bd** in ref 45) to **VII** (**Af** in ref 45) lies only about 3.2 kcal/mol above **VII** and proceeds through the intermediate **V** (**Bf** in ref 45). In this discussion all energies have been corrected for vibrational zero-point energy. The **IV'** anion is formed from the book isomer of the neutral cluster by a flip of one of the free OH groups and electron capture. The free OH flip is accompanied by an increase in the dipole moment and, hence, also by an enhanced binding of the excess electron. Our calculations indicate that this

occurs without a barrier. Moreover, **VII** is calculated to lie energetically 5.3 kcal/mol below the neutral book isomer (**IV**), which implies that the barriers for rearrangement of the anion lie energetically below the neutral cluster plus a free electron. Although the relative energies from the Becke3LYP calculations are semiquantitative at best, the conclusion that there is no net barrier between the neutral precursor **IV** plus a free electron and the **VII** anion is expected to hold up in higher level calculations such as CCSD(T).

It is also interesting to note that there are two isomers of the anion closely related to **VII**, and only slightly less stable. These are **VIII** (**Af** in ref 45) and **VI**, located in our calculations. **VI** and **VIII** are calculated to lie respectively only 0.15 and 0.21 kcal/mol above **VII**, and the barriers for rearrangement of **VI** to either **VII** or **VIII** are calculated to be only about 0.1 kcal/mol. These results suggest that the anion does not possess a well-defined rigid structure.

A.6 CONCLUSION

The present study reports for the first time calculated vibrational spectra of selected low-energy isomers of $(\text{H}_2\text{O})_6$ using geometries optimized with inclusion of high-order electron correlation effects and allowing also for coupling of the OH stretch fundamentals with overtones and combination bands. These calculations support the assignment of Diken et al.²⁷ of the book isomer as the precursor to the major $(\text{H}_2\text{O})_6^-$ isomer observed experimentally. It should be stressed that this does not necessarily imply that the book structure is the dominant $(\text{H}_2\text{O})_6$ isomer in the neutral expansion, as there could be significant population of other isomers that do not lead to the $(\text{H}_2\text{O})_6^-$ anion upon interaction with low-energy electrons. Indeed, near complete-basis set limit MP2 calculations predict the cage, book, and prism isomers of the neutral cluster

to be nearly isoenergetic (i.e., to lie within 0.25 kcal/mol).³⁴ Moreover, the calculations of Losada and Leutwyler⁵⁰ predict that the ring (chair conformer), book, cage, and prism structures are all very close in energy when vibrational zero-point effects are included and that the ring is the favored isomer below $T = 8$ K, the cage to be the dominant isomer between $T = 8$ and 26 K, and the book to be the dominant isomer for $T > 26$ K. The $(\text{H}_2\text{O})_6$ clusters characterized by Diken et al.²⁷ have attached Ar atoms, which implies cluster temperatures near $T = 40$ K, consistent with sizable population of the book isomer. The terahertz laser vibrational-rotational tunneling spectroscopic studies of Saykally et al.^{48,49} provided evidence for only the cage form of $(\text{H}_2\text{O})_6$. Also, Pribble and Zwier have concluded on the basis of their measured OH stretch vibrational spectra that the water portion of the observed benzene $\cdot(\text{H}_2\text{O})_6$ cluster has a cage structure.⁵⁷ On the basis of the calculations of Losada and Leutwyler, this would seem to imply colder clusters in the experiments of Saykally et al. and Pribble and Zwier than in those of Johnson and co-workers.

Our electronic structure calculations indicate that the most stable isomer of the anion (**VII**) can be formed from the book form of the neutral cluster with no net activation energy (i.e., that the barriers for the rearrangements to give **VII** lie energetically below the book isomer). This is consistent with the experiments of Weber et al. in which $(\text{H}_2\text{O})_6^-$ is observed upon capture by $(\text{H}_2\text{O})_6$ of near 0 eV electrons (in Rydberg electron-transfer experiments).¹⁴ The main structural change associated with this process is a donor-acceptor exchange of two adjacent water monomers analogous to that of the isolated water dimer (see Figure 1). Although this rearrangement is energetically uphill for the book form of the neutral cluster, it is accompanied by a large increase in the dipole moment and, as a result, is energetically favorable for the anion.

Acknowledgment

This research was carried out with the support of a grant from the Department of Energy. We acknowledge valuable discussions with Drs. M. Johnson, E. Sibert and F. Wang. We also thank M. Johnson for permission to reproduce the $(\text{H}_2\text{O})_6^-$ precursor spectrum obtained by his group and E. Sibert for the use of his code for carrying out the vibrational CI calculations. The calculations were performed on computers at the University's Center for Molecular and Materials Simulations and at the Pittsburgh Supercomputing Center.

References and Notes for Appendix B

1. Haberland, H.; Langosch, H.; Schindler, H.-G.; Worsnop, D. R. *J. Phys. Chem.* **1984**, *88*, 3903.
2. Coe, J. V.; Lee, G. H.; Eaton, J. G.; Arnold, S. T.; Sarkas, H. W.; Bowen, K. H.; Ludewigt, C.; Haberland, H.; Worsnop, D. R. *J. Chem. Phys.* **1990**, *92*, 3980.
3. Posey, L. A.; Johnson, M. A. *J. Chem. Phys.* **1988**, *89*, 4807.
4. Campagnola, P. J.; Cyr, D. M.; Johnson, M. A. *Chem. Phys. Lett.* **1991**, *181*, 206.
5. Posey, L. A.; Campagnola, P. J.; Johnson, M. A.; Lee, G. H.; Eaton, J. G.; Bowen, K. H. *J. Chem. Phys.* **1989**, *91*, 6536.
6. Lee, G. H.; Arnold, S. T.; Eaton, J. G.; Sarkas, H. W.; Bowen, K. H.; Ludewigt, C.; Haberland, H. *Z. Phys. D: At. Mol. Clusters* **1991**, *20*, 9.
7. Desfrancois, C.; Khelifa, N.; Lisfi, A.; Schermann, J. P.; Eaton, J. G.; Bowen, K. H. *J. Chem. Phys.* **1991**, *95*, 7760.
8. Tachikawa, D. H.; Lund, A.; Ogasawara, M. *Can. J. Chem.* **1993**, *71*, 118.
9. Misaizu, F.; Kondow, T.; Kuchitsu, K. *Chem. Phys. Lett.* **1997**, *178*, 369.
10. Maeyama, T.; Tsumura, T.; Fujii, A.; Mikami, N. *Chem. Phys. Lett.* **1997**, *264*, 292.
11. Bailey, C. G.; Kim, J.; Johnson, M. A. *J. Phys. Chem.* **1996**, *100*, 16782.
12. Ayotte, P.; Bailey, C. G.; Kim, J.; Johnson, M. A. *J. Chem. Phys.* **1998**, *108*, 444.
13. Kelley, J. A.; Weddle, G. H.; Robertson, W. H.; Johnson, M. A. *J. Chem. Phys.* **2002**, *116*, 1201.
14. Weber, J. M.; Leber, E.; Ruf, M.-W.; Hotop, H. *Eur. Phys. J. D* **1999**, *7*, 587.
15. Ayotte, P.; Weddle, G. H.; Bailey, C. G.; Johnson, M. A.; Vila, F.; Jordan, K. D. *J. Chem. Phys.* **1999**, *110*, 6268.
16. Lee, S.; Kim, J.; Lee, S. J.; Kim, K. S. *Phys. Rev. Lett.* **1997**, *79*, 2038.
17. Kim, K. S.; Lee, S.; Kim, J.; Lee, J. Y. *J. Am. Chem. Soc.* **1997**, *119*, 9329.
18. Suh, S. B.; Lee, H. M.; Kim, J.; Lee, J. Y.; Kim, K. S. *J. Chem. Phys.* **2000**, *113*, 5273.
19. Lee, H. M.; Lee, S.; Kim, K. S. *J. Chem. Phys.* **2003**, *119*, 187.
20. Tsurusawa, T.; Iwata, S. *Chem. Phys. Lett.* **1999**, *315*, 433.

21. Wang, F.; Jordan, K. D. *J. Chem. Phys.* **2003**, *119*, 11645.
22. Novakovskaya, Y. V.; Stepanov, N. F. *J. Phys. Chem. A* **1999**, *103*, 10975.
23. Smith, D. M. A.; Smets, J.; Adamowicz, L. *J. Chem. Phys.* **1999**, *110*, 3804.
24. Chen, H.-Y.; Shen, W.-S. *J. Chem. Phys.* **1999**, *110*, 9032.
25. Barnett, R. N.; Landman, U.; Makov, G.; Nitzan, A. *J. Chem. Phys.* **1990**, *93*, 6226.
26. Coe, J. V. *Int. Rev. Phys. Chem.* **2001**, *20*, 33.
27. Diken, E. G.; Robertson, W. H.; Johnson, M. A. *J. Phys. Chem. A* **2004**, *108*, 64.
28. Becke, A. D. *J. Chem. Phys.* **1993**, *98*, 5648.
29. Lee, C.; Yang, W.; Parr, R. G. *Phys. Rev. B* **1998**, *37*, 785.
30. Huisken, F.; Kaloudis, M.; Vighasin, A. A. *Chem. Phys. Lett.* **1997**, *269*, 235.
31. Diri, K.; Myshakin, E. M.; Jordan, K. D. In preparation.
32. Pople, J. A.; Head-Gordon, M.; Raghavachari, K. *J. Chem. Phys.* **1987**, *87*, 5968.
33. Tsai, C. J.; Jordan, K. D. *Chem. Phys. Lett.* **1993**, *213*, 181.
34. Xantheas, S. S.; Burnham, C. J.; Harrison, R. J. *J. Chem. Phys.* **2002**, *116*, 1493.
35. Pedulla, J. M.; Jordan, K. D. *Chem. Phys.* **1998**, *239*, 593.
36. Gregory, J. K.; Clary, D. C. *J. Phys. Chem.* **1996**, *100*, 18014.
37. Frisch, M. J.; Pople, J. A.; Binkley, J. S. *J. Chem. Phys.* **1984**, *80*, 3265.
38. Kim, K.; Jordan, K. D.; Zwier, T. S. *J. Am. Chem. Soc.* **1994**, *116*, 11568.
39. Woon, D. E.; Dunning, T. H., Jr. *J. Chem. Phys.* **1993**, *98*, 1358.
40. Kendall, R. A.; Dunning, T. H., Jr.; Harrison, R. J. *J. Chem. Phys.* **1992**, *96*, 6796.
41. Frisch, M. J.; Trucks, G. W.; et al. *Gaussian 03*, release B.05; Gaussian Inc.: Pittsburgh, PA, 2003.
42. Florio, G. M.; Zwier, T. S.; Myshakin, E. M.; Jordan, K. D.; Sibert, E. L., III. *J. Chem. Phys.* **2003**, *118*, 1735.
43. Myshakin, E. M.; Jordan, K. D.; Sibert, E. L., III; Johnson, M. A. *J. Chem. Phys.* **2003**, *119*, 10138.
44. Mayrhofer, R. C.; Sibert, E. L. *Theor. Chim. Acta* **1995**, *92*, 107.
45. Lee, H. M.; Lee, S.; Kim, K. S. *J. Chem. Phys.* **2003**, *119*, 7685.
46. Krishnan, R.; Binkley, J. S.; Seeger, R.; Pople, J. A. *J. Chem. Phys.* **1980**, *72*, 650.
47. Clark, T.; Chandrasekhar, J.; Schleyer, P. v. R. *J. Comput. Chem.* **1983**, *4*, 294.
48. Liu, K.; Brown, M. G.; Carter, C.; Saykally, R. J.; Gregory, J. K.; Clary, D. C. *Nature* **1996**, *381*, 501.
49. Liu, K.; Brown, M. G.; Saykally, R. J. *J. Phys. Chem. A* **1997**, *101*, 8995.
50. Losada, M.; Leutwyler, S. *J. Chem. Phys.* **2002**, *117*, 2003.
51. Ayotte, P.; Weddle, G. H.; Kim, J.; Johnson, M. A. *J. Am. Chem. Soc.* **1998**, *120*, 12361.
52. Robertson, W. H.; Weddle, G. H.; Kelley, J. A.; Johnson, M. A. *J. Phys. Chem. A* **2002**, *106*, 1205.
53. Barone, V. *J. Chem. Phys.* **2004**, *120*, 3059.
54. Peterson, K. A.; Gutowski, M. *J. Chem. Phys.* **2002**, *116*, 3297.
55. Gutowski, M.; Jordan, K. D.; Skurski, P. *J. Phys. Chem. A* **1998**, *102*, 2624.
56. Skurski, P.; Gutowski, M.; Simons, J. *Int. J. Quantum Chem.* **2000**, *80*, 1024.
57. Pribble, R. N.; Zwier, T. S. *Science* **1994**, *265*, 75.

APPENDIX B

CALCULATED VIBRATIONAL FREQUENCIES OF SELECTED ISOMERS OF (H₂O)₆

Table 1. Calculated vibrational frequencies of selected isomers of (H₂O)₆ at the Becke3LYP/aug-cc-pVDZ level.^{a, b}

| | Book isomer | | | Cage isomer | | | Prism isomer | | | Chair isomer | | |
|----|-------------|--------|-------|-------------|--------|-------|--------------|--------|-------|--------------|--------|-------|
| | Harm | Anharm | | Harm | Anharm | | Harm | Anharm | | Harm | Anharm | |
| 1 | 3868 | 3688 | (180) | 3873 | 3687 | (186) | 3867 | 3676 | (191) | 3869 | 3684 | (185) |
| 2 | 3865 | 3690 | (175) | 3867 | 3677 | (190) | 3866 | 3681 | (185) | 3868 | 3683 | (185) |
| 3 | 3864 | 3674 | (190) | 3863 | 3675 | (188) | 3865 | 3677 | (188) | 3868 | 3686 | (182) |
| 4 | 3864 | 3685 | (179) | 3861 | 3677 | (184) | 3783 | 3598 | (185) | 3867 | 3682 | (185) |
| 5 | 3862 | 3675 | (187) | 3726 | 3524 | (202) | 3746 | 3529 | (217) | 3867 | 3684 | (183) |
| 6 | 3702 | 3498 | (204) | 3694 | 3503 | (191) | 3720 | 3529 | (191) | 3867 | 3688 | (179) |
| 7 | 3535 | 3360 | (175) | 3648 | 3472 | (176) | 3647 | 3431 | (216) | 3422 | 3244 | (178) |
| 8 | 3520 | 3350 | (170) | 3544 | 3364 | (180) | 3643 | 3491 | (152) | 3403 | 3231 | (172) |
| 9 | 3457 | 3296 | (161) | 3478 | 3291 | (187) | 3529 | 3332 | (197) | 3403 | 3233 | (170) |
| 10 | 3345 | 3215 | (130) | 3436 | 3273 | (163) | 3474 | 3181 | (293) | 3341 | 3091 | (250) |
| 11 | 3294 | 3067 | (227) | 3388 | 3234 | (154) | 3400 | 3250 | (150) | 3341 | 3095 | (246) |

| | | | | | | | | | | | | |
|----|------|------|-------|------|------|-------|------|------|-------|------|------|-------|
| 12 | 3207 | 2971 | (236) | 3165 | 2924 | (241) | 3136 | 2888 | (248) | 3257 | 2989 | (268) |
| 13 | 1699 | 1672 | (27) | 1689 | 1655 | (34) | 1705 | 1647 | (58) | 1687 | 1624 | (63) |
| 14 | 1670 | 1633 | (37) | 1677 | 1614 | (63) | 1685 | 1627 | (58) | 1668 | 1621 | (47) |
| 15 | 1657 | 1615 | (42) | 1664 | 1618 | (46) | 1669 | 1617 | (52) | 1668 | 1623 | (45) |
| 16 | 1639 | 1607 | (32) | 1651 | 1618 | (33) | 1644 | 1611 | (33) | 1637 | 1594 | (43) |
| 17 | 1635 | 1592 | (43) | 1639 | 1588 | (51) | 1641 | 1599 | (42) | 1637 | 1596 | (41) |
| 18 | 1622 | 1578 | (44) | 1631 | 1606 | (25) | 1628 | 1626 | (2) | 1624 | 1580 | (44) |
| 19 | 1033 | 928 | (105) | 1009 | 877 | (132) | 1036 | 933 | (103) | 990 | 869 | (121) |
| 20 | 918 | 835 | (83) | 879 | 759 | (120) | 890 | 765 | (125) | 915 | 819 | (96) |
| 21 | 870 | 759 | (111) | 818 | 718 | (100) | 851 | 768 | (83) | 915 | 821 | (94) |
| 22 | 850 | 746 | (104) | 807 | 721 | (86) | 738 | 642 | (96) | 821 | 743 | (78) |
| 23 | 769 | 696 | (73) | 744 | 651 | (93) | 701 | 601 | (100) | 821 | 746 | (75) |
| 24 | 744 | 674 | (70) | 694 | 604 | (90) | 655 | 571 | (84) | 799 | 738 | (61) |
| 25 | 613 | 543 | (70) | 638 | 543 | (95) | 626 | 550 | (76) | 481 | 418 | (63) |
| 26 | 552 | 496 | (56) | 572 | 490 | (82) | 554 | 456 | (98) | 481 | 419 | (62) |
| 27 | 494 | 450 | (44) | 535 | 496 | (39) | 543 | 460 | (83) | 475 | 451 | (24) |
| 28 | 470 | 425 | (45) | 487 | 431 | (56) | 496 | 430 | (66) | 453 | 396 | (57) |
| 29 | 456 | 435 | (21) | 468 | 396 | (72) | 471 | 379 | (92) | 453 | 403 | (50) |
| 30 | 416 | 376 | (40) | 439 | 395 | (44) | 437 | 367 | (70) | 431 | 407 | (24) |
| 31 | 400 | 363 | (37) | 414 | 376 | (38) | 430 | 354 | (76) | 340 | 308 | (32) |
| 32 | 314 | 275 | (39) | 398 | 364 | (34) | 377 | 303 | (74) | 306 | 279 | (27) |
| 33 | 301 | 272 | (29) | 311 | 257 | (54) | 363 | 317 | (46) | 306 | 280 | (26) |
| 34 | 295 | 258 | (37) | 287 | 257 | (30) | 294 | 275 | (19) | 299 | 237 | (62) |
| 35 | 285 | 254 | (31) | 265 | 184 | (81) | 290 | 243 | (47) | 266 | 199 | (67) |
| 36 | 259 | 205 | (54) | 256 | 200 | (56) | 279 | 226 | (53) | 266 | 200 | (66) |
| 37 | 258 | 194 | (64) | 245 | 217 | (28) | 244 | 214 | (30) | 222 | 197 | (25) |
| 38 | 245 | 224 | (21) | 233 | 197 | (36) | 237 | 196 | (41) | 222 | 195 | (27) |
| 39 | 231 | 206 | (25) | 226 | 198 | (28) | 225 | 190 | (35) | 208 | 149 | (59) |
| 40 | 204 | 165 | (39) | 209 | 167 | (42) | 211 | 182 | (29) | 208 | 168 | (40) |

| | | | | | | | | | | | | |
|----|-----|-----|------|-----|-----|-------|-----|-----|------|-----|-----|------|
| 41 | 197 | 174 | (23) | 194 | 91 | (103) | 169 | 147 | (22) | 184 | 151 | (33) |
| 42 | 182 | 159 | (23) | 177 | 137 | (40) | 163 | 152 | (11) | 162 | 146 | (16) |
| 43 | 142 | 107 | (35) | 132 | 96 | (36) | 139 | 116 | (23) | 91 | 67 | (24) |
| 44 | 95 | 89 | (6) | 107 | 85 | (22) | 85 | 72 | (13) | 56 | 39 | (17) |
| 45 | 75 | 67 | (8) | 104 | 79 | (25) | 81 | 68 | (13) | 52 | 29 | (23) |
| 46 | 60 | 57 | (3) | 80 | 64 | (16) | 73 | 60 | (13) | 51 | 29 | (22) |
| 47 | 43 | 38 | (5) | 62 | 43 | (19) | 69 | 47 | (22) | 32 | 8 | (24) |
| 48 | 31 | 28 | (3) | 51 | 38 | (13) | 56 | -11 | (67) | 32 | 24 | (8) |

^a Experimentally observed frequencies (in cm^{-1}): 3220 (cage isomer, H-bonded OH stretch, Ref 184); 3335 (ring isomer in liquid He droplets, H-bonded OH stretch, Ref. 89); 3711, 3572, 3464, 3423, 3327, 3287, 3201, 3169 (book isomer, Ref. 90). ^b Anharmonicity corrections are given in parentheses.

BIBLIOGRAPHY

- (1) Crawford, O. H.; Dalgarno, A. *Chem. Phys. Lett.* **1967**, *1*, 23.
- (2) Brown, W. B.; Roberts, R. E. *J. Chem. Phys.* **1967**, *46*, 2006.
- (3) Garrett, W. R. *Phys. Rev. A* **1971**, *3*, 961.
- (4) Garrett, W. R. *J. Chem. Phys.* **1980**, *73*, 5721.
- (5) Garrett, W. R. *J. Chem. Phys.* **1982**, *77*, 3666.
- (6) Gutowski, M.; Skurski, P.; Boldyrev, A. I.; Simons, J.; Jordan, K. D. *Phys. Rev. A* **1996**, *54*, 1906.
- (7) Ayotte, P.; Bailey, C. G.; Kim, J.; Johnson, M. A. *J. Chem. Phys.* **1998**, *108*, 444.
- (8) Brinkman, E. A.; Berger, S.; Marks, J.; Brauman, J. I. *J. Chem. Phys.* **1993**, *99*, 7586.
- (9) Desfrancois, C.; Periquet, V.; Lyapustina, S. A.; Lippa, T. P.; Robinson, D. W.; Bowen, K. H.; Nonaka, H.; Compton, R. N. *J. Chem. Phys.* **1999**, *111*, 4569.
- (10) Compton, R. N.; Carman, H. S.; Desfrancois, C.; Abdoul-Carime, H.; Schermann, J. P.; Hendricks, J. H.; Lyapustina, S. A.; Bowen, K. H. *J. Chem. Phys.* **1996**, *105*, 3472.
- (11) Lecomte, F.; Carles, S.; Desfrancois, C.; Johnson, M. A. *J. Chem. Phys.* **2000**, *113*, 10973.
- (12) Rohr, K.; Linder, F. *J. Phys. B* **1976**, *9*, 2521.
- (13) Wong, S. F.; Schulz, G. *Phys. Rev. Lett.* **1974**, *33*, 134.
- (14) Stockdale, J. A. D.; Davis, F. J.; Compton, R. N.; Klots, C. E. *J. Chem. Phys.* **1974**, *60*, 4279.
- (15) Coe, J. V.; Lee, G. H.; Eaton, J. G.; Arnold, S. T.; Sarkas, H. W.; Bowen, K. H.; Ludewigt, C.; Haberland, H.; Worsnop, D. R. *J. Chem. Phys.* **1990**, *92*, 3980.
- (16) Dessent, C. E. H.; Bailey, C. G.; Johnson, M. A. *J. Chem. Phys.* **1995**, *102*, 6335.
- (17) Compton, R. N.; Hammer, N. I. In *Advances in Gas-Phase Ion Chemistry*; Adams, N. G., Ed.; JAI Press: Greenwich, CT, 2001; Vol. 4; pp 257.
- (18) Hammer, N. I.; Dirir, K.; Jordan, K. D.; Desfrancois, C.; Compton, R. N. *J. Chem. Phys.* **2003**, *119*, 3650.
- (19) Desfrancois, C. *Phys. Rev. A* **1995**, *51*, 3667.
- (20) Desfrancois, C.; Abdoul-Carime, H.; Khelifa, N.; Schermann, J. P. *Phys. Rev. Lett.* **1994**, *73*, 2436.
- (21) Hammer, N. I.; Hinde, R. J.; Compton, R. N.; Dirir, K.; Jordan, K. D.; Radisic, D.; Stokes, S. T.; Bowen, K. H. *J. Chem. Phys.* **2004**, *120*, 685.
- (22) Jordan, K. D.; Wang, F. *Ann. Rev. Phys. Chem.* **2003**, *54*, 367.
- (23) Gutowski, M.; Skurski, P.; Jordan, K. D.; Simons, J. *Int. J. Quantum Chem.* **1997**, *64*, 183.
- (24) Koopmans, T. *Physica (Amsterdam)* **1934**, *1*, 104.

- (25) Gutowski, M.; Jordan, K. D.; Skurski, P. *J. Phys. Chem. A* **1998**, *102*, 2624.
- (26) Raghavachari, K.; Trucks, G. W.; Pople, J. A.; Head-Gordon, M. *Chem. Phys. Lett.* **1989**, *157*, 479.
- (27) Noga, J.; Barlett, R. J. *J. Chem. Phys.* **1987**, *86*, 7041.
- (28) Tsai, M. K.; Wang, F.; Jordan, K. D. *Journal of Physical Chemistry A* **2004**, *108*, 2912.
- (29) Kendall, R. A.; Dunning, T. H.; Harrison, R. J. *J. Chem. Phys.* **1992**, *96*, 6796.
- (30) Frisch, M. J.; Trucks, G. W.; Schlegel, H. B. e. a. Gaussian 98; Gaussian, Inc.: Pittsburgh, PA, 1998.
- (31) Yokoyama, K.; Leach, G. W.; Kim, J. B.; Lineberger, W. C.; Boldyrev, A. I.; Gutowski, M. *J. Chem. Phys.* **1996**, *105*, 10706.
- (32) Gutowski, M.; Skurski, P. *Recent Res. Dev. Phys. Chem.* **1999**, *3*, 245.
- (33) Gutowski, M.; Skurski, P. *Chem. Phys. Lett.* **1999**, *300*, 331.
- (34) Crawford, O. H.; Garrett, W. R. *Journal of Chemical Physics* **1977**, *66*, 4968.
- (35) Desfrancois, C.; AbdoulCarime, H.; Schermann, J. P. *International Journal of Modern Physics B* **1996**, *10*, 1339.
- (36) Compton, R. N. In *The Role of Rydberg States in Spectroscopy and Photochemistry*; Sandorfy, C., Ed.; Kluwer Academic: Dordrecht, 1999.
- (37) Mullin, A. S.; Murray, K. K.; Schulz, C. P.; Lineberger, W. C. *Journal of Physical Chemistry* **1993**, *97*, 10281.
- (38) Sommerfeld, T. *Physical Chemistry Chemical Physics* **2002**, *4*, 2511.
- (39) Møller, C.; Plesset, M. S. *Physical Review* **1934**, *46*, 618.
- (40) Kendall, R. A.; Dunning, T. H.; Harrison, R. J. *Journal of Chemical Physics* **1992**, *96*, 6796.
- (41) Simmons, J. W.; Goldstein, J. H. *J. Chem. Phys.* **1954**, *22*, 1678.
- (42) Saadi, A. H.; Lee, W. H. *Journal of the Chemical Society B-Physical Organic* **1966**, *5*.
- (43) Dorris, K. L.; Britt, C. O.; Boggs, J. E. *Journal of Chemical Physics* **1966**, *44*, 1352.
- (44) Alonso, J. L.; Cervellati, R.; Esposti, A. D.; Lister, D. G.; Palmieri, P. *Journal of the Chemical Society-Faraday Transactions II* **1986**, *82*, 357.
- (45) Purvis, G. D.; Barlett, R. J. *J. Chem. Phys.* **1982**, *76*, 1910.
- (46) Head-Gordon, M. *J. Phys. Chem.* **1996**, *100*, 13213.
- (47) Compton, R. N.; Reinhardt, P. W.; Schweinler, H. C. *International Journal of Mass Spectrometry and Ion Processes* **1983**, *49*, 113.
- (48) Stepanovic, M.; Pariat, Y.; Allan, M. *Journal of Chemical Physics* **1999**, *110*, 11376.
- (49) Bailey, C. G.; Dessent, C. E. H.; Johnson, M. A.; Bowen, K. H. *J. Chem. Phys.* **1996**, *104*, 6976.
- (50) Gutowski, M.; Skurski, P. *Chemical Physics Letters* **1999**, *300*, 331.
- (51) Adamowicz, L. *Journal of Chemical Physics* **1989**, *91*, 7787.
- (52) Adamowicz, L.; McCullough, E. A. *J. Phys. Chem.* **1984**, *88*, 2045.
- (53) Desfrancois, C.; Periquet, V.; Carles, S.; Schermann, J. P.; Smith, D. M. A.; Adamowicz, L. *Journal of Chemical Physics* **1999**, *110*, 4309.
- (54) Carles, S.; Desfrancois, C.; Schermann, J. P.; Jalbout, A. F.; Adamowicz, L. *Chemical Physics Letters* **2001**, *334*, 374.

- (55) Kisiel, Z.; Desyatnyk, O.; Bialkowska-Jaworska, E.; Pszczolkowski, L. *Physical Chemistry Chemical Physics* **2003**, *5*, 820.
- (56) Hammer, N. I.; Gao, F.; Pagni, R. M.; Compton, R. N. *Journal of Chemical Physics* **2002**, *117*, 4299.
- (57) Wrodnigg, G. H.; Besenhard, J. O.; Winter, M. *Journal of the Electrochemical Society* **1999**, *146*, 470.
- (58) Kricheldorf, H. R.; Petermann, O. *Macromolecules* **2001**, *34*, 8841.
- (59) Frisch, M. J.; Trucks, G. W.; Schlegel, H. B.; Scuseria, G. E.; Robb, M. A.; Cheeseman, J. R.; Montgomery, J., J. A.; Vreven, T.; Kudin, K. N.; Burant, J. C.; Millam, J. M.; Iyengar, S. S.; Tomasi, J.; Barone, V.; Mennucci, B.; Cossi, M.; Scalmani, G.; Rega, N.; Petersson, G. A.; Nakatsuji, H.; Hada, M.; Ehara, M.; Toyota, K.; Fukuda, R.; Hasegawa, J.; Ishida, M.; Nakajima, T.; Honda, Y.; Kitao, O.; Nakai, H.; Klene, M.; Li, X.; Knox, J. E.; Hratchian, H. P.; Cross, J. B.; Adamo, C.; Jaramillo, J.; Gomperts, R.; Stratmann, R. E.; Yazyev, O.; Austin, A. J.; Cammi, R.; Pomelli, C.; Ochterski, J. W.; Ayala, P. Y.; Morokuma, K.; Voth, G. A.; Salvador, P.; Dannenberg, J. J.; Zakrzewski, V. G.; Dapprich, S.; Daniels, A. D.; Strain, M. C.; Farkas, O.; Malick, D. K.; Rabuck, A. D.; Raghavachari, K.; Foresman, J. B.; Ortiz, J. V.; Cui, Q.; Baboul, A. G.; Clifford, S.; Cioslowski, J.; Stefanov, B. B.; Liu, G. L., A.; Piskorz, P.; Komaromi, I.; Martin, R. L.; Fox, D. J.; Keith, T.; Al-Laham, M. A.; Peng, C. Y.; Nanayakkara, A.; Challacombe, M.; Gill, P. M. W.; Johnson, B.; Chen, W.; Wong, M. W.; Gonzalez, C.; Pople, J. A. Gaussian 03, Revision C.01; Gaussian, Inc.: Pittsburgh, PA, 2003.
- (60) Amos, R. D.; Bernhardsson, A.; Berning, A. In *MOLPRO, a package of ab initio programs*; 2002.1 ed.; Werner, H.-J., Knowles, P. J., Eds.
- (61) Knowles, P. J.; Hampel, C.; Werner, H. J. *Journal of Chemical Physics* **1993**, *99*, 5219.
- (62) Desfrancois, C.; Carime, H. A.; Schermann, J. P. *Int. J. Mod. Phys. B* **1996**, *10*, 1339.
- (63) Chapman, D. A.; Balasubramanian, K.; Lin, S. H. *Physical Review A* **1988**, *38*, 6098.
- (64) Carman, H. S., Jr.; Klots, C. E.; Compton, R. N. *J. Chem. Phys.* **1993**, *99*, 1734.
- (65) Compton, R. N.; Christop.Lg; Hurst, G. S.; Reinhard.Pw. *Journal of Chemical Physics* **1966**, *45*, 4634.
- (66) Compton, R.; Christop.L; Hurst, G.; Reinhard.P. *J. Chem. Phys.* **1966**, *45*, 4634.
- (67) Martin, F.; Burrow, P. D.; Cai, Z. L.; Cloutier, P.; Hunting, D.; Sanche, L. *Physical Review Letters* **2004**, *93*.
- (68) Nesbitt, D. J. *Chem. Rev.* **1988**, *88*, 843.
- (69) Miller, R. E. *Science* **1988**, *240*, 447.
- (70) Saykally, R. J.; Blake, G. A. *Science* **1993**, *259*, 1570.
- (71) Huisken, F.; Kaloudis, M.; Kulcke, A. *J. Chem. Phys.* **1996**, *104*, 17.
- (72) Liu, K.; Brown, M. G.; Saykally, R. J. *J. Phys. Chem. A* **1997**, *101*, 8995.
- (73) Oudejans, L.; Miller, R. E. *J. Phys. Chem. A* **1997**, *101*, 7582.
- (74) Brown, M. G.; Keutsch, F. N.; Saykally, R. J. *J. Chem. Phys.* **1998**, *109*, 9645.
- (75) Brown, M. G.; Keutsch, F. N.; Braly, L. B.; Saykally, R. J. *J. Chem. Phys.* **1999**, *111*, 7801.
- (76) Buck, U.; Huisken, F. *Chem. Rev.* **2000**, *100*, 3863.
- (77) Nauta, K.; Miller, R. E. *Science* **2000**, *287*, 293.
- (78) Wormer, P. E. S.; Avoird, A. v. d. *Chem. Rev.* **2000**, *100*, 4109.

- (79) Keutsch, F. N.; Saykally, R. J. *Science* **2001**, *98*, 10533.
- (80) Goldman, N.; Fellers, R. S.; Brown, M. G.; Braly, L. B.; Keoshian, C. J.; Leforestier, C.; Saykally, R. J. *J. Chem. Phys.* **2002**, *116*, 10148.
- (81) Keutsch, F. N.; Cruzan, J. D.; Saykally, R. J. *Chem. Rev.* **2003**, *103*, 2533.
- (82) Ceponkus, J.; Karlstrom, G.; Nelander, B. *J. Phys. Chem. A* **2005**, *109*, 7859.
- (83) Honegger, E.; Leutwyler, S. *J. Chem. Phys.* **1988**, *88*, 2582.
- (84) Xantheas, S. S.; Dunning, T. H., Jr. *J. Chem. Phys.* **1993**, *99*, 8774.
- (85) Kim, K.; Jordan, K. D.; Zwier, T. S. *J. Am. Chem. Soc.* **1994**, *116*, 11568.
- (86) Kim, J.; Kim, K. S. *J. Chem. Phys.* **1998**, *109*, 5886.
- (87) Sadlej, J.; Buch, V.; Kazimirski, J. K.; Buck, U. *J. Phys. Chem. A* **1999**, *103*, 4933.
- (88) Lee, J. Y.; Kim, J.; Lee, H. M.; Tarakeshwar, P.; Kim, K. S. *J. Chem. Phys.* **2000**, *113*, 6160.
- (89) Burnham, C. J.; Xantheas, S. S.; Miller, M. A.; Applegate, B. E.; Miller, R. E. *J. Chem. Phys.* **2002**, *117*, 1109.
- (90) Diken, E. G.; Robertson, W. H.; Johnson, M. A. *J. Phys. Chem. A* **2004**, *108*, 64.
- (91) Jung, J. O.; Gerber, R. B. *J. Chem. Phys.* **1996**, *105*, 10332.
- (92) Sabo, D.; Bacic, Z.; Graf, S.; Leutwyler, S. *J. Chem. Phys.* **1998**, *109*, 5404.
- (93) Myshakin, E. M.; Diri, K.; Jordan, K. D. *J. Phys. Chem. A* **2004**, *108*, 6758.
- (94) Diri, K.; Myshakin, E. M.; Jordan, K. D. *J. Phys. Chem. A* **2005**, *109*, 4005.
- (95) Becke, A. D. *J. Chem. Phys.* **1993**, *98*, 5648.
- (96) Mills, I. M. In *Molecular Spectroscopy: Modern Research*; Rao, K. N., Mathews, C. W., Eds.; Academic Press: New York, 1972; Vol. 1; pp 115.
- (97) Martin, J. M. L.; Francois, J. P.; Gijbels, R. *J. Chem. Phys.* **1992**, *96*, 7633.
- (98) Lee, T. J.; Martin, J. M. L.; Taylor, P. R. *J. Chem. Phys.* **1995**, *102*, 254.
- (99) Csaszar, A. G.; Mills, I. M. *Spectrochim. Acta A* **1997**, *53*, 1101.
- (100) Bludsky, O.; Chocholousova, J.; Vacek, J.; Huisken, F.; Hobza, P. *J. Chem. Phys.* **2000**, *113*, 4629.
- (101) Neugebauer, J.; Hess, B. A. *J. Chem. Phys.* **2003**, *118*, 7215.
- (102) Pople, J. A.; Head-Gordon, M.; Raghavachari, K. *J. Chem. Phys.* **1987**, *87*, 5968.
- (103) Barone, V. *J. Chem. Phys.* **2005**, *122*, 014108.
- (104) Dunn, M. E.; Evans, T. M.; Kirschner, K. N.; Shields, G. C. *J. Phys. Chem. A* **2006**, *110*, 303.
- (105) Huang, Z. S.; Miller, R. E. *J. Chem. Phys.* **1989**, *91*, 6613.
- (106) Bentwood, R. M.; Barnes, A. J.; Orville-Thomas, W. J. *J. Mol. Spectrosc.* **1980**, *84*, 391.
- (107) Braly, L. B.; Liu, K.; Brown, M. G.; Keutsch, F. N.; Fellers, R. S.; Saykally, R. J. *J. Chem. Phys.* **2000**, *112*, 10314.
- (108) Kim, K. S.; Mhin, B. J.; Choi, U.-S.; Lee, K. *J. Chem. Phys.* **1992**, *97*, 6649.
- (109) Gregory, J. K.; Clary, D. C. *J. Phys. Chem.* **1996**, *100*, 18014.
- (110) Munoz-Caro, C.; Nino, A. *J. Phys. Chem. A* **1997**, *101*, 4128.
- (111) Groenenboom, G. C.; Wormer, P. E. S.; van der Avoird, A.; Mas, E. M.; Bukowski, R.; Szalewicz, K. *J. Chem. Phys.* **2000**, *113*.
- (112) Wright, N. J.; Gerber, R. B. *J. Chem. Phys.* **2000**, *112*, 2598.
- (113) Del Bene, J. E.; Jordan, M. J. T. *J. Mol. Struct. (THEOCHEM)* **2001**, *573*, 11.

- (114) Keutsch, F. N.; Brown, M. G.; Petersen, P. B.; Saykally, R. J.; Geleijns, M.; van der Avoird, A. *J. Chem. Phys.* **2001**, *114*, 3994.
- (115) Park, C. Y.; Kim, Y.; Kim, Y. *J. Chem. Phys.* **2001**, *115*, 2926.
- (116) Rekik, N.; Valcescu, A.; Blaise, P.; Henri-Rousseau, O. *Chem. Phys.* **2001**, *273*, 11.
- (117) Smit, M. J.; Groenenboom, G. C.; Wormer, P. E. S.; van der Avoird, A.; Bukowski, R.; Szalewicz, K. *J. Phys. Chem. A* **2001**, *105*, 6212.
- (118) Tobias, D. J.; Jungwirth, P.; Parrinello, M. *J. Chem. Phys.* **2001**, *114*, 7036.
- (119) Atamas, N. A.; Yaremko, A. M.; Bulavin, L. A.; Pogorelov, V. E.; Berski, S.; Latajka, Z.; Ratajczak, H.; Abkowitz-Bienko, A. *J. Mol. Struct.* **2002**, *605*, 187.
- (120) Chaban, G. M.; Gerber, R. B. *Spectrochim. Acta A* **2002**, *58*, 887.
- (121) Dykstra, C. E.; Shuler, K.; Young, R. A.; Bacic, Z. *J. Mol. Struct. (THEOCHEM)* **2002**, *591*, 11.
- (122) Sandorfy, C. *J. Mol. Struct.* **2002**, *614*, 365.
- (123) Alparone, A.; Millefiori, S. *Chem. Phys.* **2003**, *290*, 15.
- (124) Belhayara, K.; Chamma, D.; Henri-Rousseau, O. *J. Mol. Struct.* **2003**, *648*, 93.
- (125) Florio, G. M.; Zwier, T. S.; Myshakin, E. M.; Jordan, K. D.; Sibert III, E. L. *J. Chem. Phys.* **2003**, *118*, 1735.
- (126) Rai, V. K.; Rai, S. B.; Rai, D. K. *Spectrochim. Acta A* **2003**, *59*, 1299.
- (127) Stefov, V.; Pejov, L.; Soptrajanov, B. *J. Mol. Struct.* **2003**, *651-653*, 793.
- (128) Yamamoto, N.; Shida, N.; Miyoshi, E. *Chem. Phys. Lett.* **2003**, *371*, 724.
- (129) Heyne, K.; Huse, N.; Dreyer, J.; Nibbering, E. T. J.; Elsaesser, T. *J. Chem. Phys.* **2004**, *121*, 902.
- (130) Smedarchina, Z.; Fernandez-Ramos, A.; Siebrand, W. *Chem. Phys. Lett.* **2004**, *395*, 339.
- (131) Perchard, J. P. *Chem. Phys.* **2001**, *273*, 217.
- (132) Wales, D. J. *Energy Landscapes : With Applications to Clusters, Biomolecules and Glasses*; Cambridge University Press: Cambridge, UK, 2003.
- (133) Losada, M.; Leutwyler, S. *J. Chem. Phys.* **2002**, *117*, 2003.
- (134) Pedulla, J. M.; Kim, K.; Jordan, K. D. *Chem. Phys. Lett.* **1998**, *291*, 78.
- (135) Clary, D. C.; Gregory, J. K. In *Recent Theoretical and Experimental Advances in Hydrogen Bonded Clusters*; Xantheas, S. S., Ed.; Kluwer Academic Publishers, 2000; Vol. 561; pp 187.
- (136) Millot, C.; Stone, A. J. *Mol. Phys.* **1992**, *77*, 439.
- (137) Bowman, J. M. *J. Chem. Phys.* **1978**, *68*, 608.
- (138) Gerber, R. B.; Ratner, M. A. **1979**, *68*, 195.
- (139) Bowman, J. M. *Acc. Chem. Res.* **1986**, *19*, 202.
- (140) Wierzbicki, A.; Bowman, J. M. *Comp. Phys. Comm.* **1988**, *51*, 225.
- (141) Chaban, G. M.; Jung, J. O.; Gerber, R. B. *J. Chem. Phys.* **1999**, *111*, 1823.
- (142) Yagi, K.; Hirao, K.; Taketsugu, T.; Schmidt, M. W.; Gordon, M. S. *J. Chem. Phys.* **2004**, *121*, 1383.
- (143) Bouteiller, Y.; Perchard, J. P. *Chem. Phys.* **2004**, *305*, 1.
- (144) Barone, V. *unpublished*.
- (145) Mhin, B. J.; Kim, H. S.; Kim, H. S.; Yoon, C. W.; Kim, K. S. *Chem. Phys. Lett.* **1991**, *176*, 41.
- (146) Tsai, C. J.; Jordan, K. D. *Chem. Phys. Lett.* **1993**, *213*, 181.

- (147) Xantheas, S. S.; Burnham, C. J.; Harrison, R. J. *J. Chem. Phys.* **2002**, *116*, 1493.
- (148) Dirí, K.; Myshakin, E. M.; Jordan, K. D. *unpublished*.
- (149) Martin, J. M. L.; Lee, T. J.; Taylor, P. R.; François, J. *J. Chem. Phys.* **1995**, *103*, 2589.
- (150) Losada, M.; Leutwyler, S. *J. Chem. Phys.* **2003**, *119*, 304.
- (151) Grev, R. S.; Janssen, C. L.; Schaefer III, H. F. *J. Chem. Phys.* **1991**, *95*, 5128.
- (152) Liu, K.; Brown, M. G.; Carter, C.; Saykally, R. J.; Gregory, J. K.; Clary, D. C. *Nature* **1996**, *381*, 501.
- (153) Steinbach, C.; Andersson, P.; Melzer, M.; Kazimirski, J. K.; Buck, U.; Buch, V. *Phys. Chem. Chem. Phys.* **2004**, *6*, 3320.
- (154) Ayotte, P.; Johnson, M. A. *J. Chem. Phys.* **1997**, *106*, 811.
- (155) Hart, E. J.; Boag, J. W. *J. Am. Chem. Soc.* **1962**, *84*, 4090.
- (156) Campagnola, P. J.; Lavrich, D. J.; DeLuca, M. J.; Johnson, M. A. *J. Chem. Phys.* **1991**, *94*, 5240.
- (157) Weber, J. M.; Kim, J.; Woronowicz, E. A.; Weddle, G. H.; Becker, I.; Cheshnovsky, O.; Johnson, M. A. *Chem. Phys. Lett.* **2001**, *339*, 337.
- (158) Bragg, A. E.; Verlet, J. R. R.; Kammrath, A.; Cheshnovsky, O.; Neumark, D. M. *Science* **2004**, *306*, 669.
- (159) Paik, D. H.; Lee, I.-R.; Yang, D.-S.; J. S. Baskin; Zewail, A. H. *Science* **2004**, *306*, 672.
- (160) Long, F. H.; Lu, H.; Eisenthal, K. B. *Phys. Rev. Lett.* **1990**, *64*, 1469.
- (161) Kimura, Y.; Alfano, J. C.; Walhout, P. K.; Barbara, P. F. *J. Phys. Chem.* **1994**, *98*, 3450.
- (162) Baltuška, A.; Emde, M. F.; Pshenichnikov, M. S.; Wiersma, D. A. *J. Phys. Chem. A* **1999**, *103*, 10065.
- (163) Emde, M. F.; Baltuska, A.; Kummrow, A.; Pshenichnikov, M. S.; Wiersma, D. A. *Phys. Rev. Lett.* **1998**, *80*, 4645.
- (164) Kummrow, A.; Emde, M. F.; Baltuska, A.; Pshenichnikov, M. S.; Wiersma, D. A. *J. Phys. Chem. A* **1998**, *102*, 4172.
- (165) Silva, C.; Walhout, P. K.; Yokoyama, K.; Barbara, P. F. *Phys. Rev. Lett.* **1998**, *80*, 1086.
- (166) Yokoyama, K.; Silva, C.; Son, D. H.; P.K. Walhout; Barbara, P. F. *J. Phys. Chem. A* **1998**, *102*, 6957.
- (167) Coe, J. V.; Lee, G. H.; Eaton, J. G.; Arnold, S. T.; Sarkas, H. W.; Bowen, K. H.; Ludewigt, C.; Haberland, H.; Worsnop, D. R. *J. Chem. Phys.* **1990**, *92*, 3980.
- (168) Kim, J.; Becker, I.; Cheshnovsky, O.; Johnson, M. A. *Chem. Phys. Lett.* **1998**, *297*, 90.
- (169) Verlet, J. R. R.; Bragg, A. E.; Kammrath, A.; Cheshnovsky, O.; Neumark, D. M. *Science* **2005**, *307*, 93.
- (170) Hammer, N. I.; Roscioli, J. R.; Johnson, M. A. *J. Phys. Chem. A* **2005**, *109*, 7896.
- (171) Roscioli, J. R.; Johnson, M. A. *J. Chem. Phys.* **2006**, *Submitted*.
- (172) Lee, H. M.; Lee, S.; Kim, K. S. *J. Chem. Phys.* **2003**, *119*, 187.
- (173) Hammer, N. I.; Shin, J.-W.; Headrick, J. M.; Diken, E. G.; Roscioli, J. R.; Weddle, G. H.; Johnson, M. A. *Science* **2004**, *306*, 675.
- (174) Posey, L. A.; DeLuca, M. J.; Johnson, M. A. *Chem. Phys. Lett.* **1986**, *131*, 170.

- (175) Gerhards, M.; Unterberg, C.; Gerlach, A. *Phys. Chem. Chem. Phys.* **2002**, *4*, 5563.
- (176) Shin, J.-W.; Hammer, N. I.; Headrick, J. M.; Johnson, M. A. *Chem. Phys. Lett.* **2004**, *399*, 349.
- (177) Lee, H. M.; Suh, S. B.; Kim, K. S. *Journal of Chemical Physics* **2003**, *118*, 9981.
- (178) Wang, F.; Jordan, K. D. *J. Chem. Phys.* **2001**, *114*, 10717.
- (179) Wang, F.; Jordan, K. D. *J. Chem. Phys.* **2002**, *116*, 6973.
- (180) Sommerfeld, T.; Diri, K. unpublished work.
- (181) Herbert, J. M.; Head-Gordon, M. *J. Phys. Chem. A* **2005**, *109*, 5217.
- (182) Herbert, J. M.; Head-Gordon, M. *Proceedings of the National Academy of Sciences of the United States of America* **2006**, *103*, 14282.
- (183) Roscioli, J. R.; Johnson, M. A. *J. Chem. Phys.* **2007**, *126*, 024307.
- (184) Paul, J. B.; Collier, C. P.; Saykally, R. J. *J. Phys. Chem. A* **1997**, *101*, 5211.